Analysis of Autophagy Induction through ATG16L1 Phosphorylation

Wensheng Tian

Thesis submitted to the University of Ottawa in partial fulfillment of the requirements for the degree of Master of Science, Cellular and Molecular Medicine

Department of Cellular and Molecular Medicine

Faculty of Medicine

University of Ottawa

Abstract

Autophagy is a degradative program that maintains cellular homeostasis and is responsible for clearing potentially toxic elements from the cell. Defects in autophagy have been described in pathophysiology including neurodegeneration, cancer, and inflammatory bowel disease. However, analysis of autophagy rates can be challenging, particularly in rare cell populations or *in vivo*, due to inherent limitations of current tools available for measuring autophagy pathway induction. Here, we describe a novel method to monitor autophagy by measuring post-translational modification of the protein ATG16L1. We developed and characterized a monoclonal antibody that can detect phospho-ATG16L1 endogenously in mammalian cells by western blot, immunofluorescence, and immunohistochemistry. We demonstrate that phosphorylation of ATG16L1 provides a readout for the level of active E3-like enzyme responsible for lipidating LC3B, which can be used to determine autophagy rates. Importantly, phospho-ATG16L1 is only present on newly-forming autophagosomes. Therefore, its levels are not affected by prolonged stress or late-stage autophagy blocks, which can confound autophagy analysis. Moreover, we show ATG16L1 phosphorylation by the autophagy kinase ULK1 is a conserved signaling pathway that is activated by numerous autophagy-inducing stressors. Taken together, analysis of ATG16L1 phosphorylation represents an exciting new tool for researchers to study autophagy induction.

Author and co-author/collaborator contributions

Wensheng Tian (the author) was primarily responsible for data production in all figures of the results section except for immunofluorescence and IHC panels in Figs. 17, 22, and supplemental video. Reham Alsaadi assisted with immunofluorescence experiments and data analysis. Zhihao Guo was responsible for optimizing pATG16L1 antibody protocols for immunofluorescence and IHC. Alena Kalinina and Diane Lagace provided the mice used for the study and assisted with IHC experimental planning and tissue staining. Micael Carrier. and Marie-Eve Tremblay imaged EM samples. Baptiste Lacoste provided expertise and guidance for EM sample preparation. Ryan Russell oversaw manuscript planning and conceived of the study.

Table of Contents

List of Figures

List of Abbreviations

4EBP1	eIF4E binding protein
AA	Amino acid
ADP	Adenosine diphosphate
Akt	Protein kinase B
AMP	Adenosine monophosphate
AMPK	AMP-activated protein kinase
ATG	Autophagy-related
ATP	Adenosine Triphosphate
Baf A1	Bafilomycin A1
Bcl-2	B-cell lymphoma 2
CCCP	Carbonyl cyanide m-chlorophenyl hydrazine
CD	Crohn’s disease
CTEP	2-chloro-4-[2-[2,5-dimethyl1-[4-(trifluoromethoxy)phenyl]imidazol-4-yl]ethynyl]pyridine
DEPTOR	DEP domain containing mTOR interacting Protein
DMEM	Dulbecco's Modified Eagle'smedium
ER	Endoplasmic reticulum
FBS	Fetal bovine serum
FIP200	Focal adhesion kinase family interacting protein of 200kD
GAP	GTPase activating protein
GDP	Guanosine 5’-diphosphate
GFP	Green Fluorescent Protein
GTP	Guanosine 5’-triphosphate
HBSS	Hank’s balanced salt solution
HCT116	Human colorectal carcinoma cell line.
HEK293A	Human embryonic kidney cells 293
HOPS	Homotypic fusion and vacuole protein sorting
IF	Immunofluorescence

IHC	Immunohistochemistry
IKKα	IκB kinase subunit
IRGM	Immunity related GTPase M
KO	Knockout
MAP1LC3	Microtubule-associated protein 1 light chain 3
LIR	LC3-interacting region
MDCK	Madin-Darby Canine Kidney
MEF	Mouse embryonic fibroblasts
mLST8	Mammalian homolog of lethal with sec-13 gene 8
mTORC1	The mechanistic target of rapamycin complex 1
NDP52	Nuclear domain 10 protein 52
NOD2	Nucleotide-binding oligomerization domain-containing protein 2
NPC	Neural progenitor cells
NR	Nutrient-rich
OCT	Optimal temperature cutting compound
p62/SQSTM1	Sequestosome 1
pATG16L1^{s278}	Phospho-serine 278 ATG16L1
PBS	Phosphate-buffered saline
PFA	Paraformaldehyde
PIKK	Phosphatidylinositol-kinase-related kinase
PRAS40	Proline-rich Akt substrate of 40 kDa
PtdEth	Phosphatidylethanolamine
PtdIns	Phosphatidylinositide
PtdIns(3)P	Phosphatidylinositol(3)phosphate
Raptor	Regulatory associated protein of mTOR
Rheb	Ras homolog enriched in brain
RPE1	Retinal pigmented epithelial
Rubicon	RUN domain Beclin 1-interacting and cysteine-rich containing protein
S6K	p70S6 kinase
SDS-PAGE	Sodium dodecyl sulfate – polyacrylamide gel electrophoresis
ST	*Salmonella typhimurium*

TBST	Tris-buffered saline tween
TEM	Transmission electron microscopy
TSC2	Tuberous sclerosis complex 2
ULK	unc-51-like kinase
UVRAG	UV irradiation resistance-associated gene
VMP1	Vacuole membrane protein 1
VPS34	Vacuolar protein sorting 34
WB	Western blot
WIPI	WD-repeat protein interacting with phosphoinositides

Acknowledgments

I would like to thank my master's thesis supervisor Dr. Ryan Russell for his continued support and guidance, without whom I could not have achieved what I have accomplished today. Dr. Russell has provided me with valuable advice and encouragement for me to grow as a graduate student and develop the necessary skills as an independent researcher. Next, I would like to thank my Thesis Advisory Committee members, Dr. John Copeland and Dr. Morgan Fullerton, and my co-supervisor, Dr. Steven Gee, for their constructive comments and feedback throughout my research. In addition to their insightful advice, their comments have assisted me to consider perspectives from researchers of other fields than my own and better present my research to a broad audience.

I would like to thank my collaborators Dr. Diane Lagace, Dr. Baptise Lacoste, Dr. Marie-Eve Tremblay, their students Alena and Micael, and fellow lab member co-authors Reham Alsaadi and Zhihao Guo for their assistance and contribution in preparing and publishing the manuscript. The uOttawa PALM-Histology Core Facility for processing the IHC tissue samples, the Cell Biology and Image Acquisition Core (CBIA) for assistance in three-dimensional reconstruction and rendering of brain imaging, N. Vernoux for technical assistance in electron microscopy, J.A. Lunde for technical assistance in collecting mouse skeletal muscle samples

I am grateful to my fellow Russell lab members: Reham, Cloe, Mercy, Karyn and Yujin for their assistance and encouragement throughout my studies, and for providing a fun and supportive work environment. Our lab technician Zhihao for his work to keep the lab running smoothly. Last but not least, I would like to express my deepest gratitude to my family for their love and encouragement. Especially to my parents, for their unwavering support that enabled me to pursue my scientific dreams.

Sources of Funding

This work was supported by Canadian Institutes of Health Research (CIHR) Project Grants awarded to Ryan Russell (#PJT153034).

Introduction

Macroautophagy (hereafter referred to as autophagy) is a heavily regulated degradative process activated by a range of cellular stressors including nutrient starvation, unfolded protein aggregates, and pathogen infection. Autophagy serves to remove potentially harmful elements from the cytosolic environment such as proteins aggregates, damaged organelles, and foreign pathogens. Additionally, autophagy is an adaptive response able to maintain cellular energy homeostasis through the breakdown of macromolecules upon exposure to environmental stressors[1]. The process begins with the formation of double-membrane vesicles called autophagosomes. Cellular cargo designated for degradation by autophagy is recruited and sequestered by the autophagosomes as they expand and eventually enclose. The mature autophagosome then fuses with the lysosome to form the autolysosome, where acid-activated hydrolases breakdown the cargo in an acidic environment sequestered from the cytosol. The autophagy pathway is driven by a set of highly conserved autophagy-related (ATG) proteins, with each protein playing specific roles in the pathway at either the initiation of autophagy or autophagosome biogenesis steps.

History of autophagy

The first researcher to coin the term “autophagy” was Belgian scientist Christan de Duve, whose pioneering research 70 years ago lead to the discovery of the lysosome and its associated intracellular protein degradation functions. In 1949, de Duve and his colleagues were studying a blood sugar regulating phosphatase enzyme. As a control, de Duve’s group monitored acid phosphatase activity in their experiments where they

fractionated subcellular organelles with ultra-centrifugation. When they measured the acid phosphatase activity in the fractions, it was much lower compared to the expected value. Interestingly, old samples that were left in the fridge for days showed an increase of phosphatase activity in all fractions[2]. The group then hypothesized that the acid phosphatase was sequestered in tiny membrane sacs, which resulted in the lower than expected enzymatic activity in fresh samples. In older samples, the freeze-thaw cycles damaged these sacs and released the acid phosphatase, thus explaining the increased enzymatic activity observed. Four acid hydrolases were later identified from these tiny membrane sacs, which de Duve then named the “lysosome” for the lytic enzyme cargos they carry[3]. In 1974, de Duve received a Nobel prize of physiology and medicine for his discovery of the lysosome.

The natural question then arose was what were the biological functions of those newly discovered lysosomes. In the mid-1950s, Werner Straus, who was studying renal endocytosis, observed that lysosomes droplets that were rich in acid hydrolases at the proximal tubule of the kidney were responsible for storage and degradation of reabsorbed proteins[4]. In the 1960s, Zanvil Cohn and James Hirsch discovered bacterial lipids and proteins accumulated in the lysosomes of macrophages that engulfed bacteria earlier[5]. These were the first data linking lysosomal digestion to endocytotic uptake of materials such as pathogens or cellular debris. Around the same time, Marilyn Farquhar and her colleagues observed vesicles containing engulfed cytoplasmic material, they hypothesized these vesicles were early-stage lysosomes that have not yet digested its cargo, or “pre-lysosomes”. These “pre-lysosomes” are what we now know as autophagosomes. Autophagosomes originate in the cytoplasm as cup-shaped membrane

structures call phagophores, which expands and eventually fuses its edges to form a double-membraned mature autophagosome[6]. During the expansion process, autophagosomes recruit macromolecules or damaged organelles to their inward surface, and once a mature autophagosome forms, it then fuses with lysosome delivering its cargo for degradation[6]. De Duve recognized that the cargos in the autophagosomes usually originate from the same cells, he coined the term “autophagy” from the Greek roots “auto” (self) and “phagos” (eat) to describe this newly discovered process.

Scientists truly began to understand and appreciate the importance of autophagy in the 2000s after genetic experiments in the late 1990s identified key individual proteins involved in the autophagy pathway. Japanese scientist Yoshinori Ohsumi led the effort in identifying 15 new autophagy-related (ATG) genes from yeast nitrogen withdrawal genetic screens, the first of which – Atg1, was characterized in 1997[7]. Ohsumi’s pioneering work in identifying yeast ATG genes opened the floodgates for a wave of new autophagy research to look for their homologs in higher eukaryotes. The first mammalian ATG genes, ATG5 and ATG12, were characterized by Ohsumi’s student Mizushima in 1998[8]. ATG5 and ATG12 are part of a critical ubiquitin-like conjugation system of the autophagy pathway that conjugates the ubiquitin-like protein ATG8 onto autophagosomes. Shortly after this discovery, the mammalian homolog of ATG8, MAP1LC3 (LC3) was also identified by Ohsumi and colleagues[9]. As more mammalian homologs of yeast ATG proteins are identified, efforts began to shift in characterizing the autophagy signaling pathway in higher eukaryotes. As early as 1995, inhibition of the TOR (target of rapamycin) kinase by the macrolide rapamycin was found to stimulate autophagy in rat hepatocytes[10]. In 2009, the ULK-ATG13-FIP200 kinase complex was found to mediate

autophagy activation directly downstream of mTOR (mammalian TOR) signal[11]. Mizushima *et al* first discovered mammalian autophagosome formation occurred in a step-wise manner with the gradual expansion of the nascent autophagosomal membrane through tracking fluorescently labeled ATG5 in mouse embryonic stem cells[12]. In 2013, through delicately designed live-cell imaging experiments, his group was able to demonstrate the temporal hierarchy of mammalian ATG protein recruitment to the autophagosome, thereby providing a comprehensive picture of the autophagy pathway[13]. Currently, over 41 ATG genes have been identified, and further details of the autophagy signaling pathway continue to be uncovered. Ohsumi was awarded the 2016 Nobel Prize in Physiology or Medicine for his pioneering work on autophagy. Today, autophagy remains a hot topic of biological research as its implications in a variety of physiological conditions such as metabolism, cancer, and neurodegeneration are continually uncovered.

Key Proteins of Autophagy

Autophagy initiation

1. mTOR complex 1

The autophagy pathway is evolutionarily conserved from yeast to mammals and plays important roles in maintaining cellular homeostasis against environmental stressors[14]. Metabolic stress has been by far the most well-studied autophagy stressor, as evident by the success of nitrogen withdrawal as a selection factor for Ohsumi's pioneering 1993 yeast genetic screen in identifying autophagy proteins. Starvation-induced autophagy is primarily controlled by the mTOR complex. Two mTOR complexes exist in mammals, mTORC1 and mTORC2. mTORC1 is sensitive to nutrients while mTORC2 responds to

growth factor and PI3K signaling[15]. mTORC1 is a master regulator of eukaryotic cell growth and metabolism regulated by a variety of intracellular and environmental stresses such as nutrient starvation, hypoxia, or DNA damage[16]. mTORC1 consists of three core components: mTOR, Raptor (regulatory associated protein of mTOR), and mLST8 (mammalian lethal with Sec13 protein 8). mTOR is a member of the PIKK (phosphatidylinositol-kinase-related kinase) family of serine and threonine kinases[17]. Raptor functions as a scaffold protein recruiting canonical mTOR substrates such as S6K1 (p70S6 kinase) and 4EBP1 (eIF4E binding protein) to the complex through interacting with the TOS (TOR signaling) motif on the substrate proteins. Raptor also regulates the cellular localization of mTORC1[18]. Recent studies of mLST8 suggest it is dispensable for the critical role of mTORC1, although it has been described to promote mTORC1 catalytic functions[19]. Aside from these three core components, mTORC1 also associate with two inhibitory subunits PRAS40 (proline-rich Akt substrate of 40 kDa) and DEPTOR (DEP domain-containing mTOR interacting protein)[17].

mTORC1 kinase activity can be regulated by the energy state of the cell, specifically, through upstream factors such as insulin, growth factors and certain amino acids and their derivatives (Fig. 1)[20].

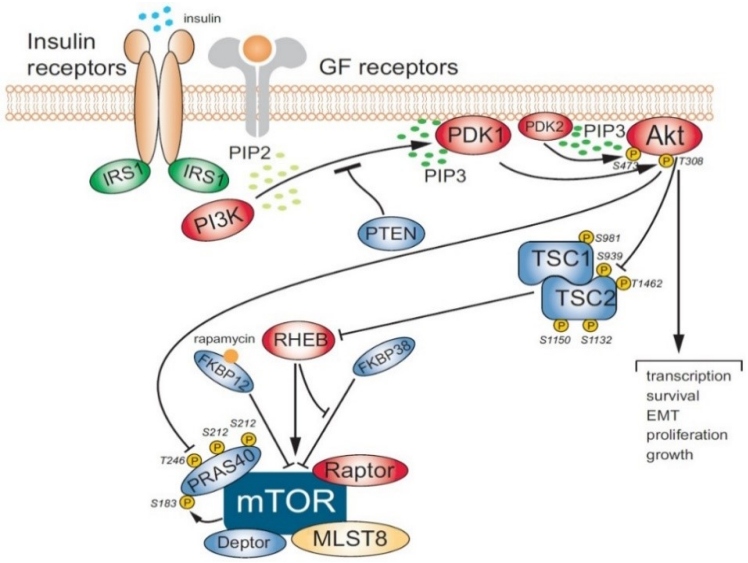

This figure was modified from figure 2 Tchevkina and Komelkov, 2012

Figure 1. mTORC activity is regulated primarily by insulin, growth factor, and amino acids[21]. *TSC is directly upstream of mTORC and is regulated by upstream signals, TSC activity negatively regulates the small GTPase Rheb that stimulates mTORC activity.*

mTORC1 is active under energy-rich states and is localized to the lysosomal membrane, which is required for its activation[22]. Synthetically tethered mTORC1 to the lysosomal membrane is constitutively activated regardless of the cellular nutrient levels, while disruption of mTORC1-lysosome interaction abrogates amino acid activation of mTORC1[23]. mTORC1 is also activated by the small GTPase Rheb, Rheb is sensitive to the change in GTP and GDP levels[24]. When GTP is available, Rheb works as a potent activator of mTORC1 kinase activity[23]. However, the exact mechanism of how Rheb stimulates mTORC1 kinase activity remains unclear.

Tuberous Sclerosis Complex (TSC) is a negative regulator of mTORC1 activity. TSC is a heterotrimeric complex consisting of TSC1, TSC2, and TBC1D7 (Tre2-Bub2-CDC16 (TBC) 1 domain family member 7)[25]. TSC2 possesses a GTPase activating protein (GAP) domain, which can convert Rheb from the GTP-bound active form to a GDP-bound

inactive form[25]. Signaling through several growth factors and mitogen-dependent pathways promotes Akt mediated phosphorylation of TSC2 on at least four serine and threonine residues[26]. Phosphorylated TSC dissociates from the lysosomal membrane, allowing GTP-bound Rheb to accumulate and promote mTORC1 activity[26].

mTORC1 is a master regulator of cellular anabolic and catabolic processes[17]. At times of nutrient stress, mTORC1 activity is inhibited and result in the activation of catabolic processes such as autophagy. In a nutrient-rich state, mTORC1 has important roles in promoting synthetic metabolic processes and cellular growth through activating cap-dependent translation, nucleotide synthesis, and lipid synthesis, while suppressing catabolic metabolism. Overall, mTORC1 activity regulates the cellular balance between anabolism and catabolism in response to a myriad of intrinsic and extrinsic environmental conditions[16].

2. ULK

The ULK (unc 51-like kinase) protein, also known as ATG1 in yeast, has two homologs in mammals, ULK1 and ULK2. The ULK1&2 complexes are the most upstream element of the autophagy pathway and are one of the first detectable proteins at nascent autophagosomes[13]. Unsurprisingly, their kinase activity is critical for autophagy initiation[27]. ULK1 and ULK2 have largely overlapping targets and roles in promoting autophagy[28] and are collectively referred to as ULK hereafter. Autophagic ULK complex consists of ULK itself serving as the catalytic component of the serine/threonine kinase, along with ATG13, FIP200 (or RB1CC1), and ATG101[11,29–32]. Binding of ULK with ATG13 or FIP200 has been shown to increase stability and subsequent kinase activity of ULK, along with ULK phosphorylation of FIP200. ATG101 associates with the ULK-ATG13-

FIP200 complex, possibly via direct interaction with ATG13[11], it has been shown to recruit downstream factors to the phagophore[30]. ULK complexes are potently inhibited through direct phosphorylation by the mammalian target of rapamycin complex 1 (mTORC1)[11,11,32]. Under stress, ULK is potently activated by the release of mTORC1 inhibition, phosphorylating downstream targets to promote autophagy [11,11,32](Fig. 2). Moreover, ULK is required for the recruitment of downstream ATG proteins that drive autophagosome biogenesis[28].

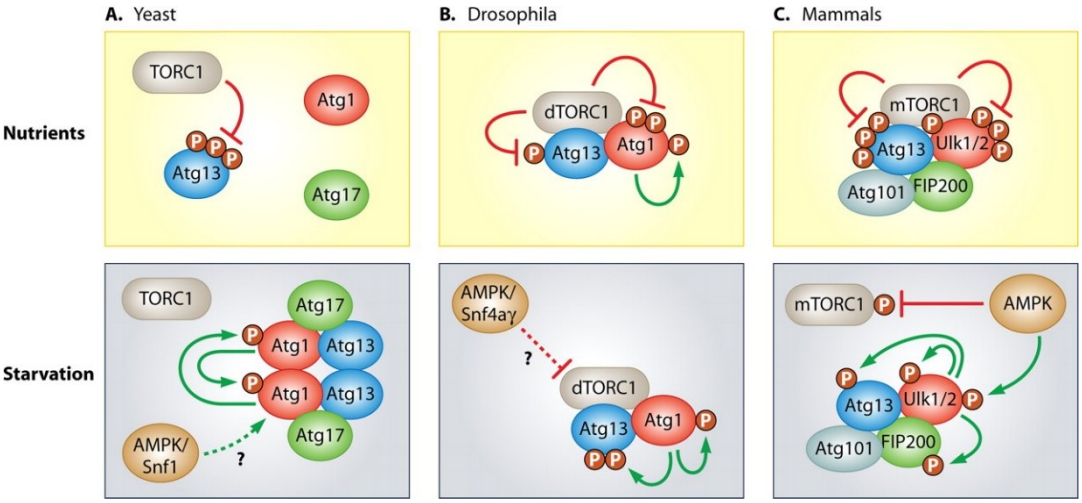

This figure was modified from figure 1 of Alers et al, 2011

Figure 2. TORC1 and ULK(Atg1) are highly conserved upstream regulators of autophagy from yeast to human[33]. *Under nutrient-rich states TORC1 activity suppresses ULK. During starvation, TORC1 is inhibited and ULK becomes active through both the loss of TORC1 inhibition and AMPK activation.*

Autophagosome Biogenesis

Autophagosome biogenesis refers to the formation process autophagosomes go through during autophagy[34]. Autophagosome formation begins as phagophores, which are small cytoplasmic crescent-shaped membrane structures with high degrees of membrane curvature. The origin of the membrane is unclear, with the ER, endosomes, and

mitochondria being the prime suspects. Autophagy proteins are recruited to the phagophore through attraction to its high membrane curvature and facilitate the elongation of the phagophore on both sides. As the nascent autophagosome grows, autophagic cargos are also transported to the inward-facing membrane during this step. Eventually, the nascent autophagosome grows to a mature autophagosome and fully encloses its content. It then fuses with the lysosome, allowing lysosomal acid hydrolases to begin breaking down the autophagic cargo (Fig. 3)[35]. 4 key protein/protein complexes are involved in the autophagosome formation process, including 1) the class iii phosphoinositide 3-kinase/VPS34 complex I, 2) two ubiquitin-like protein conjugation systems (ATG12–ATG5-ATG16L1 and MAP1LC3 (LC3), the mammalian ortholog of yeast ATG8), 3) WIPI proteins, and 4) transmembrane proteins ATG9 and VMP1[34].

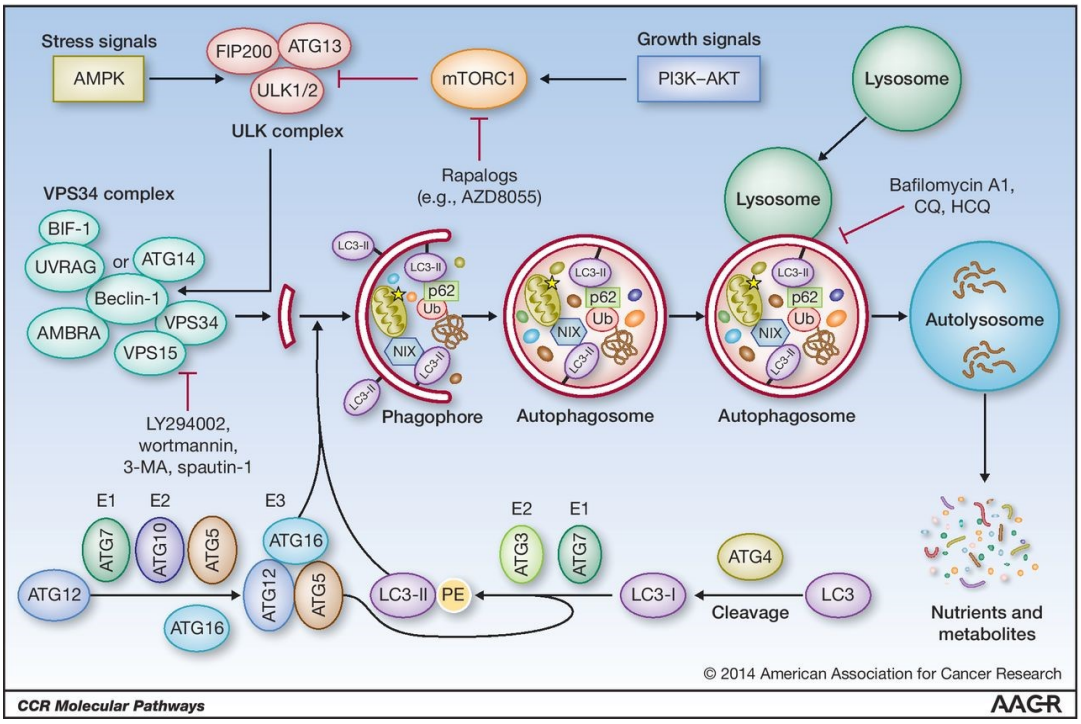

This figure was modified from figure 1 of Cicchini et al, 2014

Figure 3. Overall schematic of the autophagy pathway. Including the major ATG proteins involved in the autophagosome biogenesis process[35].

1. The Class III Phosphoinositide (PtdIns) 3-Kinase Complex/VPS34 Complex I

The VPS34 complex is involved in a variety of essential cellular functions in autophagy, endocytic trafficking, cytokinesis, phagocytosis, and nutrient sensing[36]. VPS34 is a member of the PtdIns 3-kinase family of lipid kinases and exists in several different complexes to regulate a wide range of cellular processes[36]. The VPS34 complexes associated with the autophagy pathway consist of: the catalytic subunit VPS34, the scaffold VPS15, and the regulatory beclin-1 (homolog of yeast Atg6), and either ATG14 or UVRAG subunits (Fig. 4)[38].

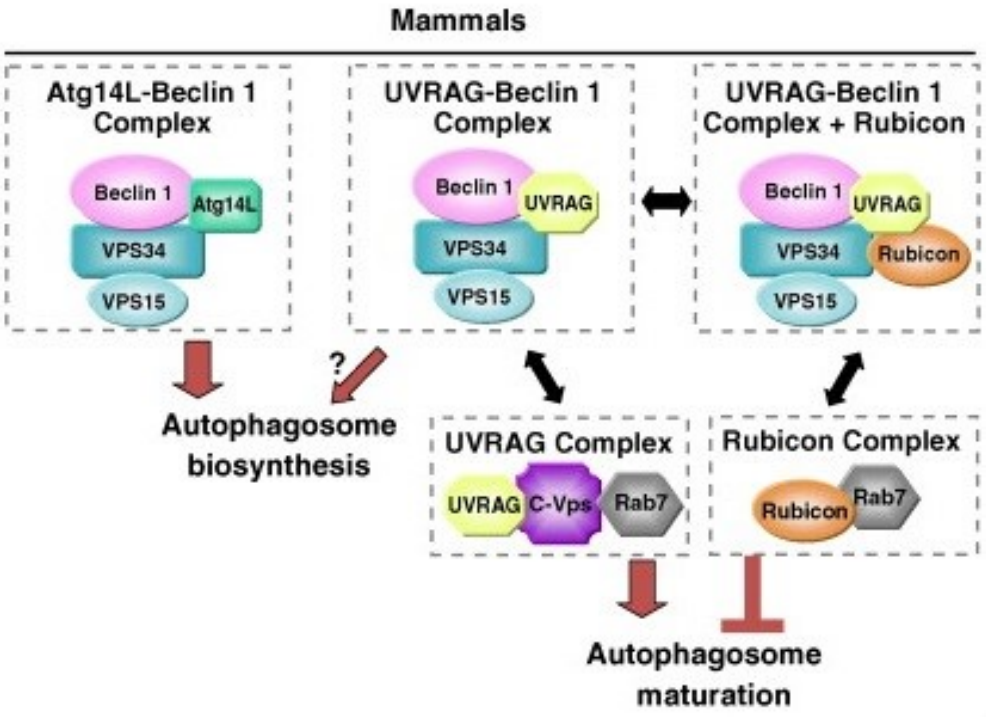

This figure was modified from figure 1B of Funderburk et al, 2010

Figure 4. Multiple types of VPS34 complexes exist in mammals[38]. ATG14L-containing VPS34 complex is the main form associated with autophagy. Non-VPS34 associated UVRAG complex promotes autophagy while non-VPS34 associated Rubicon complex inhibits autophagosome maturation.

Pro-autophagic VPS34 complexes are activated by nutrient starvation, through two upstream initiators ULK and AMPK[32]. Limitation of amino acids leads to mTORC1 inhibition and ULK activation, which then phosphorylates the catalytic subunit VPS34 on S249[39], the beclin-1 subunit on S14[40], the ATG14 subunit on S29[41], and AMBRA1 on unidentified sites[42]. Conversely, under glucose starvation AMPK is activated and directly phosphorylates beclin-1 on S90/93 (Fig 3)[43].

ULK and AMPK phosphorylation not only induce the lipid kinase activity of the VPS34 complex but also serve to recruit VPS34 to the nascent autophagosomal membrane. The active VPS34 then catalyzes the phosphorylation of phosphatidylinositol (PtdIns) to PtdIns-3-phosphate (PtdIns(3)P) on the autophagosomal membrane, which in turn recruits a class of PtdIns(3)P-binding proteins[44,45]. The PtdIns(3)P-binding proteins recruit downstream components of the autophagy pathway and are indispensable for the formation of the autophagosome[46]. Examples of functional classes of core ATG proteins are discussed in the following sections. In addition, the UVRAG subunit further promotes autophagy initiation by enhancing the interaction of beclin-1 with VPS34 and upregulates the activity of VPS34 complexes. UVRAG has also been described to facilitate autophagosome maturation via binding to the HOPS (homotypic fusion and vacuole protein sorting) complex and promoting lysosomal fusion with autophagosome (Fig. 4)[47].

Under nutrient-rich conditions, VPS34 activity is negatively regulated by mTORC1, Bcl-2, and Rubicon. mTORC1 directly phosphorylates VPS34 complex subunit ATG14[48], suggesting that the ATG14 subunit functions mediate the negative regulation of VPS34 complex by mTORC1. Indeed, in vitro incubation of VPS34-VPS15-Beclin 1 complexes with mTORC1 failed to inhibit the lipid kinase activity of VPS34[49]. Bcl-2 contains a

hydrophobic groove that interacts with the BH3 domain of beclin-1, which disrupts the beclin-1/VPS34 binding, reduces lipid kinase activity, and subsequently inhibits autophagy induction[50]. Bcl2-beclin1 interaction is disrupted upon stresses, which alleviates the inhibition of VPS34 activity[50]. Rubicon is another negative regulator of VPS34 acting to disrupt the UVRAG-HOPS interaction through binding to the UVRAG subunit of VPS34 complexes, resulting in decreased VPS34 lipid kinase activity (Fig. 4)[47]. The Rubicon-UVRAG interaction is further enhanced by mTORC1 directly phosphorylating UVRAG[49]. Taken together, VPS34 activity is tightly regulated by upstream nutrient sensors mTORC1, ULK, and AMPK. This ensures autophagy can be activated rapidly in response to cellular energy stresses and inhibited once energy homeostasis is restored.

2. Ubiquitin-like protein conjugation systems - ATG12–ATG5-ATG16L1 and MAP1LC3 (LC3)

Among all the ATG proteins characterized so far two, ATG12 and LC3 (mammalian homolog of ATG8), are structurally related to ubiquitin[48]. These two proteins each form a distinct ubiquitin-like conjugation system, which is critical for autophagosome biogenesis (Fig. 5)[51].

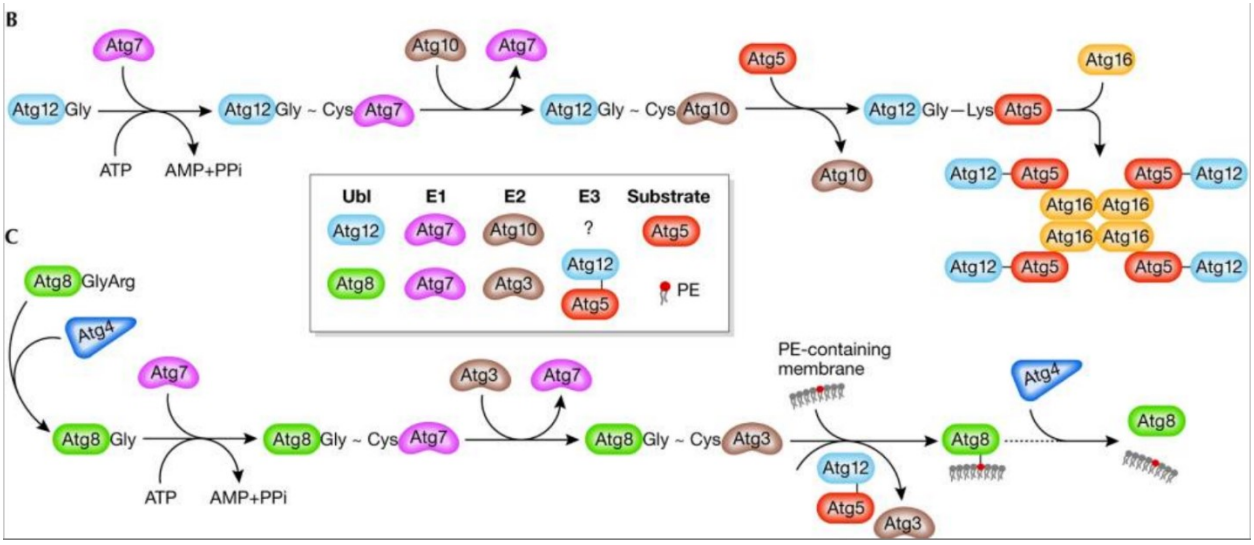

This figure was modified from figure 2 of Geng and Klionsky, 2008

Figure 5. Overview of the two ubiquitin-like conjugation systems of the autophagy pathway[51].

First, ATG12 is activated by the E1-like enzyme ATG7 through the formation of a thioester bond[53]. Active ATG12 is recruited to the E2-like enzyme ATG10, which results in ATG12 conjugation to its target protein ATG5[50]. The ATG12-ATG5 linkage produced is covalent, so ATG12 and ATG5 primarily exist in conjugated forms[50]. ATG5 interacts with the coiled-coil domain of ATG16L1, forming a trimeric ATG16L1-ATG5-ATG12 complex. The ATG16L1 complex serves as the E3-like enzyme in the LC3 ubiquitin-like conjugation chain and is essential for the expansion and formation of the autophagosomes through its function in LC3 lipidation (Fig. 6)[55,56].

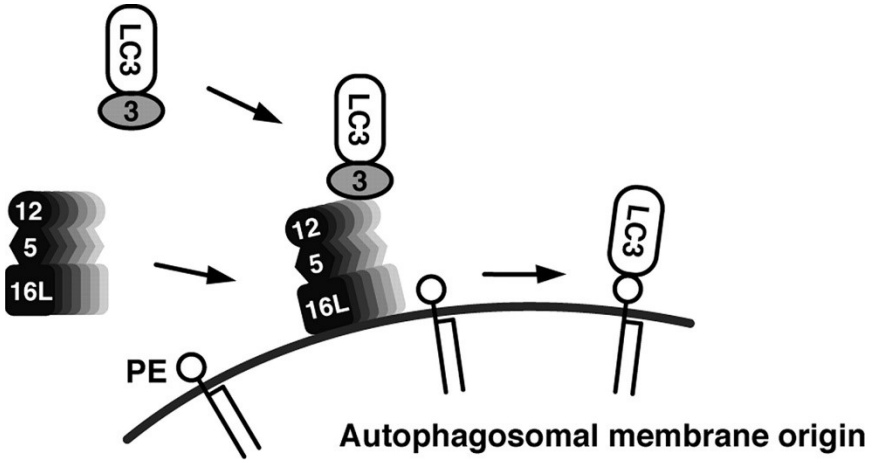

This figure was modified from figure 7 of Fujita et al, 2008

Figure 6. The dynamic localization model of LC3 lipidation[56]. *The E3-like ATG16L1-ATG5-ATG12 complex recruits LC3-I from ATG3 and conjugates LC3-I to PtdEth on the autophagosomal membrane.*

The second ubiquitin-like conjugation system processes the LC3 protein from its initial pro-LC3 form to the phosphatidylethanolamine (PtdEth)-conjugated form, this process is commonly referred to as LC3- lipidation[53]. First, the C-terminus of newly synthesized pro-LC3 is cleaved by the protease ATG4, producing the non-conjugated, ATG4-cleaved LC3 protein is known as LC3-I (Fig. 5). LC3-I is transferred to and activated by the E1-like enzyme ATG7[53]. ATG7 then transfers LC3-I to the E2-like enzyme ATG3, which then passes LC3-I onto the E3-like enzyme complex ATG16L1-ATG5-ATG12[57]. Each subunit of the trimeric ATG16L1-ATG5-ATG12 has a distinct function in the processing of LC3[52]. Collectively, ATG16-5-12 is required for linking LC3-I bound at ATG3 to PtdEth on the membrane. The ATG16L1 subunit is responsible for targeting the enzyme complex to autophagosomal membrane[58]. While the covalently linked ATG12-ATG5 promotes lipidation of LC3-I to phosphatidylethanolamine (PtdEth) present on the membrane of expanding autophagosomes (Fig. 6)[58,59]. The lipidated form of LC3 is now known as LC3-II. LC3 lipidation catalyzed by ATG16L1 complex is a critical rate-limiting step to the

autophagy pathway and therefore LC3 is the most commonly used marker for the measurement for autophagy induction as well as detection of autophagosomes[51]. Functionally, LC3-II is involved in cargo recognition and autophagosome maturation. LC3-II present on the autophagosomal membranes serves as docking sites for autophagy adaptor proteins carrying autophagic cargos (Fig. 3). This interaction is mediated by the LC3 interacting region (LIR) motifs found in the autophagy adaptor proteins[60] and allows the cargos to be sequestered by immature autophagosome as it continues to grow. There is also evidence suggesting LC3-II being involved in the closure of autophagosomes[61].

3. WIPI proteins

The WIPI (WD-repeat protein interacting with phosphoinositides) proteins are an evolutionarily conserved protein family consisting of four members (WIPI1 to WIPI4) along with their splice variants[58]. WIPI1 and WIPI2 have been shown to localize at the inner and outer membrane of autophagosomes. They are part of the aforementioned group of downstream autophagy effectors recruited to the nascent autophagosomal membrane through binding to PtdIns(3)P, specifically mediated through evolutionarily conserved WD repeat domains[62,63](Fig. 7). WIPI2 also binds the E3-like ATG16L1 complex through interactions of the WD repeat domains present on both proteins. These interactions allow WIPI2 to recruit the to the LC3 lipidation machinery to the phagophore site (Fig. 7)[63]. Thereby, linking VPS34-mediated PtdIns(3)P production to LC3 lipidation and autophagosome formation.

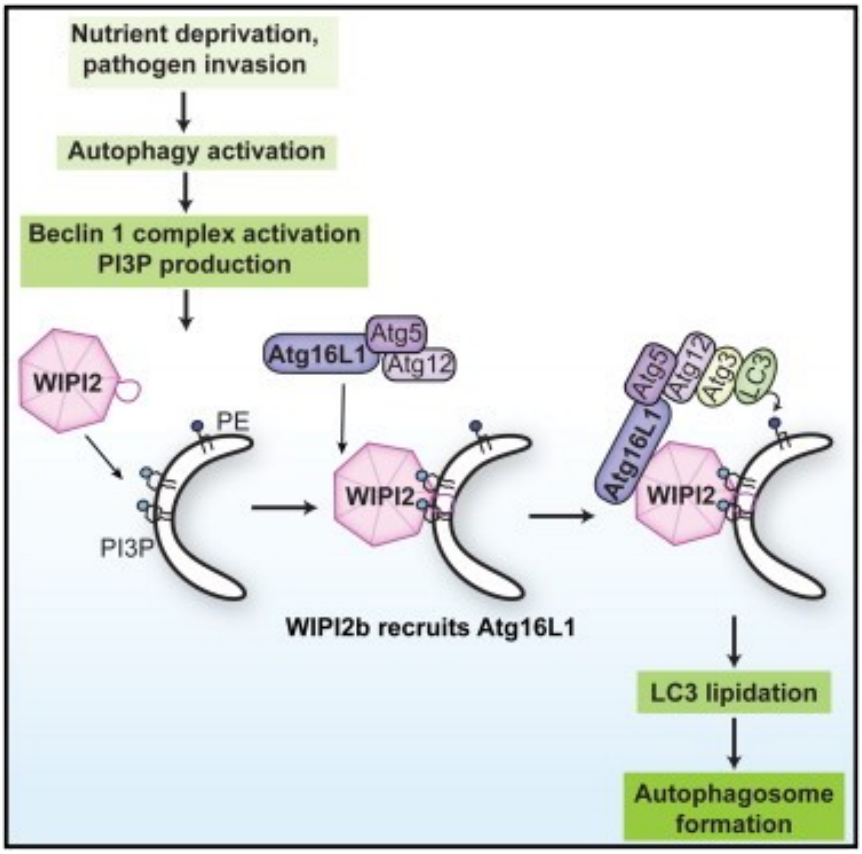

This figure was modified from the graphical abstract of Dooley et al, 2014

Figure 7. WIPI2 binds to PI3P marked phagophore membrane and subsequently recruits the ATG16L1 complex to conjugate LC3-I onto the phagophore membrane[63].

Transmembrane Autophagy Proteins

Two transmembrane proteins, ATG9 and VMP1, are required for the proper functioning of the autophagy pathway[64]. Under cellular energy stress, ATG9 translocates from its locations in the Golgi network and late endosomes to peripheral sites overlapping with LC3-positive autophagosomes[65]. The starvation-mediated cycling of ATG9 is dependent on both ULK and VPS34 complex activity[66,67]. ATG9 cycling has been shown to regulate membrane delivery from potential sources such as the ER membrane to the nascent

autophagosome[68] and continues to be a widely studied protein in the ongoing efforts to locate the primary source of autophagosome membranes.

VMP1 is an ER transmembrane protein that has recently emerged as a key player in the early autophagy pathway. Unlike most ATG proteins, VMP1 is only present in high eukaryotes. It was found to be indispensable for mammalian autophagy. Overexpression of VMP1 was shown to promote autophagy even under nutrient-rich conditions[69–71]. Its autophagy involvement includes binding to the VPS34 complex subunit beclin-1, possibly regulating the transfer of membrane material from the ER to nascent autophagosomes (Fig. 8)[72,73]. Additionally, a recent study identified TP53INP2 as a novel VMP1-binding protein involved in recruiting beclin-1 and LC3 to autophagosomal sites, potentially via its interaction with VMP1[74]. In summary, a role for VMP1 is emerging in the recruitment of both membrane components and downstream autophagy effectors to the phagophore.

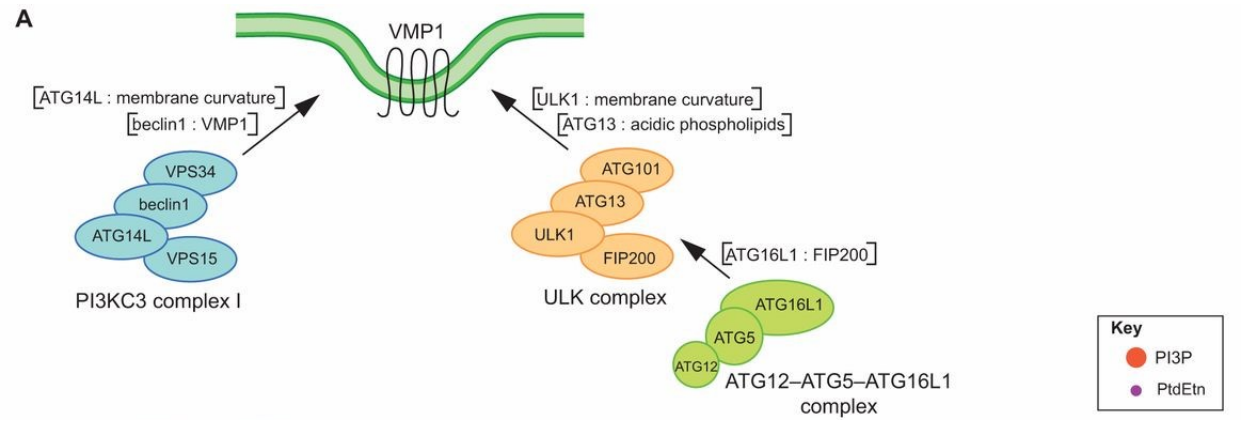

This figure was modified from figure 2A of Carlsson and Simonsen, 2015

Figure 8. VMP1 recruits VPS34 complex through binding with Beclin-1 and creates membrane curvature which facilitates recruitment of ATG14L and ULK1[72].

Autophagy and human health

As autophagy research rapidly expanded over the past two decades, the impact of autophagy on human health and disease has become a focal point of study. Multiple conditions including cancer, neurodegeneration, cardiovascular diseases and autoimmune disorders have been linked with autophagy defects[75]. Understanding the role of autophagy in the pathogenesis of these diseases is therefore highly valuable in contributing to the search for therapeutic solutions.

1. Cancer

The genetic link between cancer and autophagy was first discovered in 2003 by Beth Levine's laboratory. Their research demonstrated beclin-1 as a conserved essential autophagy gene and a haploinsufficient tumour suppressor[76]. The beclin-1+/- mutant mice used in the experiment displayed high incidences of spontaneous tumours. Analysis of beclin-1 mRNA and protein levels of the tumour cells showed wild-type expression of beclin-1, confirming the fact that it is a haploinsufficient tumour suppressor. Similarly, ATG4C deficient mice were also found to have had an increased rate of tumour growth by another group[77]. Together, these studies highlight the tumour-suppressing ability of autophagy.

Conversely, autophagy has also been found to enhance tumour growth in advanced stage cancers. In the central part of solid tumours, tumour cells often suffer from stressful growth conditions such as hypoxia and nutrient deprivation. Autophagy can fulfill the metabolic demands of these tumour cells through the production of nutrients from the breakdown of macromolecules[78]. Contrary to the case of beclin-1 +/- mice, the deletion of beclin-1 has been shown to promote death of cancer cells with impaired apoptotic response under

metabolic stress[79]. The apparent paradox can be explained by considering different stages of tumourigenesis and potential defects in apoptosis. Defective autophagy produces cells with cytotoxic components such as damaged mitochondria and protein aggregates. Without proper function of apoptosis, these cells would eventually develop DNA damage and become oncogenic[1]. Therefore, autophagy likely prevents cancer in pre-cancerous environments. However, it can become oncogenic in assisting in cancer cell survival upon stress after key DNA mutations have been acquired and the tumour increases in size.

2. Neurodegenerative disease

One of the hallmark pathological events in neurodegenerative diseases is the aggregation of misfolded proteins in neuronal cells[80]. Since autophagy is a critical intracellular mechanism for removing protein aggregates, it has unsurprisingly been implicated in several neurodegenerative diseases [81]. One such example is Huntington's disease (HD), a neurodegenerative disease caused by the accumulation of the Huntington protein (Htt), resulting in gradual neuronal cell death with age[82]. Simply inhibiting mTOR activity to induce autophagy was shown to be protective against neurodegeneration in fly and mice models[83]. Study on a potential Huntington drug CTEP (2-chloro-4-[2-[2,5-dimethyl1-[4-(trifluoromethoxy)phenyl]imidazol-4-yl]ethynyl]pyridine) revealed treatment led to decrease in Htt protein aggregate burden in a transgenic mice Huntington model strain, along with increased motor function and autophagy activation[84]. CTEP is able to inhibit the metabotropic glutamate receptor 5 (mGluR5) resulting in the activation of autophagy through a GSK3b and ZBTB16-related pathway, the inhibition of mGluR5 lead to the removal of inhibitory phosphorylation on GSK3b and loss of ZBTB16 stability. ZBTB16 is

a component of an E3 ubiquitin ligase that regulated ATG14 degradation[84]. Therefore, CTEP treatment promoted autophagy through the stabilization of ATG14. Also, as mGLuR5 phosphorylation of ULK suppresses its activity. CTEP treatment also promoted ULK activity as evidenced by the observed increase of ATG13 phosphorylation (a product of ULK activity) and beclin-1 protein levels. Generally speaking, activation of autophagy has been found to be beneficial in nearly all neurodegenerative diseases[85,86] and much emphasis has been put on developing autophagy-activating pharmaceutical solutions as a treatment method for these diseases.

3. Cardiovascular diseases

Defects of autophagy regulation have been observed in cardiovascular diseases such as cardiomyopathies, cardiac hypertrophy, ischemic heart disease, and heart failure[87]. Upregulation of autophagy is observed in failing hearts as a coping mechanism for cardiac stress[88]. Cardiac-specific ATG5-deficient mice have shown defects in left ventricular dilatation and contraction, cardiac hypertrophy, and increased levels of ubiquitinated proteins in cardiac tissues[88]. At a subcellular level, ATG5 deficiency produced abnormal sarcomere structure, mitochondrial misalignment and aggregation[88]. In summary, there is a baseline level of cardiac autophagy that serves to maintain cardiac health and proper function, and disruptions in basal cardiac autophagy can lead to the development of cardiovascular defects.

4. Immune system

Xenophagy, a specific form of autophagy targeting invading pathogens, is an innate defense mechanism of eukaryotic cells against intracellular pathogens[1]. A variety of cell-invading bacteria have been shown to be targeted by xenophagy, including pathogenic

species in humans such as *Listeria monocytogenes*, *Salmonella enterica*, *Shigella flexneri*, *Toxoplasma gondii*, *Streptococcus pyogenes*, and *Mycobacterium tuberculosis*[89–94]. Xenophagy selectively targets invading pathogens through specific autophagic adaptor proteins, for example, the human autophagy adaptor protein NDP52 has been shown to target ubiquitinated *Salmonella* and facilitate its capture by autophagosomes[90]. In addition to innate immunity, autophagy has also been observed to promote adaptive immune response through facilitating efficient MHC class I and II presentation of viral antigens[95,96].

Defects in autophagy have been linked to the onset of inflammatory bowel diseases where the residential microbiota is a major contributing factor. Crohn's disease (CD) is a chronic inflammatory bowel disease typically affecting multiple separate segments of the gastrointestinal tract, with highly heterogeneous symptoms profiles[97]. Both genetic and environmental factors are believed to be involved in the development of CD[98]. Genome-wide association studies have identified several autophagy-related genes as high susceptibility regions of CD onset, including proteins involved in the xenophagy pathway such as ATG16L1, IRGM and NOD2[99]. A particular SNP of ATG16L1 resulting in a substitution mutation of the 300th threonine to alanine has been identified to be susceptible to CD development[100]. This CD-associated ATG16L1 is susceptible to caspase-mediated cleavage[101–103], which directly inhibits autophagic activity as ATG16L1 is an essential autophagy gene. The inhibition of autophagy leads to upregulation of local inflammatory response in the gut environment, which likely contributes to the development of CD[104–106]. The example of this specific ATG16L1 mutation demonstrates

the profound effect of autophagy in maintaining homeostasis of the bacteria-rich gut environment.

Existing Methods for Monitoring Autophagy

1. Electron microscopy

Autophagy was first observed by transmission electron microscopy (TEM) in the 1950s. Today, while not the most commonly used method to measure autophagy, TEM remains as a gold standard for detecting autophagic activity in cell culture or tissue samples[6]. The value of TEM as a research tool in autophagy comes from the fact that it is the sole method to be able to not only visualize autophagosomes but also membrane structures at different stages of the autophagosome biogenesis process, all down to nanometer levels of resolution[6] (Fig. 9). TEM also allows researchers to directly observe the types of cargos captured in the autophagosomes, with notable examples being mitochondria and intracellular bacteria. Finally, quantitative analysis with TEM is also possible given that the data were recorded in accordance with the proper sampling rules.

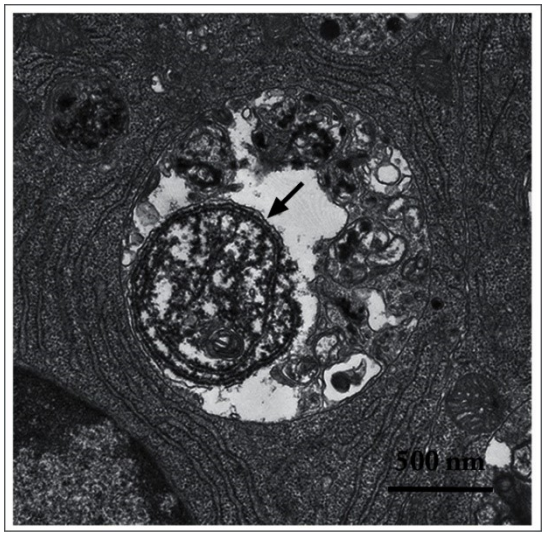

This figure was modified from figure 2 of Klionsky et al, 2016

Figure 9. TEM provides direct visualization of autophagosomes[6]**.** *An autophagic body in a large lysosome of a mouse epithelial cell from a seminal vesicle in vitro. The arrow shows the single limiting membrane covering the sequestered rough ER.*

It is also possible to investigate a specific protein of interest through immunogold EM, which utilizes gold particle conjugated antibodies to label and visualizes antigens in TEM images. Immuno-EM is especially useful for identifying protein localization on high specific structures difficult to decipher in other imaging techniques, such as the phagophore membrane. LC3 immunogold labeling can also uncover novel degradative organelles within autophagy compartments. It has led to the discovery of the autophagoproteasome[107], where LC3 and ubiquitin-proteasome system (UPS) antigens were co-stained.

Despite being able to reliably verify autophagic activity and providing a highly detailed view of the process, TEM is not often used by researchers examining autophagy due to a few significant drawbacks. The primary concern is the difficulty and length of sample

preparation, where technical expertise is required at all stages of the process in order to obtain quality data[6]. Even after this is achieved, data analysis to properly identify autophagic structures also requires lots of experience and can be very time-consuming, as many membranous vesicles have appearances similar to autophagosomes. The difficulties and amounts of time required for data analysis also make large scale experimental designs impractical. In summary, TEM is a powerful tool to detect autophagic activity; however, its static nature fails to relay much about the rate of autophagy. Technical constraints further limit its use to specific experimental designs. Therefore, it is best employed in combination with additional autophagy assays.

2. LC3-based assays

The LC3 protein is by far the most widely used marker for monitoring autophagic activity. The human LC3/GABARAP family contains 6 members that are all homologs of the yeast ATG8. Among them, LC3B is the most studied and is the isoform most commonly used in nearly all autophagy assays[9,108]. Many different types of experimental assays have been developed based on LC3B[109]. Here we mainly focus on two types of LC3-based autophagy assays 1) Visualization of LC3B in immunofluorescent microscopy and 2) LC3-I/II ratio and turnover in Western blots.

Fluorescence microscopy imaging of either GFP-tagged or immunolabeled LC3B can readily detect increases in autophagy activity in the form of increased number LC3B punctate structures, where the puncta are generally assumed to each represent a single autophagic vesicle (Fig. 10)[9].

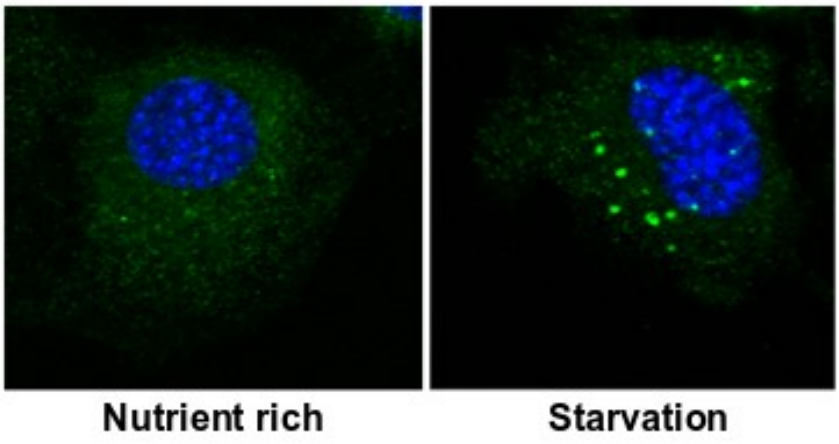

Figure 10. IF images of mouse embryonic fibroblasts under nutrient rich or starvation conditions. LC3 (green) and DNA (blue) are stained. (Unpublished, Ryan Russell lab)

The use of GFP-LC3B is especially popular in *in vivo* studies involving live imaging of either transgenic organisms (e.g. *C. elegans, D. melanogaster*) or cells expressing the GFP-LC3B transgene[9,110,111]. These live-imaging experiments are especially valuable in uncovering dynamic changes in the autophagy pathway, as the movements of each vesicle can be tracked and analyzed over time[112]. In conventional fluorescent imaging of fixed samples, autophagosomal LC3B appears as distinct puncta, thereby providing a relatively easy tool for quantification of autophagosomes[6]. Staining of LC3B puncta can also assist in highlighting the autophagic capture of any specific cargo of interest or pathogen in multi-stained samples through observing colocalizations of the cargo protein of interest to LC3[113–115]. An especially useful reporter assay developed for fluorescent microscopy is the mCherry-GFP-LC3B reporter system[116]. It takes advantage of the difference in pH sensitivity between mCherry and GFP proteins to differentiate autophagosomes from autolysosomes. In short, GFP is sensitive to the acidic pH of the

lysosome and will lose fluorescence rapidly in the autolysosome. However, the fluorescence of mCherry is consistent in the lysosome or autophagosomal pH, leading autophagosomes to appear as dual positives (GFP and mCherry) and autolysosomes to appear as single mCherry positive puncta. By comparing the number of autophagosomes to autolysosomes, researchers can infer the rate of ongoing autophagy in a particular sample. The mCherry-GFP-LC3B reporter system also allows differentiation of an actual increase in autophagy, versus blockage of autophagosome turnover, which would both appear as merely an increase in the number of LC3 puncta without the mCherry-GFP reporter system.

Another common laboratory LC3B-based autophagy assay is western blotting. This is due to the convenient fact that lipidated LC3B at the autophagosomal membrane has increased mobility on SDS-PAGE and can easily be distinguished by western blot (Fig. 11)[6]. The ability to measure autophagosome abundance through lipidated LC3B (hereafter referred to as LC3B-II) in a variety of commonly used assays has resulted in the inclusion of LC3B-II measurement in the majority of studies on the autophagy pathway[109]. However, analysis of the autophagy pathway using LC3B-II must be performed carefully as decreases in or blockages of autophagosome clearance rate often result in increased LC3B-II levels, which incorrectly infers an elevation of autophagy rates[109]. Conversely, under stress conditions rapidly turned-over LC3B-II sometimes fails to accumulate, thereby masking increased autophagy rates[109]. To overcome these obstacles, LC3B-II analysis is often done in the presence of pharmacological inhibition of the lysosomal pathway to control for autophagosome clearance rates (Fig. 11)[109]. However, the use of such drugs can be impractical *in vivo*, or introduce confounding

effects including mTORC1-inactivation if used for an extended duration *in vitro*. Despite these limitations, LC3B-II analysis has acted as the backbone of autophagy research for several years.

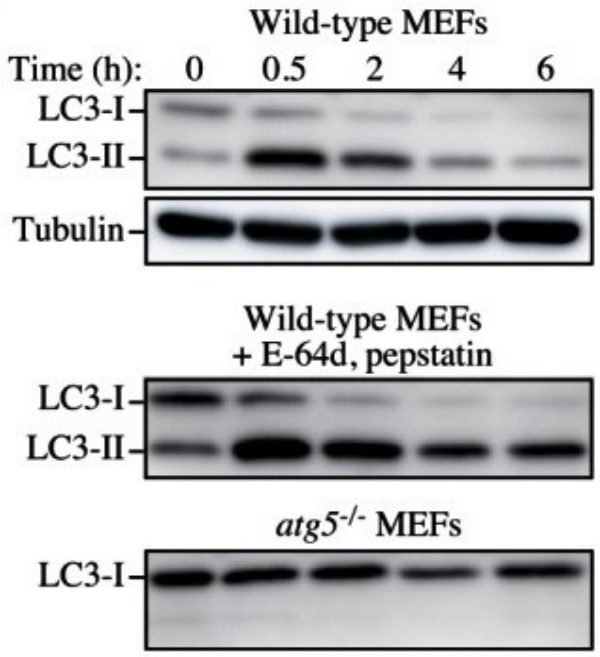

This figure was modified from figure 6A of Klionsky et al, 2016

Figure 11. Western blot analysis of LC3 lipidation[6]. *Cells were subjected under amino acid and serum starvation for the indicated time. E-64d (10 μg/ml) and pepstatin A (10 μg/ml) were added to the medium where indicated.*

3. Autophagy adaptor proteins

Analysis of autophagy adaptor clearance is another common approach to examine autophagy rates[6]. Autophagy adaptors recruit specific cargo to the interior face of the autophagosomal membrane, as a result, they are degraded along with the cargo upon the fusion of the autophagosome to the lysosome. The adaptors are recruited to LC3B in the expanding autophagosome through LIR domains[6]. The best-characterized autophagy adaptor is p62 (also known as sequestosome-1), which binds ubiquitinated

substrates and loads them into the lumen of the autophagosome[117]. p62 is rapidly cleared in response to several stressors[6], and clearance of p62 or other autophagy adaptors is indicative of an increase in autophagy flux (Fig. 12). Notably, autophagy analysis using p62 or other autophagy adaptors comes with important caveats: 1) p62 is transcriptionally regulated by stress[118,119] and in disease states[120,121], which can affect protein levels independently of autophagy flux; 2) different stressors can preferentially utilize specific autophagy adaptors[122–124], which can be problematic if the adaptor is not known or chosen *a priori*; and 3) after an initial decrease, the protein levels of autophagy adaptors remain relatively constant under continued stress and provide limited information about sustained rates of autophagy. Despite these limitations, the analysis of autophagy adaptors has been proven to be a very useful tool for autophagy researchers and is most commonly used in conjunction with LC3B-II analysis.

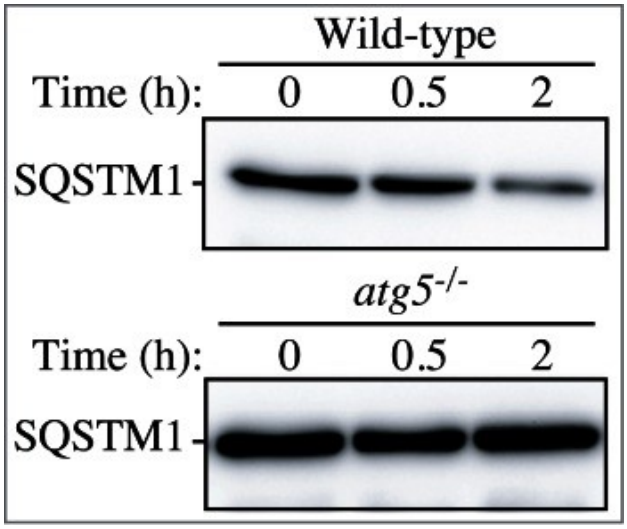

This figure was modified from figure 15 of Klionsky et al, 2016

Figure 12. p62 (SQSTM1) is readily degraded after amino acid and serum starvation[6]. *Numbers indicate the length of starvation. This degradation is autophagy dependent, as p62 levels in ATG5 null cells did not decrease under the same conditions.*

Preliminary data and rationale for the study

Previous reports have shown that FIP200, an essential cofactor for ULK-kinase activity, can bind to ATG16L1[125,126]. This binding has been reported to affect ATG16L1 localization and requires amino acids 229-242 of ATG16L1, which are not phosphorylated by ULK[127]. This implicates that FIP200 may recruit ATG16L1 to ULK-containing complexes thereby promoting ATG16L1 phosphorylation. A series of *in vitro* kinase assays with recombinant ATG16L1 proteins from an earlier project in our lab demonstrated that ULK phosphorylates ATG16L1 on S278[127](Fig. 13).

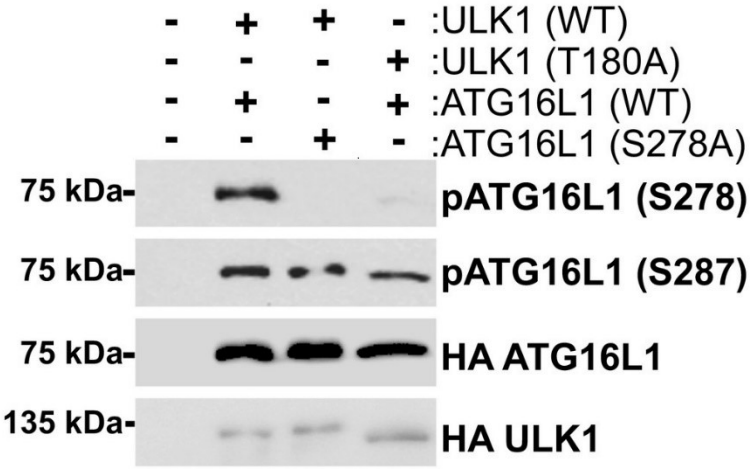

This figure was modified from figure 1E of Alsaadi et al, 2019

Figure 13. ULK phosphorylates ATG16L1 on serine residue 278[127]. *HEK293A cells were transfected with wild-type or phospho-dead ATG16L1 in the presence of wild-type or kinase-dead ULK1. Phosphorylation of ATG16L1 (S278 or S287) and inputs were examined by WB.*

As a follow up to this discovery, we recently identified a stress-sensitive signaling event that may be tied to newly forming autophagosomes. We showed that both ULK1 and

ULK2 phosphorylate the ATG16L1 subunit of the LC3B-lipidating enzyme in response to starvation (Fig. 14) and *Salmonella* infection at a conserved serine (S278).

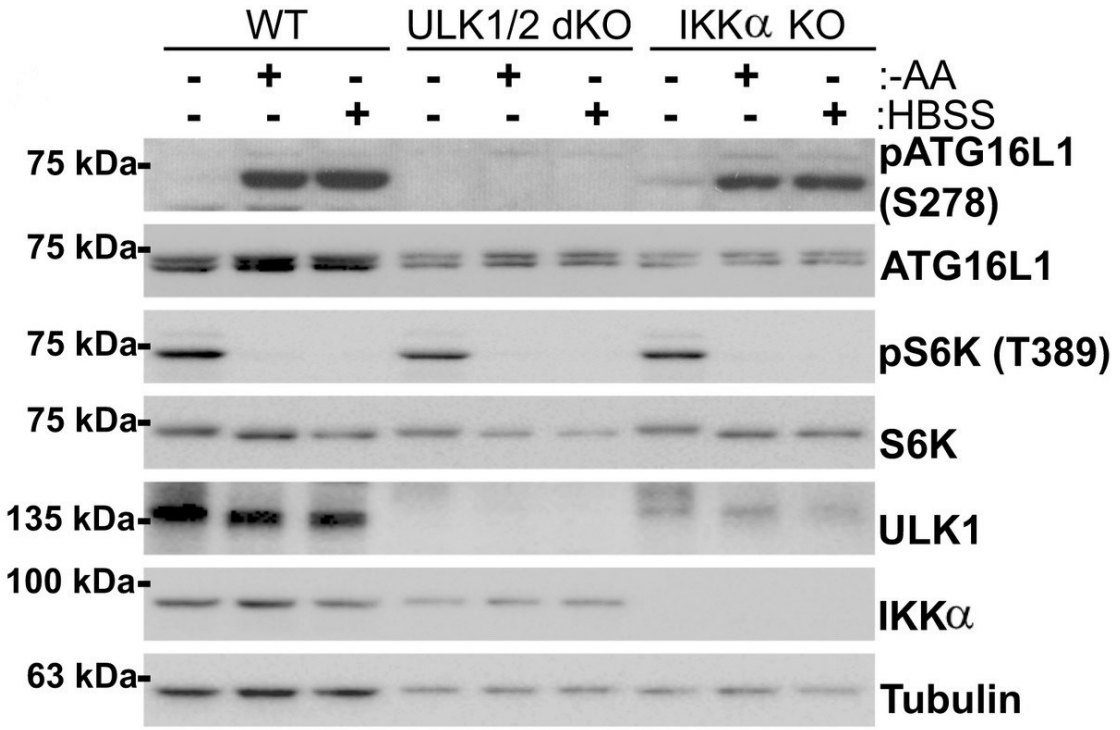

This figure was modified from figure 2A of Alsaadi et al, 2019

Figure 14. ULK-mediated ATG16L1 Ser278 phosphorylation is stimulated by starvation[127]. *Wild-type, ULK1/2 double-knockout (dKO) or IKKα KO mouse embryonic fibroblasts (MEFs) cells were incubated with either complete medium, amino acid-deficient DMEM or HBSS for 1 h. Samples were immunoblotted using the indicated antibodies.*

This may represent an essential signaling event in autophagosome formation. Indeed, ATG16L1 and ULK are essential for autophagy initiation in nearly all conditions, unlike individual members of LC3/GABARAP family or autophagy adaptors that have divergent or overlapping roles. Therefore, the newly discovered mechanistic link between ULK and the LC3-lipidating machinery may represent a common signaling event that is stimulated upon autophagy induction, regardless of the stress or cargo. In other words, this signaling

event could serve as a new marker for autophagy induction, which is compatible with multiple types of autophagy-inducing stressors and without the known caveats of LC3 or autophagy adaptor-based methods. Under this guiding rationale, we proposed to develop and characterize a novel method to monitor autophagy based on measuring ULK-mediated ATG16L1 phosphorylation. This method would retain the beneficial qualities of LC3B and autophagy adaptor-based methods in their ease of use and the availability of high-quality reagents that can be applied to multiple assays. Additionally, this method would also be more specifically tied to autophagosome formation itself, rendering it insensitive to the accumulation of dysfunctional autophagosomes or skewing by the duration of autophagy activation. To achieve this goal, we partnered with Abcam to develop a monoclonal antibody capable of detecting ATG16L1 phosphorylation on serine 278. After two years of development involving multiple rounds of hybridoma fusions and clonal screens, we successfully produced a monoclonal antibody capable of specifically detecting endogenous levels of the phospho-protein. This high-quality antibody enabled us to characterize our hypothesized new readout of autophagy measurement based on detecting ATG16L1 phosphorylation

Results

Phosphorylation of ATG16L1 is a conserved indicator of autophagy induction, which is activated by multiple stimuli

In the aforementioned past study from our lab, phosphorylation of ATG16L1 has been described following bacterial infection and shown to play a role in the defects related to Crohn's-associated mutations of ATG16L1[104,127]. Yet, the regulation of ATG16L1 phosphorylation in bulk autophagy remains unclear. IKKα has been shown to phosphorylate ATG16L1 in *in vitro* kinase assay at serine 278 (S278), but we determined that endogenously ULK, not IKKα, is the kinase responsible for ATG16L1 phosphorylation at this specific residue[127] (Fig. 14). To further study this phosphorylation, we developed a monoclonal antibody from rabbit hybridomas, which was specific against ATG16L1 phosphorylated at S278 (hereafter referred to as pATG16L1^{s278}). To test the specificity of our phospho-antibody and its ability to recognize endogenous pATG16L1^{s278}, we first created an ATG16L1 knockout (KO) HCT116 cell line using CRIPSR/Cas9 genomic editing via disruption of the first exon of ATG16L1[127]. Using these KO cells, we next tested the specificity of pATG16L1 ^{s278} detection in response to amino acid starvation, a well-established inducer of autophagy. Wildtype (WT) and ATG16L1 KO cells were treated in the presence or absence of amino acids, to relieve mTORC1-mediated repression of the autophagy pathway, and whole cell lysates were analyzed by western blot (Fig. 15A). We found phosphorylation of ATG16L1 was stimulated by amino acid withdrawal and could be detected by our monoclonal antibody endogenously in whole cell lysates (Fig. 15A). However, no signal was observed in ATG16L1 KO cells. To confirm the specificity of our antibody we reconstituted ATG16L1 KO cells with ATG16L1 (WT or

S278A mutant) and analyzed pATG16L1^{s278} under amino acid starvation. As expected, we observed that our pATG16L1 antibody specifically recognized WT and not the S278A mutant of ATG16L1 (Fig. 16A). Inhibition of ULK kinase through deletion of FIP200, a necessary cofactor of ULK1 and ULK2 kinase complexes, resulted in a complete abrogation in pATG16L1^{s278}-induction (Fig. 16B). Together, these data demonstrate that this monoclonal antibody is highly specific for ULK-mediated ATG16L1 phosphorylation on S278.

We next sought to determine whether ATG16L1 phosphorylation is induced by common stressors known to induce autophagy. We observed clear increases in ATG16L1 phosphorylation in response to *i)* catalytic inhibition of mTOR, *ii)* glucose withdrawal, *iii)* cytokine depletion, *iv)* reactive oxygen species, and *v)* mitochondrial decoupling (Figs. 15B and 16C-D). These stimuli add to amino acid withdrawal and infection that we identified previously[127]. The increase in pATG16L1^{s278} levels also correlated with autophagy induction, which was confirmed by reduction of p62 levels, and by concomitant increase in LC3B lipidation (Fig. 15B). Conversely, we also sought to determine whether ATG16L1 phosphorylation can be blocked by disruption of key upstream autophagic proteins involved in autophagy initiation. We first tested the effects of ATG5 and ATG7 knockouts on ATG16L1 phosphorylation. However we have determined that knocking out either of these two genes resulted in a dramatic destabilization of total ATG16L1 protein (Fig. 16E). We decided to target another protein upstream of the E3 enzyme and tried to inhibit VPS34 function by treating cells with a VPS34 inhibitor, since VPS34 knockout is lethal. We observed that inhibition of VPS34 ablated both starvation induced autophagy and ATG16L1 phosphorylation (Fig. 16F). The consistency with which ATG16L1

phosphorylation was detected in numerous conditions leading to autophagy induction, and its absence under early autophagy blockage indicate detection of endogenous pATG16L1^{s278} as a reliable marker of stress-induced autophagy by western blot and lead us to further characterize pATG16L1^{s278} detection as a proxy for mammalian autophagy induction. Another promising aspect of this antibody was that it was generated from a highly-conserved region of ATG16L1 (Fig. 15C), which should allow it to cross-react with most of the frequently used cell lines/organisms in autophagy research. To confirm the cross-species reactivity and cell type specificity of our antibody, we starved 8 cell lines from 5 different species (human, monkey, rat, mouse, and dog) and 6 different tissue types (uteral, retinal, renal, embryonic fibroblast, neuronal, and skeletal muscle). In all samples, we observed an increase in endogenous pATG16L1^{s278} levels under stress (Fig. 16G). Taken together, our data indicate detection of endogenous pATG16L1 as a reliable marker of stress-induced autophagy by western blot.

Figure 15

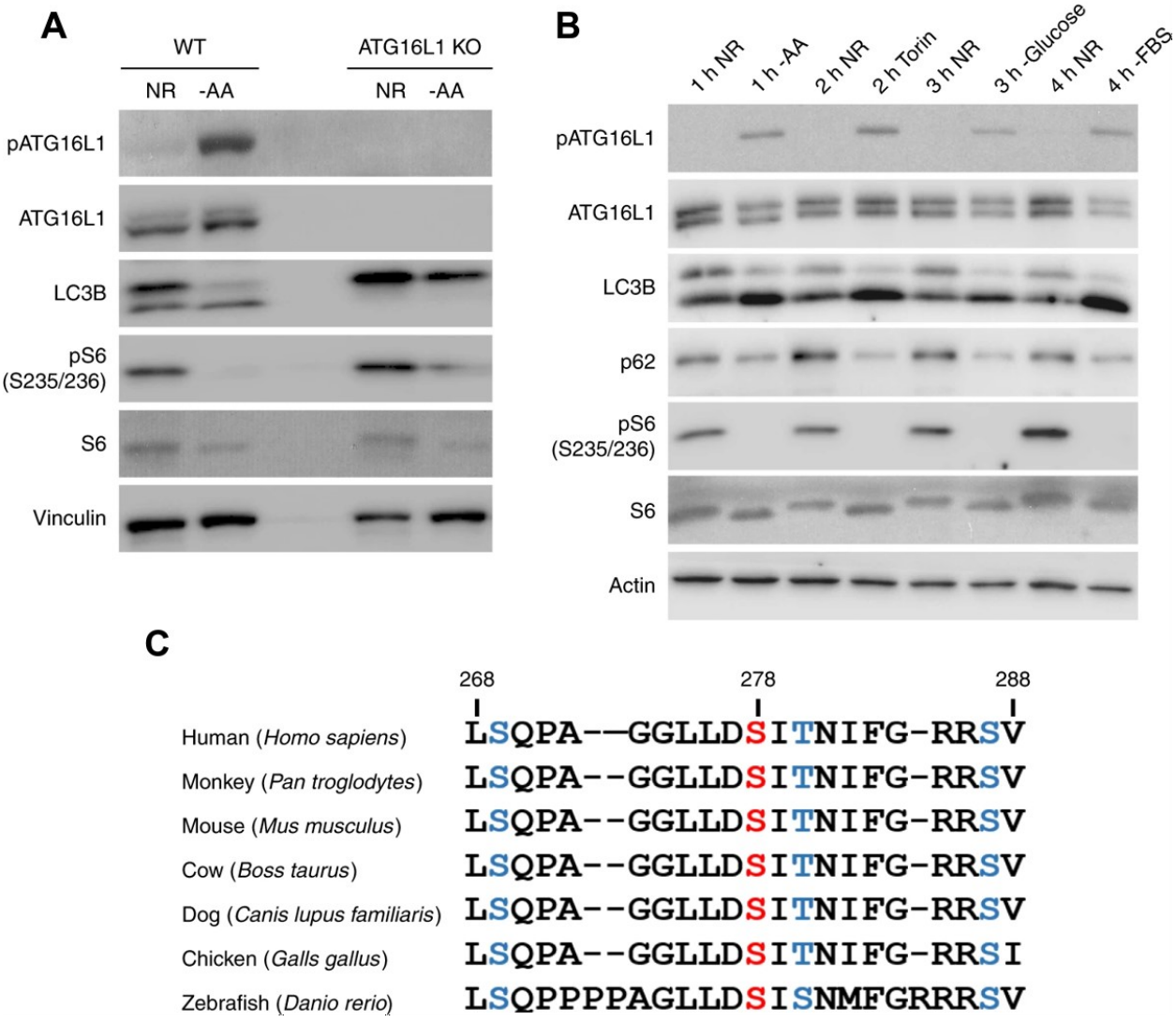

Figure 155. Phosphorylation of ATG16L1 is a conserved indicator of autophagy induction, which is activated by multiple stimuli *(**A**) Wild-type and ATG16L1 KO HCT116 cells were kept in nutrient rich complete media (NR) or starved with DMEM deficient in amino acids (-AA) for 3 hours. Cell lysates were resolved by SDS-PAGE and immunoblotted using the indicated antibodies. S6 phosphorylation was measured as a readout of mTORC1 activity. An empty lane demarcates WT and KO cell lines. (**B**) Q7 mouse brain striatal cells were incubated with either: complete media; amino acid deficient DMEM; complete media containing 200nM Torin-1 (Torin); DMEM without glucose (-glucose); DMEM without serum (-FBS) for the duration stated. Cell lysates were resolved by SDS-PAGE and immunoblotted using the indicated antibodies. (**C**) Amino acid sequence proximal to serine 278 of human ATG16L1 aligned to indicated species displaying high degree of conservation. The 278 serine residue is marked in red. Additional conserved serine and threonine residues are marked in blue.*

Figure 16

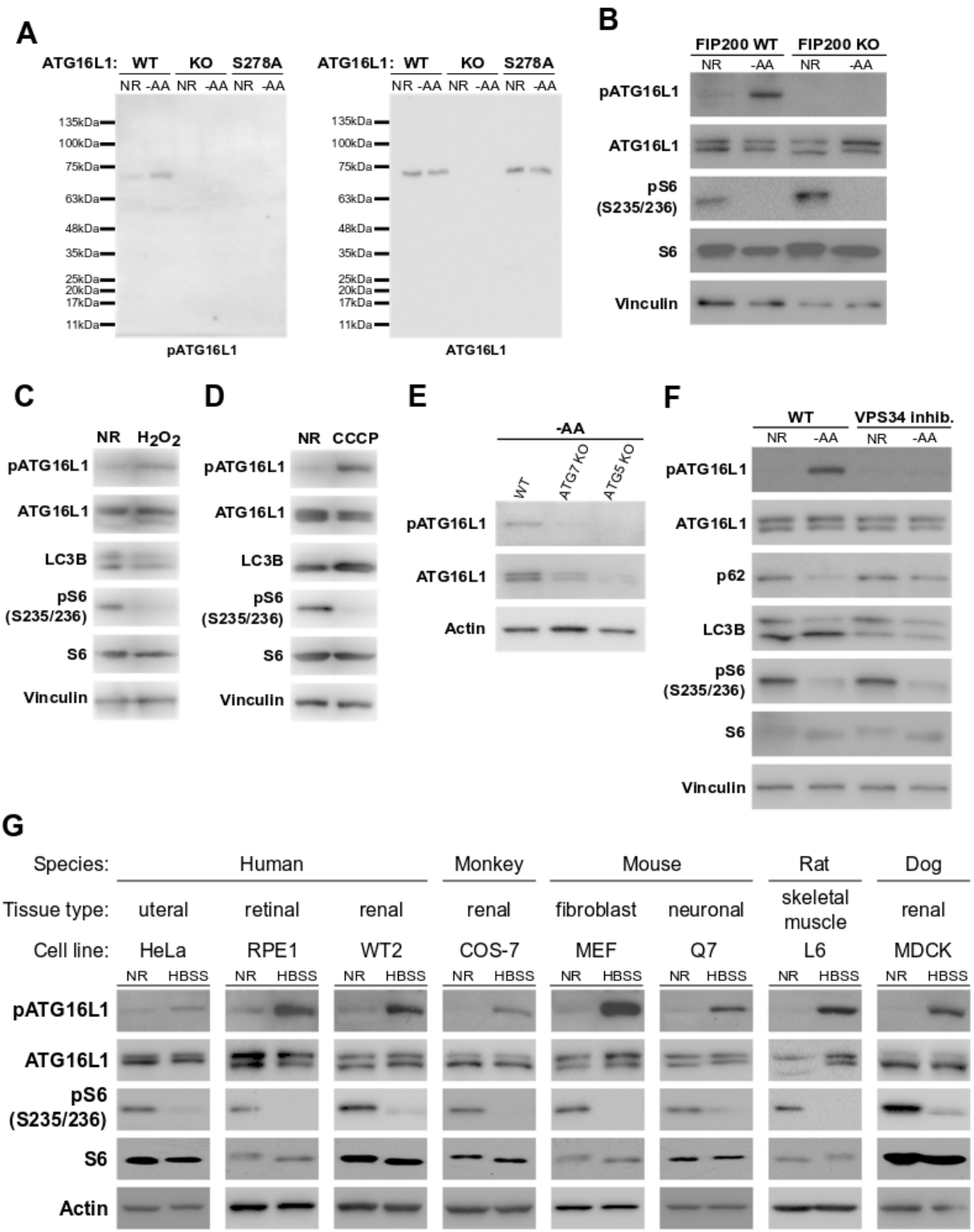
A
ATG16L1: WT KO S278A
NR -AA NR -AA NR -AA
135kDa
100kDa
75kDa
63kDa
48kDa
35kDa
25kDa
20kDa
17kDa
11kDa
pATG16L1
ATG16L1
B
FIP200 WT FIP200 KO
NR -AA NR -AA
pATG16L1
ATG16L1
pS6 (S235/236)
S6
Vinculin
C
NR H2O2
pATG16L1
ATG16L1
LC3B
pS6 (S235/236)
S6
Vinculin
D
NR CCCP
pATG16L1
ATG16L1
LC3B
pS6 (S235/236)
S6
Vinculin
E
-AA
WT
ATG7 KO
ATG5 KO
pATG16L1
ATG16L1
Actin
F
WT VPS34 inhib.
NR -AA NR -AA
pATG16L1
ATG16L1
p62
LC3B
pS6 (S235/236)
S6
Vinculin
G
Species: Human Monkey Mouse Rat Dog
Tissue type: uteral retinal renal renal fibroblast neuronal skeletal muscle renal
Cell line: HeLa RPE1 WT2 COS-7 MEF Q7 L6 MDCK
NR HBSS
pATG16L1
ATG16L1
pS6 (S235/236)
S6
Actin

Figure 16. pATG16L1s278 signaling is regulated by upstream autophagy factors and is conserved across multiple species. *(**A**) HCT116 cells of the indicated genotype were incubated in either complete DMEM (NR) or amino acid deficient media (-AA) for 3 hours. Cell lysates were resolved by SDS-Page and immunoblotted using either pATG16L1 or ATG16L1 antibodies. Full length blots are shown. (**B**) FIP200 knockout or wild-type mouse embryonic fibroblasts (MEFs) were treated for 3 hours with nutrient rich (NR) or amino acid deficient DMEM (-AA). Cell lysates were resolved by SDS-PAGE and immunoblotted using the indicated antibodies. (**C**) L6 cells were incubated in complete media in the presence or absence of H_2O_2 for 1 hour. Cells lysates were resolved by SDS-PAGE and immunoblotted using the indicated antibodies. (**D**) WT2 cells were incubated in complete media in the presence or absence of carbonyl cyanide m-chlorophenylhydrazone (CCCP) for 5 hours. Cells lysates were resolved by SDS-PAGE and immunoblotted using the indicated antibodies. NR, nutrient rich. (**E**) Wild-type, ATG5 knockout, and ATG7 knockout MEFs were incubated with amino acid deficient DMEM for 3 hours. Cell lysates were resolved by SDS-PAGE and immunoblotted using the indicated antibodies. (**F**) Wild-type MEFs were incubated in nutrient rich or amino acid deficient DMEM, in the presence or absence of VPS34 inhibitor (Calbiochem, 100nm) for 3 hours. Cell lysates were resolved by SDS-PAGE and immunoblotted using the indicated antibodies. (**G**) 8 cell lines of different species and/or tissue origins, as labeled, were incubated in either complete media or HBSS for 2 to 4 hours. Cell lysates were resolved by SDS-PAGE and immunoblotted using the indicated antibodies. KO, knockout; NR, Nutrient rich; -AA, no amino acid; -FBS, no serum; HBSS, Hanks Balanced Salt Solution.*

pATG16L1^{s278} can be detected endogenously by immunofluorescence microscopy and is upregulated in amino acid starved cells

Immunofluorescent (IF) staining of autophagy-related proteins is another widely used method to monitor autophagy. Importantly, IF allows for analysis of autophagy at the single-cell level, which can be critical for rare cell populations or mixed cultures. Therefore, we next sought to determine if our antibody was compatible with IF and how it compared to other established autophagy markers. First, we verified the specificity and reactivity of our antibody for IF staining in both ATG16L1 wild-type and knockout cells. We stained for both endogenous pATG16L1^{s278} and total ATG16L1 and observed that pATG16L1^{s278} puncta were completely absent in both knockout cells and cells treated with VPS34 inhibitor (Fig. 17A). Strikingly, we found that the localization of pATG16L1 was almost exclusively punctate when compared to total ATG16L1, which exhibited a staining pattern both a punctate and diffuse (Fig. 17A). Furthermore, nearly all (97%) of the pATG16L1^{s278} puncta colocalized with total ATG16L1 puncta, which combined with the lack of signal in the negative controls, indicates the pATG16L1^{s278} antibody was specific and compatible with IF. To further validate that our antibody was exclusively staining the phosphorylated form of ATG16L1, we next performed the same experiment in ATG16L1 knockout cells stably reconstituted with epitope-tagged versions of either wild-type or phospho-dead S278A mutant ATG16L1. Similar to the knockout cells, we did not observe any pATG16L1^{s278} puncta in the S278A mutant, indicating the antibody was specific to ATG16L1 phosphorylated on serine 278 (Fig. 18A). We postulated that pATG16L1^{s278} may be selectively associated with autophagosomal structures due to its exclusive punctate staining, since punctate staining of autophagy-related proteins is often associated with autophagosomes. To investigate whether pATG16L1^{s278} puncta are

indeed autophagosome-associated, we analyzed pATG16L1^{s278} puncta colocalization with LC3B and sensitivity to starvation. Co-staining of endogenous pATG16L1^{s278} and LC3B revealed a starvation-induced upregulation of both puncta as well as a consistent but partial colocalization (Fig. 17B, 18B).

pATG16L1^{s278} is not essential for starvation induced autophagy

In order to determine if ATG16L1 phosphorylation is required for autophagy induction we stably reconstituted ATG16L1 (WT or S278A) in ATG16L1 knockout cells and monitored autophagosome induction under starvation by staining for endogenous LC3B. We observed a similar induction of autophagosomes in both cell lines indicating that pATG16L1^{s278} is not required for starvation induced autophagy (Fig. 18C). Additionally, we tested the ability of ATG16L1 to localize to WIPI2, which has been described to directly bind ATG16L1[63]. Cells were transfected with WIPI2 and co-stained with total ATG16L1. We observed no appreciable difference in ATG16L1-WIPI2 binding, underscoring that ATG16L1 phosphorylation is not required for ATG16L1 binding to WIPI2 under starvation (Fig. 18D). This is consistent with our previous observation that this particular modification of ATG16L1 is important in antibacterial autophagy but dispensable for starvation-induced autophagy[127]. However, it should be noted that the most commonly used indicators for autophagy monitoring, such as LC3B and p62, are similarly not essential for autophagy[128,129]. In the case of LC3B, multiple orthologs can act in a functionally redundant manner in promoting autophagy. As a result, the most commonly studied modification in autophagy, the lipidation of LC3B, is not strictly required for autophagosome formation. This serves to underscore that the lack of a requirement for

an autophagy-related modification in the autophagy pathway (ATG16L1 phosphorylation, p62 degradation etc.) does not relate to its utility for monitoring autophagy.

pATG16L1^{s278} is primarily located on early stage autophagosomes

In order to confirm the autophagosomal nature of pATG16L1^{s278} puncta, we also analyzed colocalization between pATG16L1^{s278} and p62 in nutrient rich or starved conditions. p62 recruits cargo to the autophagosome and is observable as punctate structures when present in the autophagosome[130]. Consistent with our observations of pATG16L1^{s278}/LC3B colocalization, we detected pATG16L1^{s278}/p62 double-positive puncta primarily in amino acid starved cells (Fig. 17C, 18E). Triple staining for revealed a higher degree of colocalization between p62 and LC3B than was found for pATG16L1^{s278} with either LC3B or p62 (Fig. 17D, 18F). As p62 and LC3B are both found on fully formed autophagosomes this raises the possibility that pATG16L1^{s278} associates with the autophagic membrane prior to autophagosome closure, similarly to the described localization pattern proteins involved in autophagy initiation[13]. The possibility of selective localization of pATG16L1^{s278} to immature autophagosomes is particularly interesting as quantifying these structures would provide a readout for the rate of autophagy initiation in the cell.

In order to decipher the stage at which pATG16L1^{s278} promotes autophagosome biogenesis, we performed high-resolution confocal microscopy, allowing resolution to 120nm, on cells triple-stained for pATG16L1^{s278}, LC3B and WIPI1. WIPI2 has been described to recruit the E3-like enzyme complex (ATG16L1-5-12) to nascent autophagosomal membranes and can directly interact with both PtdIns(3)P and ATG16L1[63]. GFP-tagged WIPI1 was transfected as no commercial antibody was suitable

for detection of endogenous protein by IF. Importantly, fluorescently tagged WIPI1 was previously found only on expanding autophagosomal structures and not on mature autophagosomes[13]. Using 3-dimensional reconstruction of z-stacks of high-resolution images we were able to observe distinct patterns of co-staining, which could be attributed to different stages of autophagosome biogenesis. For example, we observed puncta that exhibited colocalization between pATG16L1^{s278}/WIPI1, pATG16L1 ^{s278}/LC3B, and pATG16L1^{s278}/WIPI1/LC3B (Fig. 17E). However, we did not observe any WIPI1/LC3B in the absence of pATG16L1 ^{s278} (Fig. 17E).

The correlation of pATG16L1^{s278} with early markers of autophagy initiation does not preclude the possibility that pATG16L1^{s278} also plays a role on late stage autophagosomes. Therefore, we next sought to determine if pATG16L1^{s278} localized to autolysosomes. Autolysosomes were identified by endogenous staining for lysosomal and autophagosomal markers LAMP1 and LC3B, which were co-stained with pATG16L1^{s278} in cells treated with BafA1 to enrich for autolysosomes. Consistent with our previous analysis we found that starvation induced a significant percentage of pATG16L1 positive autophagosomes (17.5%) with less than 1% of autolysosomes showing colocalization with pATG16L1^{s278} (Fig. 18G). To corroborate this observation we stained pATG16L1^{s278} in cells stably expressing eGFP-mCherry-LC3B. In these cells eGFP fluorescence is quenched when the autophagosome fuses with the lysosome. Consistent with our previous analysis we observed a significant colocalization between pATG16L1 and autophagosomes (eGFP-mCherry-positive puncta), while the vast majority of autolysosomes (mCherry-positive puncta) did not colocalize with pATG16L1^{s278} (Fig. 18H). Taken together these data suggest that the majority of

phosphorylated ATG16L1 is associated with newly forming autophagosomes. This series of autophagosomal structures suggests a working model of autophagosomal initiation where pATG16L1^{s278} is targeted to newly forming autophagosomes to promote LC3B-lipidation and dissociates along with WIPI-proteins upon autophagosomal maturation (Fig. 17F).

Figure 17

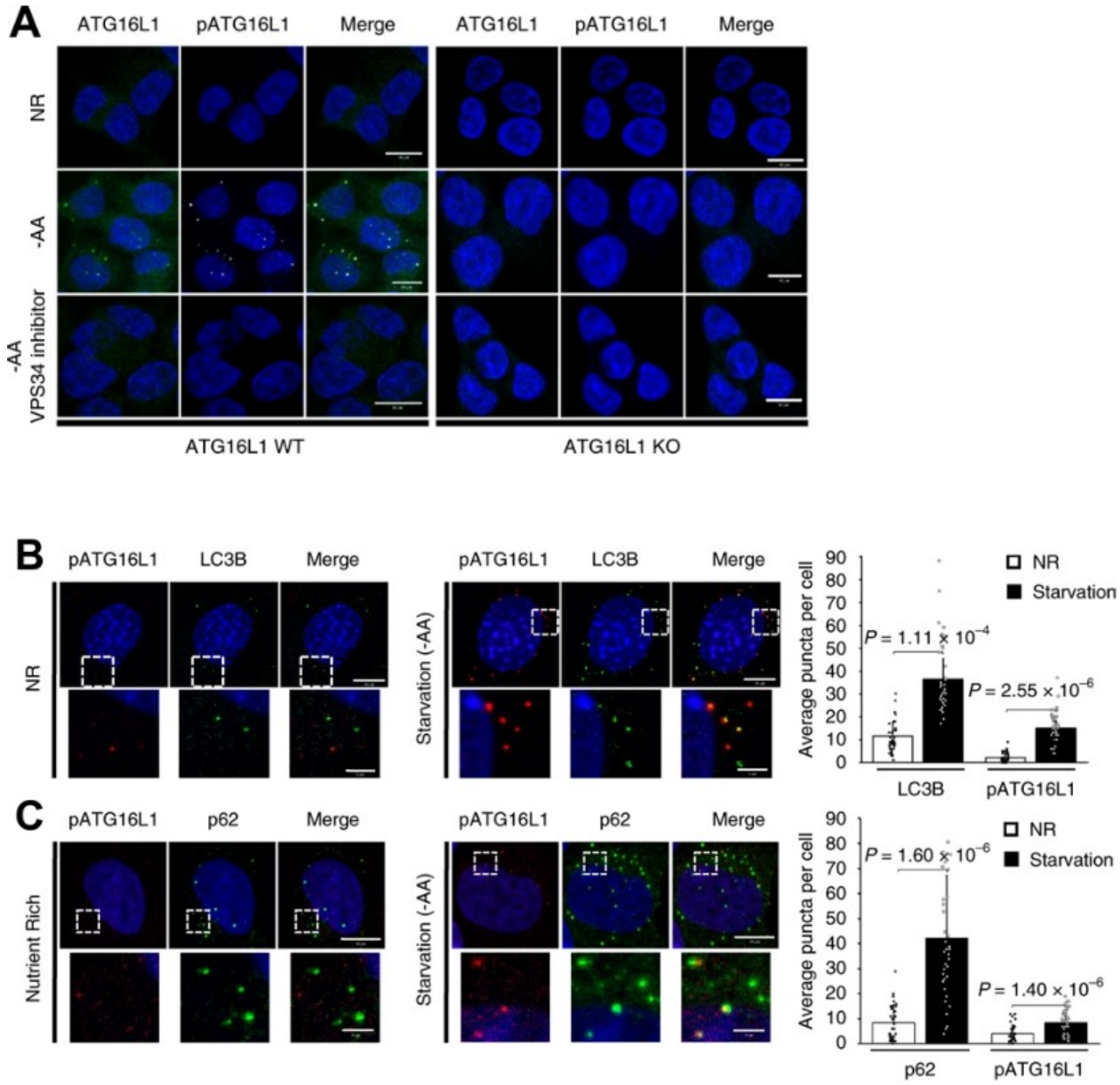

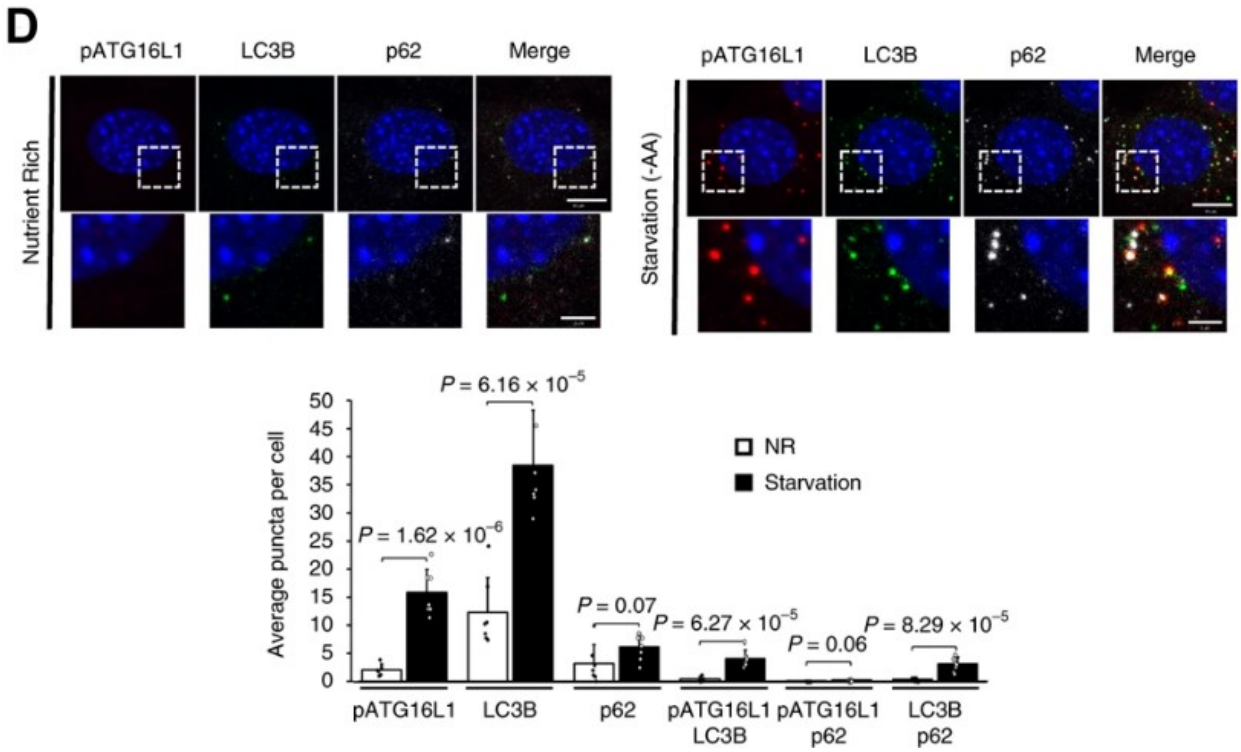
D
pATG16L1
LC3B
p62
Merge
Nutrient Rich
Starvation (-AA)
Average puncta per cell
NR
Starvation
P = 6.16 × 10−5
P = 1.62 × 10−6
P = 0.07
P = 6.27 × 10−5
P = 0.06
P = 8.29 × 10−5
pATG16L1
LC3B
p62
pATG16L1 LC3B
pATG16L1 p62
LC3B p62

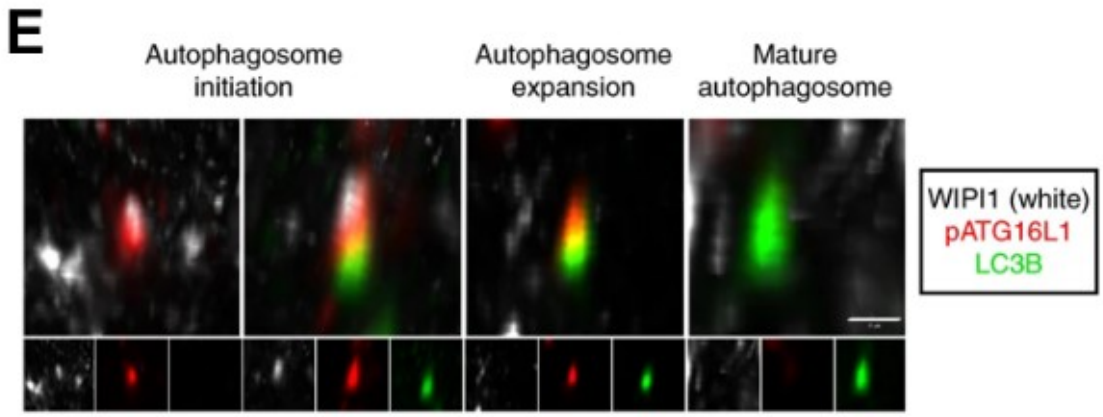
E
Autophagosome initiation
Autophagosome expansion
Mature autophagosome
WIPI1 (white)
pATG16L1
LC3B

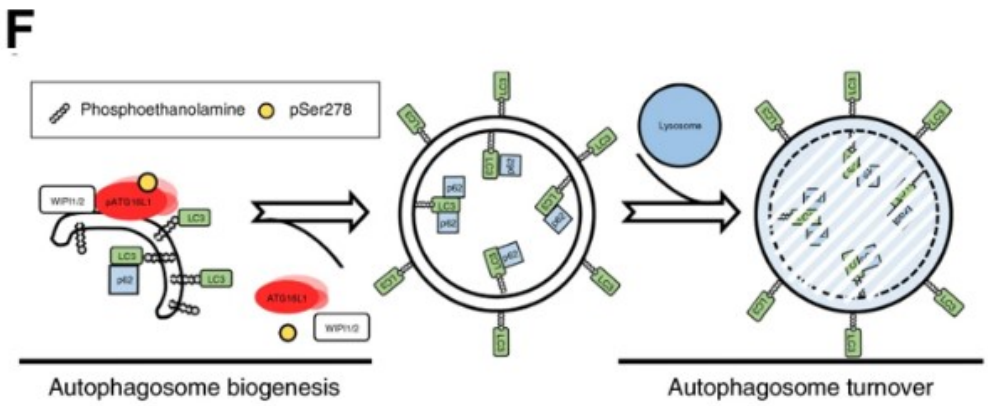

Figure 16 .pATG16L1^{s278} can be detected endogenously by immunofluorescence microscopy in amino acid starved cells and is primarily located on early stage autophagosomes.*(**A**) HCT116 WT and ATG16L1 KO cells were treated with the indicated treatments for 2 h. Endogenous ATG16L1 (green), pATG16L1 (white) and DNA (blue) were stained. Representative images are shown (scale bars, 10 µm). (**B**), Endogenous pATG16L1 (red), LC3B (green) and DNA (blue) were stained in Q7 cells incubated in either complete medium or amino acid-deficient DMEM for 1 h. Representative images are shown (scale bars, top row, 10 µm; bottom row, 3 µm). Quantification of one representative experiment is shown, independently repeated three times (n = 3) with similar results. Error bars represent standard deviation. Statistical analysis was performed using two-sided Student's t-test; asterisks denote P < 0.05. (**C**) Endogenous pATG16L1 (red), p62 (green) and DNA (blue) were stained in Q7 cells incubated in either complete medium or amino acid-deficient DMEM for 1 h. Representative images are shown (scale bars, top row, 10 µm; bottom row, 2 µm). Quantification of one representative experiment is shown, independently repeated three times (n = 3) with similar results. Error bars represent standard deviation. Statistical analysis was performed using two-sided Student's t-test; asterisks denote P < 0.05. (**D**), Endogenous pATG16L1 (red), LC3B (green), p62 (white) and DNA (blue) were stained in Q7 cells incubated in either complete medium or amino acid-deficient DMEM for 1 h. Representative images are shown (scale bars, top row, 10 µm; bottom row, 3 µm). Quantification of one representative experiment is shown, independently repeated three times (n = 3) with similar results. Error bars represent standard deviation. Statistical analysis was performed using two-sided Student's t-test; asterisks denote P < 0.05. (**E**), MEFs transiently expressing GFP-tagged WIPI1 were incubated in either complete medium or amino acid-deficient DMEM for 1 h. Endogenous pATG16L1 and LC3B were stained and analyzed along with GFP by AiryScan high-resolution fluorescent microscopy. Four representative images corresponding to different stages of autophagosome expansion are shown. Experiment was repeated three times (n = 3) with similar results. For consistency pATG16L1 was pseudocolored red, LC3B green and GFP-WIPI1 white (scale bars, 2 µm). (**F**), Simplified schematic of autophagosome biogenesis with respect to the roles of WIPI1/2, ATG16L1, LC3 and p62.*

Figure 18

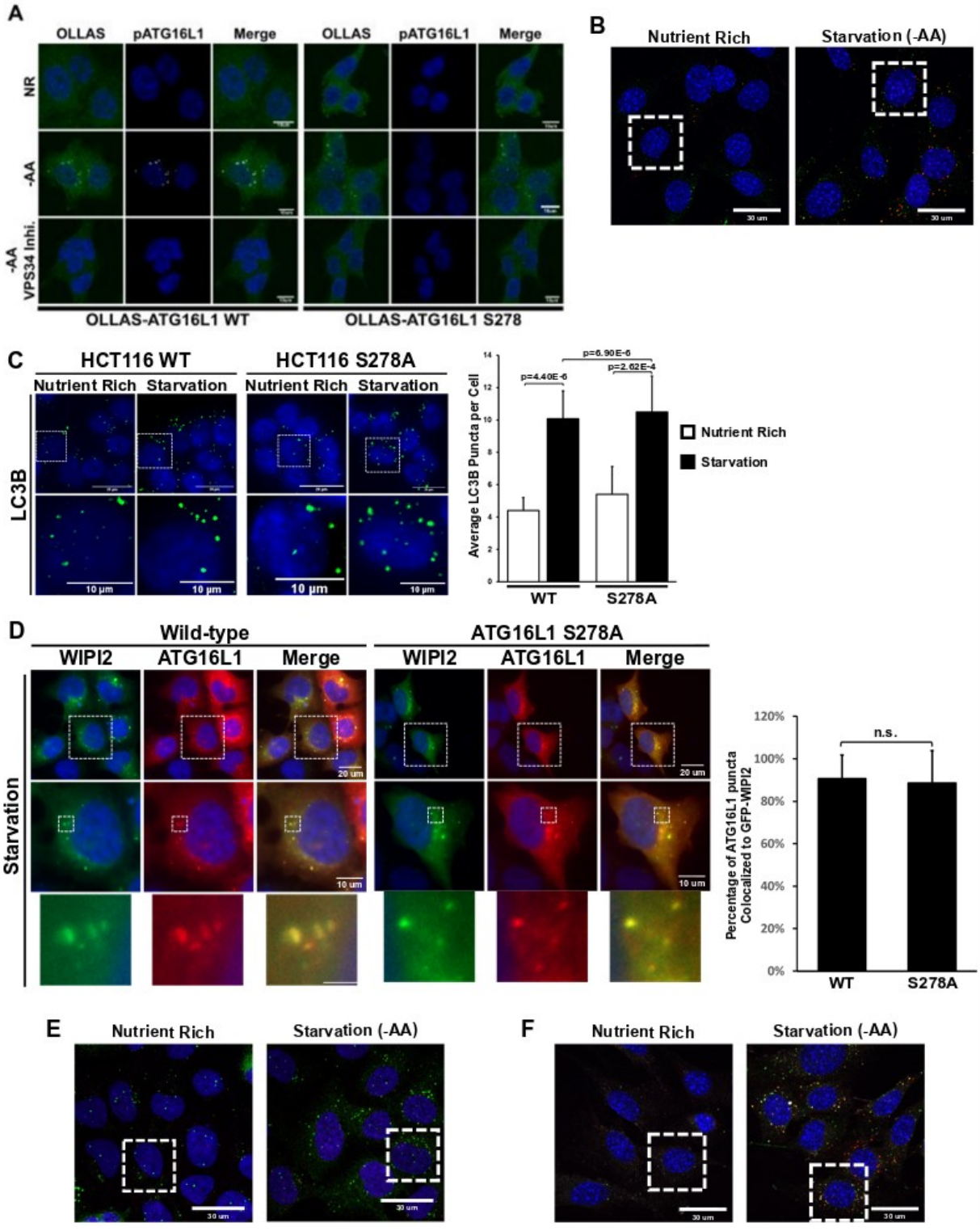
A
OLLAS
pATG16L1
Merge
OLLAS
pATG16L1
Merge
NR
-AA
-AA VPS34 Inhi.
OLLAS-ATG16L1 WT
OLLAS-ATG16L1 S278
B
Nutrient Rich
Starvation (-AA)
C
HCT116 WT
HCT116 S278A
Nutrient Rich
Starvation
Nutrient Rich
Starvation
LC3B
10 μm
p=4.40E-6
p=6.90E-6
p=2.62E-4
Average LC3B Puncta per Cell
Nutrient Rich
Starvation
WT
S278A
D
Wild-type
ATG16L1 S278A
WIPI2
ATG16L1
Merge
WIPI2
ATG16L1
Merge
Starvation
20 um
10 um
Percentage of ATG16L1 puncta Colocalized to GFP-WIPI2
120%
100%
80%
60%
40%
20%
0%
n.s.
WT
S278A
E
Nutrient Rich
Starvation (-AA)
30 um
F
Nutrient Rich
Starvation (-AA)
30 um

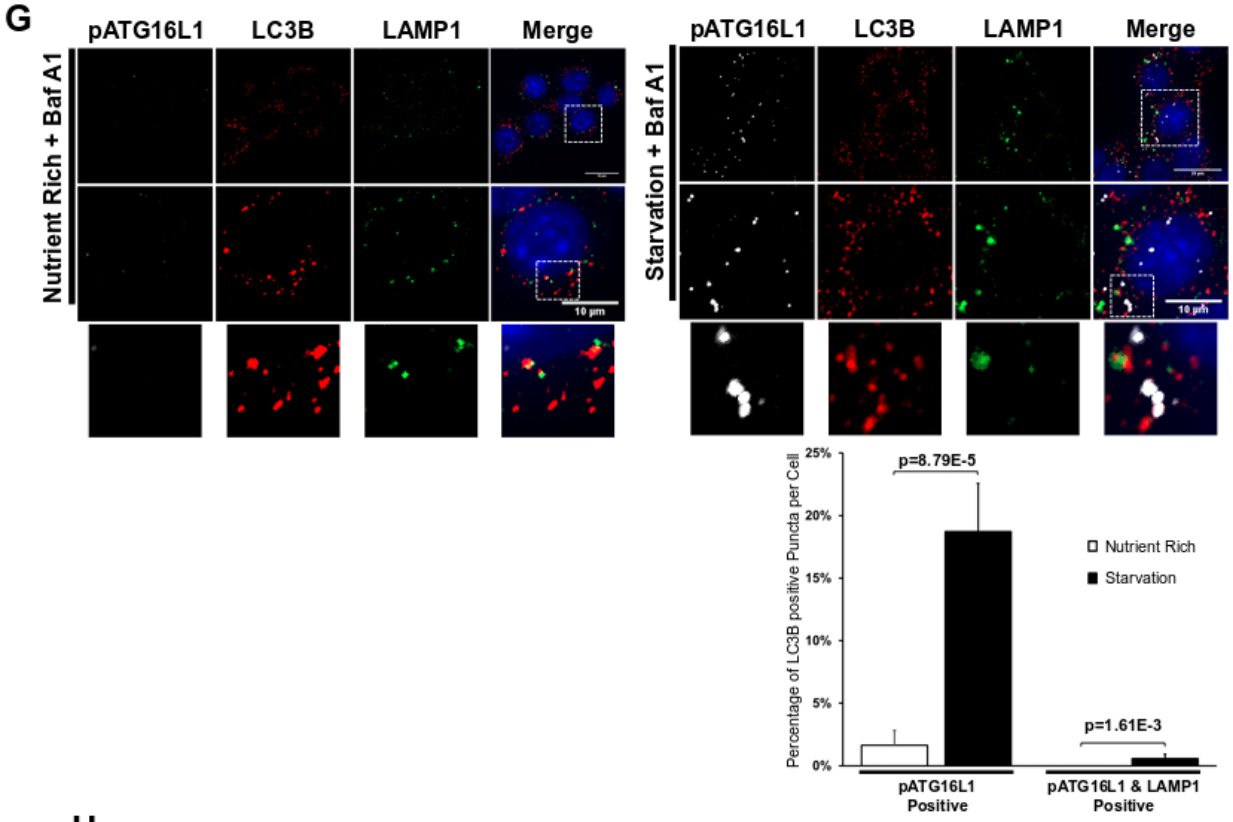
G
pATG16L1
LC3B
LAMP1
Merge
Nutrient Rich + Baf A1
Starvation + Baf A1
10 μm
p=8.79E-5
p=1.61E-3
Percentage of LC3B positive Puncta per Cell
25%
20%
15%
10%
5%
0%
Nutrient Rich
Starvation
pATG16L1 Positive
pATG16L1 & LAMP1 Positive

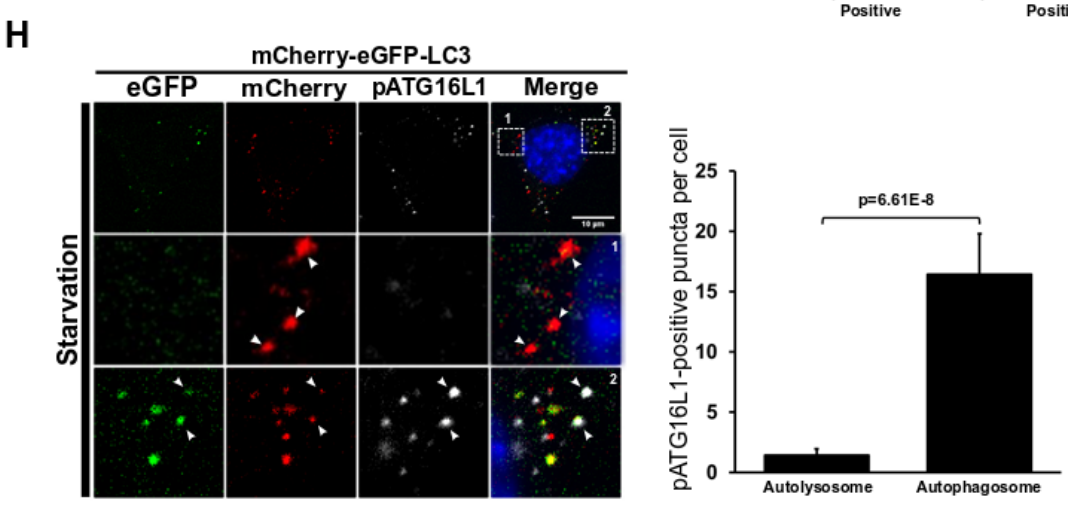
H
mCherry-eGFP-LC3
eGFP
mCherry
pATG16L1
Merge
Starvation
1
2
10 μm
p=6.61E-8
pATG16L1-positive puncta per cell
25
20
15
10
5
0
Autolysosome
Autophagosome

Figure 18. pATG16L1^{s278} can be detected endogenously by immunofluorescence microscopy in amino acid starved cells and is not essential for autophagosome biogenesis. *(**A**) HCT116 ATG16L1 knock-out cells reconstituted with either OLLAS tagged wild-type or S278A ATG16L1 were treated with the indicated treatments for 2 hours. OLLAS (green), pATG16L1 (white) and DNA (blue) were stained. Representative images are shown (scale bars: 10μm). Experiment was repeated 3 times (n=3) independently with similar results. (**B**) Enlarged multicell view of Fig. 17B showing all channels merged. Experiment was independently repeated 3 times (n=3) with similar results. (**C**) Wild-type and ATG16L1 S278A mutant HCT116 cells were incubated in DMEM or amino acid deficient media for 2 hours. LC3B was stained and representative immunofluorescent images are shown. Quantification of one representative experiment is shown, independently repeated 3 times with similar results. Error bars represent standard deviation. Statistical analysis was performed using two-sided Student's Ttest, asterisk denote p<0.05. (**D**) GFP-WIPI2 was transiently expressed in HCT116 cells stably expressing either wild-type or S278A mutant ATG16L1. Cells were starved in amino acid deficient media for 2 hours. ATG16L1 (red) was stained and analyzed with GFP signal (green). Representative immunofluorescent images are shown. Quantification of one representative experiment is shown, independently repeated 3 times (n=3) with similar results. Error bars represent standard deviation. Statistical analysis was performed using two-sided Student's T-test, asterisk denote p<0.05. (**E**) Enlarged multicell view of Fig. 17C showing all channels merged. Experiment was independently repeated 3 times (n=3) with similar results. (**F**) Enlarged multicell view of Fig. 17D showing all channels merged. Experiment was independently repeated 3 times (n=3) with similar results. (**G**) Wild-type MEFs were incubated in DMEM or amino acid deficient media for 2 hours in the presence of Bafilomycin A1 (200nm). The specified proteins were stained and representative immunofluorescent images are shown. Quantification of one representative experiment is shown, independently repeated 3 (n=3) times with similar results. Error bars represent standard deviation. Statistical analysis was performed using two-sided Student's T-test, asterisk denote p>0.05. (**H**) mCherry-eGFP-LC3 knockin MEFs were incubated in complete DMEM or amino acid deficient media for 240 minutes. pATG16L1 (white) was stained and representative immunofluorescent images are shown. White arrows in enlarged view #1 indicate autolysosomes (mCherry singlepositive puncta) absent of pATG16L1 signal. White arrows in enlarged view #2 indicate autophagosomes (mCherry-eGFP double-positive puncta) colocalized with pATG16L1. Quantification of one representative experiment is shown, independently repeated 4 (n=3) times with similar results. Error bars represent standard deviation. Statistical analysis was performed using two-sided Student's T-test, asterisk denote p<0.05.*

pATG16L1^{s278} level provides a reliable measurement of autophagy rates independent of late stage autophagy block

The ability of pATG16L1^{s278} to specifically target newly forming autophagosomes indicates that this marker for autophagy should be insensitive to blockages in

autophagosome clearance. A persistent problem in the autophagy research field is that blockade of autophagosomal turnover leads to accumulation of LC3B-positive vesicles, resembling a potent induction of autophagy[109]. To correct for this, inhibitors of autophagosome turnover, such as bafilomycin A1 (Baf A1), are commonly used to aid the measurement of autophagy flux by LC3B. Baf A1 inhibits lysosomal V-ATPase, thereby preventing acidification and clearance of lipidated LC3B in autophagosomes. However, use of Baf A1 and related inhibitors are not always feasible or may produce unintended changes *in vivo*[131], limiting the information on autophagy rates from animal or patient samples. To test if pATG16L1^{s278} levels are altered by accumulation of mature autophagosomes, we treated cells with Baf A1 under nutrient rich conditions and analyzed LC3B and pATG16L1^{S278} using IF. As expected, LC3B puncta were dramatically increased when autophagosome turnover was inhibited under nutrient rich conditions, despite no increase in the overall rate of autophagy (Fig. 19A). Excitingly, we observed that pATG16L1^{s278} staining was indistinguishable between Baf A1 treated cells and untreated, consistent with the actual rate of autophagy induction under nutrient rich conditions (Fig. 19A). We next performed a time-course experiment under nutrient rich conditions in the presence or absence of lysosomal inhibitors, and found that pATG16L1^{s278} was not increased at any time point by western blot (Fig. 19B). Altogether, these findings indicate that pATG16L1^{s278} could be very useful in discriminating between autophagy induction and autophagosome accumulation.

We next sought to compare the kinetics of pATG16L1^{s278} induction to established markers of autophagy flux (e.g. LC3B lipidation in the presence of flux inhibitors and clearance of autophagy adaptors). To compare pATG16L1^{s278} to LC3B lipidation, we performed time-

course experiments using Baf A1 under starvation and measured LC3B-II accumulation and pATG16L1 levels by western blot. Interestingly, we constantly observed a correlation between the peak signals for LC3B-II and pATG16L1 (Fig. 19C). These data indicate that analysis of ATG16L1 phosphorylation could be used as a substitute to LC3B lipidation analysis with flux inhibitors, which has been a pillar in the measurement of autophagy rates.

Another widely used method to monitor autophagic flux is the analysis of autophagy adaptor protein clearance. Autophagy adaptors typically bind LC3B and ubiquitin to selectively recruit cargo into newly forming autophagosomes, and as such are cleared at rapid rates when autophagy is strongly induced. The most commonly analyzed autophagy adaptor is p62, whose levels are inversely correlated with autophagic activity[6]. Decreased autophagy adaptor protein p62 levels can be observed without the use of late stage inhibitors, which prompted us to conduct a similar experiment as described in Fig. 19C, but in the absence of Baf A1 in order to compare the analysis of autophagic flux using clearance of autophagy adaptors or induction of ATG16L1phosphorylation. As expected, by 2 hours of starvation we observed a potent decrease in p62 protein levels and a concomitant increase in ATG16L1 phosphorylation over nutrient rich conditions, consistent with autophagy induction (Fig. 19D). However, we noted that these two methods of monitoring autophagy gave slightly different information at both early and late time points. After 40min starvation we observed a dramatic increase in pATG16L1^{s278} levels and a statistically insignificant reduction in p62 levels (Fig. 19D). This is consistent with an early point in the autophagic flux, where several new autophagosomes are being formed (pATG16L1^{s278} high) but only few have fused with the lysosome to degrade p62

(Fig. 16F). However, beyond 120min starvation p62 levels remain low making it difficult to determine changes in autophagy flux after the initial clearance of autophagy adaptors. As a consequence, the increase we see pATG16L1^{s278} and LC3B-II levels around 3-4 hours (Figs. 19C, D) is not observable by p62 clearance. These data indicate the potential for a unique advantage of analyzing autophagy through phosphorylation of ATG16L1, which is not sensitive to the duration of starvation. Moreover, stress-induced degradation of p62 has been described to correlate with an upregulation of its transcription[132], potentially confounding autophagy analysis unlike phosphorylation/dephosphorylation, which is rapid and reversible making it the ideal indicator for autophagic activity.

Figure 19

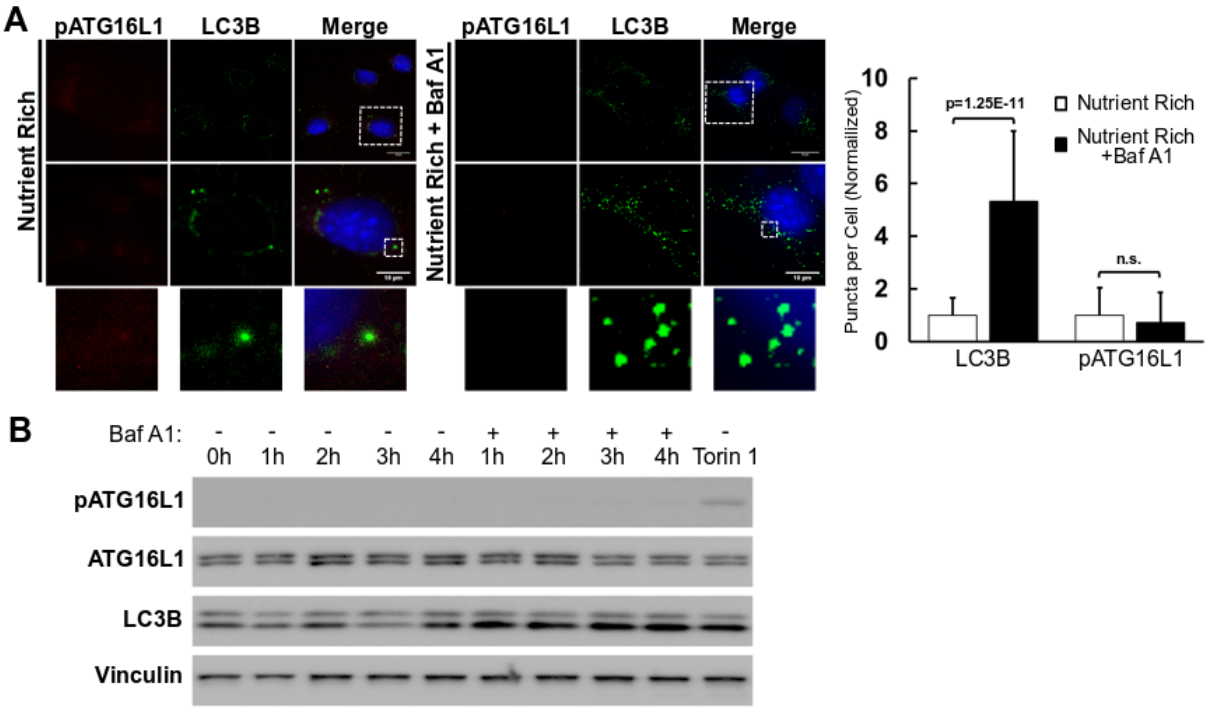

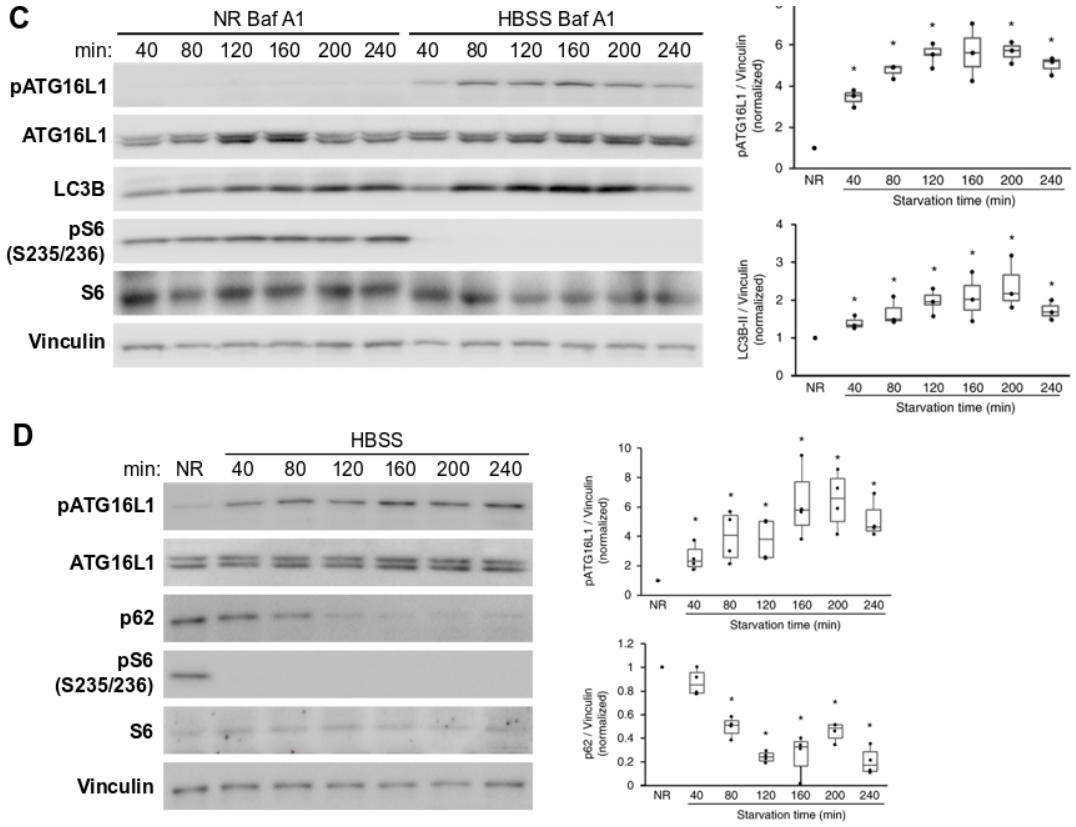

Figure 179. pATG16L1^{s278} level provides a reliable measurement of autophagy rates independent of late stage autophagy block. *(**A**) Q7 cells were incubated in complete medium in the presence or absence of Baf A1. pATG16L1, LC3B and DNA were stained and analyzed by immunofluorescence. Representative images are shown (scale bars, top row, 20 µm; bottom row, 10 µm). Quantification of one representative experiment is shown, independently repeated three times (n = 3) with similar results. Error bars represent standard deviation. Statistical analysis was performed using two-sided Student's t-test; asterisk denotes P < 0.05. (**B**) Immunoblot of Q7 cells incubated in complete media in the presence or absence of Baf A1. Cell lysates were collected at the time points indicated. Cells were treated with Torin-1 for 2 hours as a positive control for induction of ATG16L1 phosphorylation. Experiment was repeated 3 times independently with similar results (**C**), Q7 cells were incubated in either complete medium or HBSS in the presence of Baf A1 . Cell lysates were collected at the time points indicated and immunoblotted with the indicated antibodies. Quantification of western blot protein relative intensities normalized against the NR sample from three independently repeated experiments (n = 3) is shown. Error bars represent standard deviation. Statistical analysis was performed using two-sided Student's t-test; asterisk denotes P < 0.05. (**D**), Q7 cells were incubated in either complete medium or HBSS. Cell lysates were collected at the time points indicated and immunoblotted with the indicated antibodies. Quantification of western blot protein relative intensities normalized against the NR sample from four independently repeated experiments (n = 4) is shown. Error bars represent standard deviation. Statistical analysis was performed using two-sided Student's t-test; asterisk denotes P < 0.05.*

pATG16L1^{s278} correlates with the production of newly forming autophagosomes

In order to validate the peak in autophagy rates we observed by LC3B and pATG16L1^{s278} around 3-4 hours starvation, we performed a temporal analysis of autophagosome formation using the eGFP-mCherry-LC3B reporter. In MEF cells stably expressing this reporter, eGFP-mCherry dual positive puncta are newly formed autophagosomes and mCherry-single positives are matured autolysosomes. We quantified both autophagosomes and autolysosomes at the time points previously used for our western analysis of pATG16L1^{s278} and confirmed that autophagosome formation was still elevated at 3-4 hours starvation, consistent with our pATG16L1^{s278}, and LC3B-II western blots (Fig. 20A). We also quantified pATG16L1^{s278} puncta and determined that peaks in pATG16L1^{s278}-positive vesicles occur between 3 and 4 hours (Fig. 20B). We previously showed that pATG16L1^{s278} puncta are on autophagosomes not autolysosomes (Fig. S2G, S2H) and that autolysosome and autophagosome number peak at 3-4 hours confirming the peak in autophagic flux shown by pATG16L1^{s278} and LC3B-II western blot. Next, we utilized the autophagosome-specific live cell stain CytoID^{tm} and similarly found that autophagosome formation peaked between 3 and 4 hours (Fig. 20C). Finally, we duplicated plates at 4 hours starvation and analyzed pATG16L1^{s278} levels by western blot and electron microscopy (EM). We observed an increase in autophagic vesicles by in EM images (Fig. 20D), which correlated with an increase in pATG16L1^{s278} levels by western blot (Fig. 20E). Together, our findings establish pATG16L1^{s278} as a robust indicator of autophagic rate, independent of late stage autophagy block, with the potential to provide a more accurate readout and/or simpler readout of autophagy induction than widely-used markers such as p62 and LC3B.

Figure 20

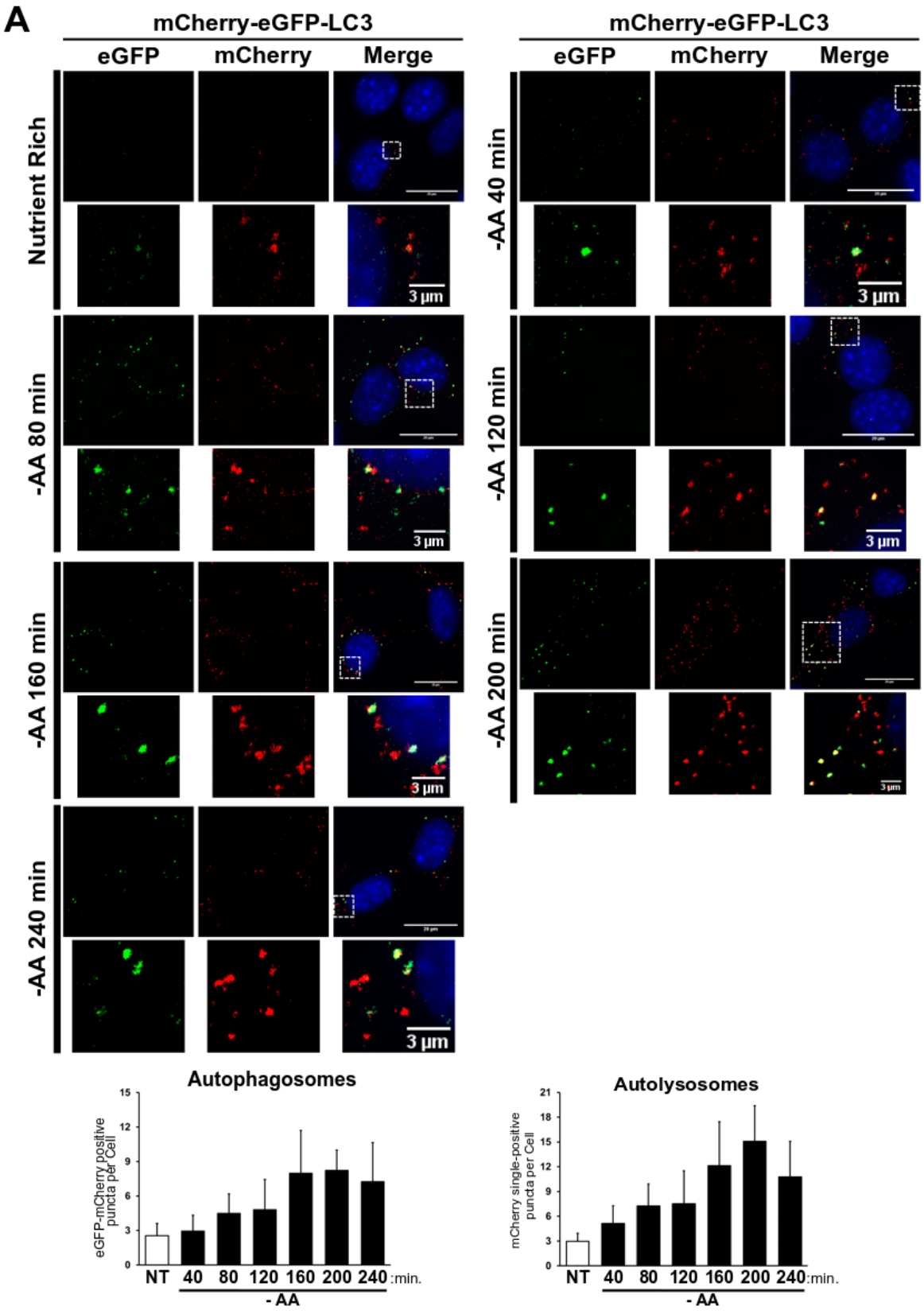
A
mCherry-eGFP-LC3
eGFP
mCherry
Merge
Nutrient Rich
-AA 40 min
-AA 80 min
-AA 120 min
-AA 160 min
-AA 200 min
-AA 240 min
3 μm
Autophagosomes
eGFP-mCherry positive puncta per Cell
NT 40 80 120 160 200 240 :min.
- AA
Autolysosomes
mCherry single-positive puncta per Cell
NT 40 80 120 160 200 240 :min.
- AA

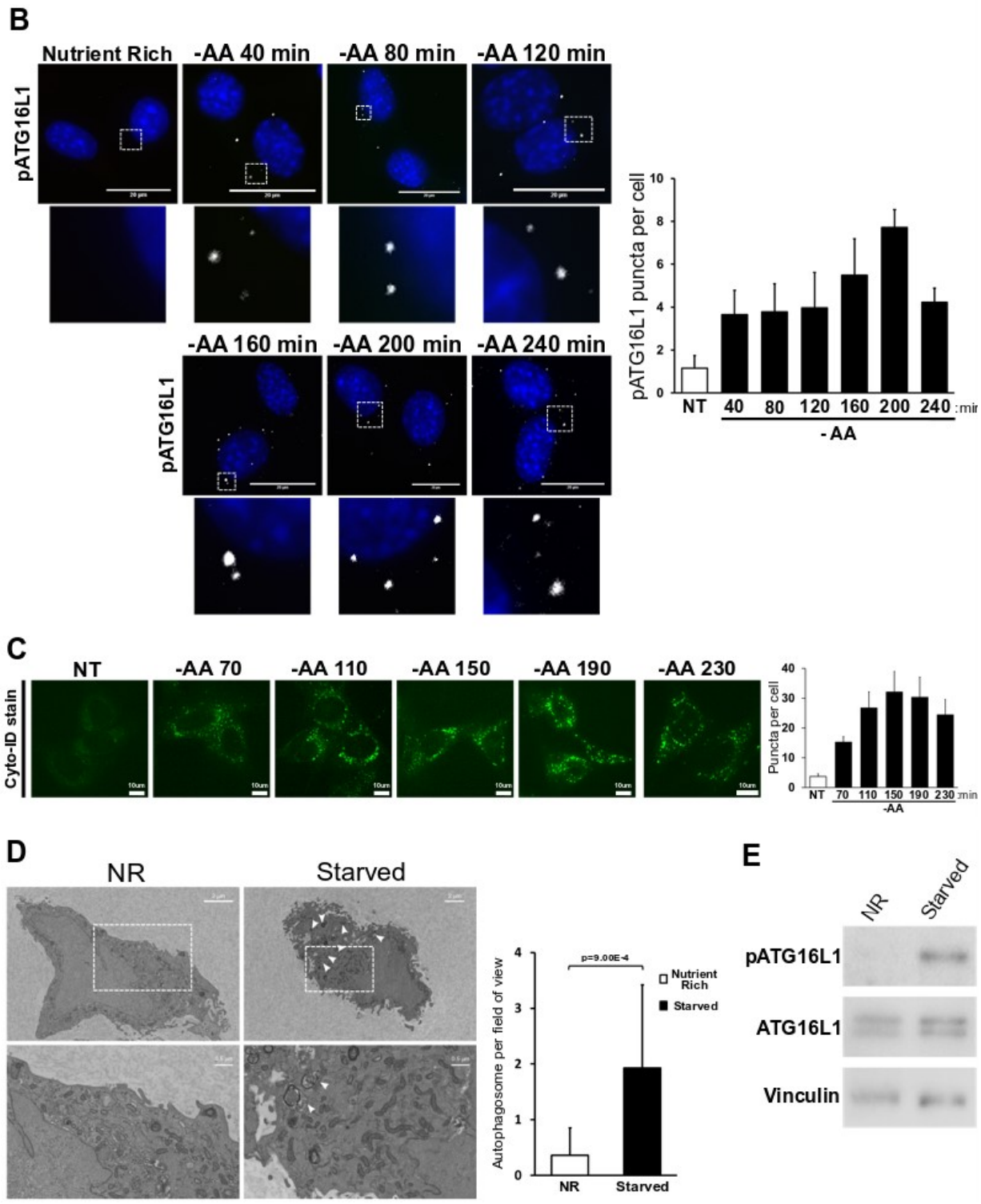

Figure 20. pATG16L1^{s278} signal correlates with production of newly forming autophagosomes. *(A) mCherry-eGFP-LC3 knockin MEFs were incubated in DMEM or amino acid deficient media for the specified time. mCherry (red) and GFP (green) signals were analyzed and representative immunofluorescent images*

*are shown. The number of autophagosomes (GFP, mCherry dual-positives) and autolysosomes (mCherry signal only) per timepoint were quantified separately from one representative experiment, repeated 3 times with similar results. Error bars represent standard deviation. Statistical analysis was performed using two-sided Student's T-test, asterisk denote p<0.05. (**B**) mCherry-eGFP-LC3 knockin MEFs were incubated in DMEM or amino acid deficient media for the specified time. Endogenous pATG16L1 (white) was stained and representative immunofluorescent Representative images are shown. The number pATG16L1 puncta per timepoint was quantified from one representative experiment, repeated 3 times with similar results. Error bars represent standard deviation. Statistical analysis was performed using two-sided Student's T-test, asterisk denote p<0.05. (**C**) Wild-type MEFs were incubated in either complete DMEM or HBSS and stained at specified timepoints with Cyto-ID Autophagy Detection Kit 2.0 (Enzo). Representative live cell images are shown. The number of stained vesicles (green) for each timepoint were quantified from one representative experiment, repeated 2 times with similar results. Error bars represent standard deviation. Statistical analysis was performed using two-sided Student's T-test, asterisk denote p<0.05. (**D**) Q7 cells were incubated in either complete DMEM or HBSS for 240 min. Cells were then fixed, agarose-embedded, sectioned and analyzed by electron microscopy. White arrows denote autophagosomes. Scale bars, top row, 2 µm; bottom row, 0.5 µm. Quantification of one representative experiment is shown, independently repeated three times (n = 3) with similar results. Measure of center represents mean value and error bars represent standard deviation. Statistical analysis was performed using two-sided Student's t-test; asterisk denotes P < 0.05. (**E**), Representative immunoblot from duplicate set of cells treated with the same conditions as panel (**D**). Experiment was independently repeated three times (n = 3) with similar results.*

pATG16L1 ^{s278} is a better indicator of autophagy rate than other mTORC1 and ULK phosphorylation targets

Since the initiation of autophagy is directly regulated by the mTORC1 pathway through its inhibition of the ULK complex, we next examined the possibilities of using mTORC1 and ULK phosphorylation targets to measure autophagy, as well as how these markers compare to pATG16L1^{s278}. One of the main concern for such methods is that mTORC1 activity is rapidly inhibited upon autophagy induction by starvation, while most of the autophagic cargo turnover have no occurred yet. Indeed, we have observed that mTORC1 activity (as a readout of S6K phosphorylation) was lost in merely 10-20 minutes

after starvation, while cargo turnover (as a readout of p62 levels) only begins around 45 minutes (Fig. 21A). Moreover, in contrast of the fluctuating pATG16L1^{s278} and LC3B-II levels representative of autophagy rates we observed (Fig. 19C), no further information could be gained from mTORC1 activity readout as it is completely abolished after 20 minutes starvation (Fig. 21A). Additionally the increased distance of mTORC1 to the autophagosome formation step in the autophagy pathway also makes mTORC1 activity assay more vulnerable to disruption by other factors. Case-in-point, we previously showed that *Salmonella* infection results in a complete blockage of autophagy even when mTORC1 is inhibited by amino acid withdrawal or Torin-1, a catalytic inhibitor of mTOR[133]. We tested the cotreatment of Torin-1 with Salmonella and analyzed pATG16L1^{s278} in addition to mTOR-targets and LC3B and p62. Under these conditions pATG16L1^{s278}, but not mTORC1-target phosphorylation accurately reflected rates of autophagic induction (Fig. 21B). This data illustrates that the more direct the relationship between the assay (ATG16L1 phosphorylation and the phenomenon measured (autophagosome biogenesis) the less likely of confounding variables affecting the integrity of the assay. Finally, we also examined phosphorylation of ATG13, another ULK target, and compared its ability to accurately measure autophagy rates with that of pATG16L1^{s278}. While pATG13 did seem to show an increase when under starvation, its levels were also relatively high in the untreated samples (Fig. 21C). The high basal levels of pATG13 confounded the analysis of autophagy induction, and as a result pATG13 was far less consistent in measuring autophagy as opposed to pATG16L1^{s278} (Fig. 21C)

Figure 21

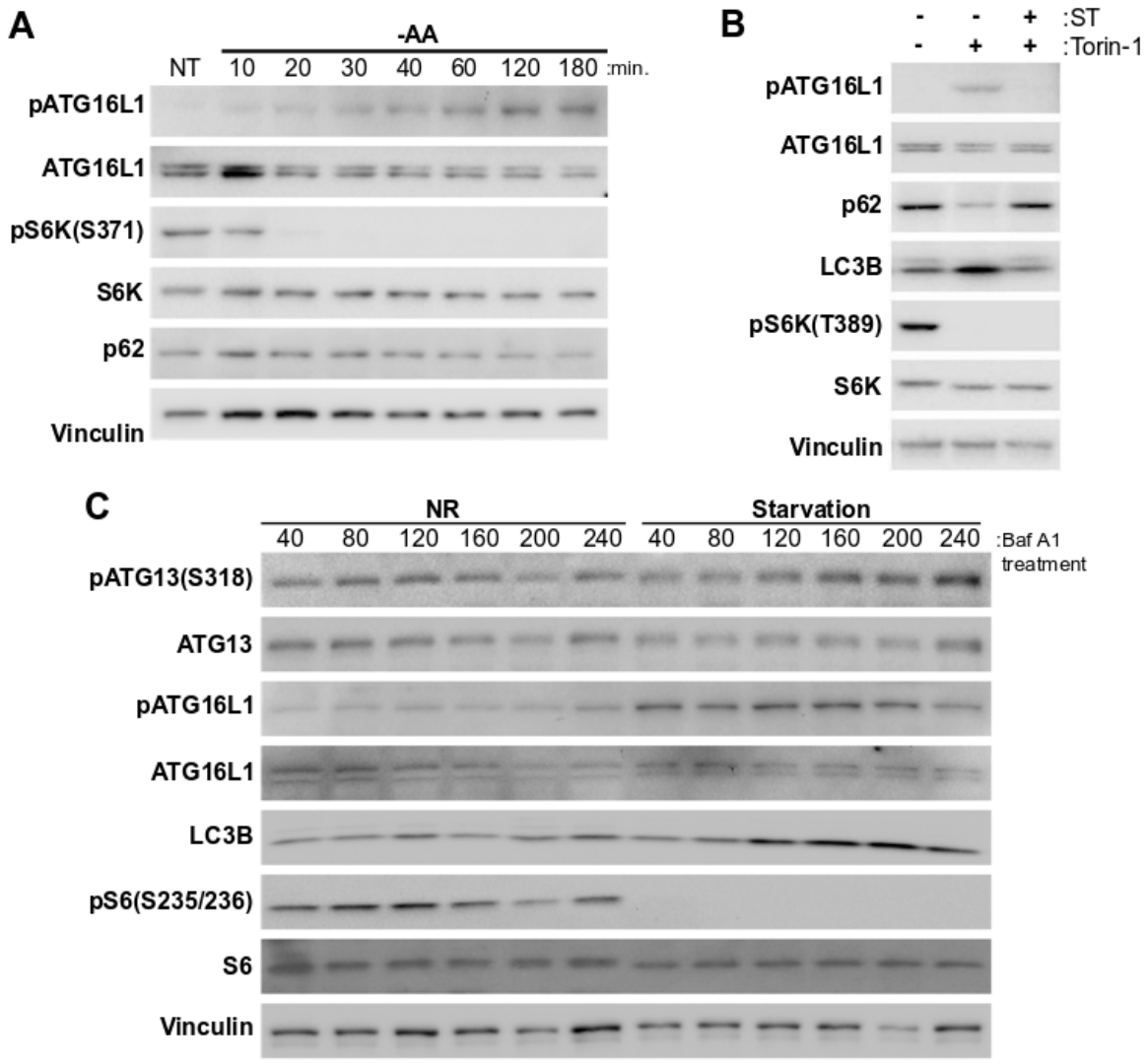

Figure 21. pATG16L1^{s278} is a better indicator of autophagy rate than other mTORC1 and ULK phosphorylation targets. *(**A**) Immunoblot of wild-type MEFs incubated in DMEM (NT) or Hank's Balanced Salt Solution (HBSS) for the indicated period of time. Experiment was independently repeated 3 times with similar results. (**B**) Immunoblot of wild-type MEFs incubated in DMEM and treated with salmonella (ST) and/or Torin-1 (200nm) as indicated for 1 hour. Experiment was independently repeated 3 times with similar results. (**C**) Immunoblot of wild-type MEFs incubated in DMEM (NR) or Hank's Balanced Salt Solution (HBSS) with Bafilomycin A1 (Baf A1, 200nm) for the indicated period of time. Experiment was independently repeated 3 times with similar results.*

pATG16L1^{s278} is compatible with immunohistochemistry staining of tissue samples to measure autophagic activities *in vivo*

We next sought to determine if pATG16L1^{s278} levels could be monitored *in vivo* from histological sections. Samples were generated from mice that were either fed *ad libitum* or starved for 16 hours, which was previously shown to activate autophagy in skeletal muscle[134]. Samples were then stained for pATG16L1 and LC3B and analyzed by confocal microscopy. Cryopreserved muscle samples showed punctate pATG16L1^{s278} staining when compared to secondary antibody alone, indicating immunoreactivity (Fig. 22A). More importantly, we observed that the number of puncta per cell increased significantly in starved muscles indicating that elevated pATG16L1^{s278} is detectable by immunohistochemistry (Fig. 22A, 23A). LC3B-staining in cryopreserved samples was increased across starvation samples but did not achieve statistical significance due to a large variance in LC3B puncta in one animal of the fed group (Fig. 22A, 23A). Consistent with the cryo-preserved samples, paraffin-formalin samples displayed pATG16L1^{s278} as a punctate pattern that was absent in controls (Fig. 22B). Additionally, punctate pATG16L1 staining was increased in starved samples compared to fed controls (Fig. 22B, 23B). LC3B staining was also specific and increased in starved samples (Fig. 22B, 23B). Notably, using this protocol LC3B staining gave more consistent staining in controls and was previously identified as optimal for LC3B immunohistological staining[135]. While we are using an LC3B antibody that has previously been validated for IHC, other antibodies may give improved results or require alternate tissue preparation protocols. We next sought to determine if pATG16L1^{s278} was suitable for IHC of liver or brain sections. These organs were harvested after transcardial perfusion with PBS followed by 4% PFA,

which greatly reduced background staining and aided in interpretation of pATG16L1^{s278} staining. We found that staining of both liver and hippocampal sections yielded a specific and punctate staining pattern for ATG16L1^{s278} (Fig. 22C-D). We further characterized the specificity of pATG16L1^{S278} staining in the brain through analysis of Atg5-null dividing neural progenitor cells (NPCs) from fixed slices of the hippocampus from adult brain. As previously described Atg5 was removed from the NPCs through injection of a 1:1 ratio of *CAG-GFP-Cre* and control RFP (*CAG-RFP*) retrovirus that specifically infects in vivo the dividing NPCs in the hippocampus of the *Atg5*$^{flox/flox}$ mice[136]. Atg5-null NPCs have been characterized and exhibit a reduction in autophagic activity[136]. Staining of these sections showed that the Atg5-null NPCs were void of pATG16L1 when compared to the surrounding tissue (Supplemental Video). Taken together, these results show that pATG16L1^{s278} staining is compatible with autophagy analysis using immunohistochemistry.

Figure 22

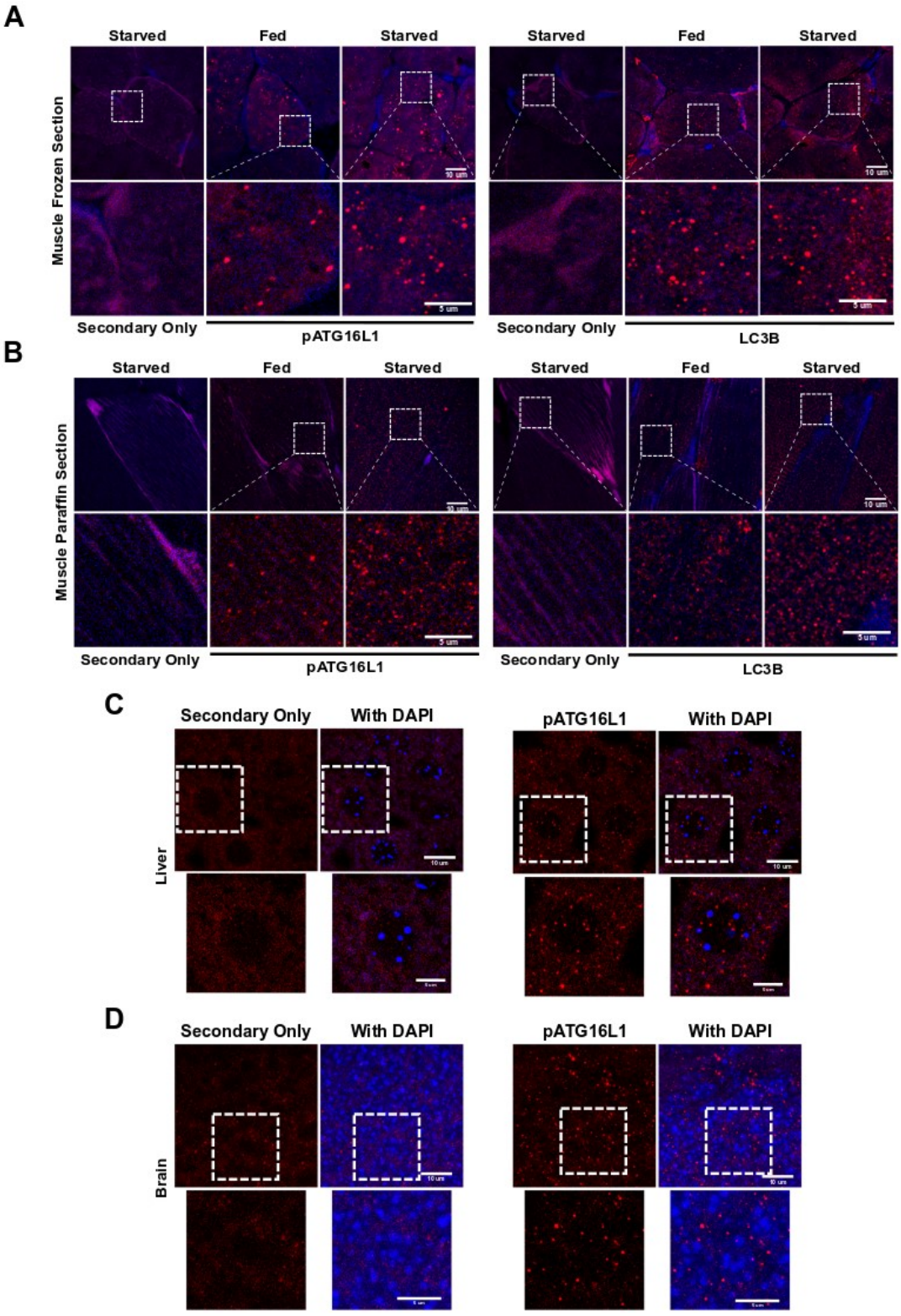
A
Starved
Fed
Starved
Starved
Fed
Starved
Muscle Frozen Section
Secondary Only
pATG16L1
Secondary Only
LC3B
B
Starved
Fed
Starved
Starved
Fed
Starved
Muscle Paraffin Section
Secondary Only
pATG16L1
Secondary Only
LC3B
C
Secondary Only
With DAPI
pATG16L1
With DAPI
Liver
D
Secondary Only
With DAPI
pATG16L1
With DAPI
Brain

Figure 22. pATG16L1S278 is compatible with immunohistochemistry staining of tissue samples to measure autophagic activities in vivo. (***A***) *Tissue sections from quadriceps of either fed or starved mice were cryopreserved and sectioned into 10-µm-thick slices. Staining was done using the indicated primary antibodies, followed by incubation with fluorophore-conjugated secondary antibody. Samples stained with secondary antibody alone are shown to provide a baseline of background fluorescence. Representative confocal microscopy images from a total of three biological replicates (n = 3) are shown (scale bars, 10 µm). (**B**) Tissue sections from quadriceps of either fed or starved mice were fixed with 10% formalin, paraffin embedded and sectioned into 4-µm-thick slices. Staining was performed using the indicated primary antibodies, followed by incubation with fluorophore-conjugated secondary antibody. Samples stained with secondary antibody alone are shown to provide a baseline of background fluorescence. Representative confocal microscopy images from a total of five biological replicates (n = 5) are shown (scale bars, 10 µm). (**C**) Mouse liver tissue sections were stained with pATG16L1 antibody. Secondary-only images are shown to distinguish specific pATG16L1 staining. Representative images are shown from a total of five biological replicates (n = 5) (scale bars, top row, 10 µm; bottom row, 5 µm). (**D**) Mouse brain hippocampus tissue sections were stained with pATG16L1 antibody. Secondary-only images are shown to distinguish specific pATG16L1 staining. Representative images are shown from a total of four biological replicates (n = 4) (scale bars, top row, 10 µm; bottom row, 5 µm).*

Figure 23

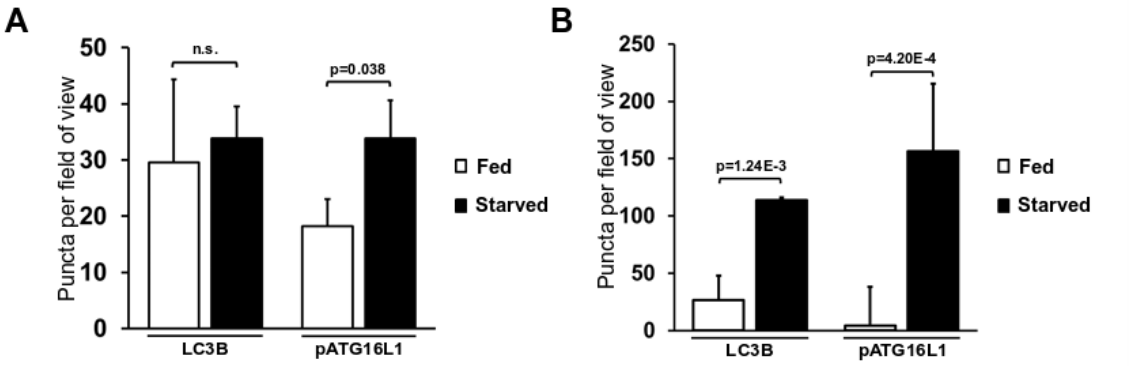

Figure 23. Quantitative analysis of pATG16L1S278 and LC3B staining in mice skeletal muscle. *(**A**) Quantification of LC3B and pATG16L1 puncta for Fig. 22A. n=3/group. Statistical analysis was performed using two-sided Student's T-test with p<0.05. (**B**) Quantification of LC3B and pATG16L1 puncta for Fig. 22B. n=5/group. Statistical analysis was performed using two-sided Student's T-test with p<0.05.*

Materials and Methods

Cell Culture

HeLa, RPE1, COS-7, Q7, L6, HCT116, MEF and MDCK cells were obtained from American Type Culture Collection (ATCC; Rockville, MD). 293A cells were obtained from ThermoFisher Scientific. Cells were cultured at 37°C in a humidified 5% CO_2 atmosphere. HCT116 ATG16L1 knockouts were generated using CRISPR/Cas9 targeting exon 1. Guide RNA sequence: 5' AAACCCGCTGGAAGCGCCACATCTC 3'. HCT116 ATG16L1 KO reconstituted cells were generated using the same guides. WT2 cells were generated by stable reconstitution of VHL in the 786-0 background as previously described[137]. ATG5 and ATG7 knockout MEFs were generated using CRISPR/Cas9 and has been previously described[138]. FIP200 knockout MEFs were a generous gift from Jun-Lin Guan (University of Cincinnati). All cell lines were maintained in Dulbecco's modified Eagle's medium (DMEM) supplemented with 10% Bovine Calf Serum (BCS - VWR Life Science Seradigm), with the exception of L6 cells which were grown in alpha modified Eagle's medium (AMEM) supplemented with 10% heat-inactivated fetal bovine serum (FBS). eGFP-mCherry-LC3B stable MEF cells was generated from infection of wild-type MEFs with a lentivirus containing the transgene. A stable polyclonal population was obtained through puromycin (1 μg/ml) selection for stable integration of the transgene.

Mammalian expression plasmids

GFP-WIPI2 DNA plasmid was a gift from Dr. Proikas-Cezanne and has been described previously[139]. Transfection was performed with polyethylenimine (PEI, 4:1 v/w ratio to DNA) and cells were used for experiment 48 hours post transfection.

Phospho-antibody development

Phospho-peptide flanking S278 of ATG16L1 was used to immunize 4 rabbits. Sera were screened against *in vitro* phosphorylated ATG16L1. Hybridomas were made from the most reactive rabbit. Hybridoma supernatants were screened for reactivity against phospho-peptide, recombinant phospho-protein, and endogenous phospho protein. Clones that were successful in all phases of screening were then tested for reactivity in IF. A single clone (211) from the second hybridoma fusion was reactive in all assays. This antibody has now been cloned and is commercially available (ab195242).

Antibodies

Anti-phospho-S6 (4858), S6 (2317), were purchased from Cell Signalling Technology. Anti-ATG16L1 (ab187617), anti-ATG13 (ab201467) were purchased from Abcam. Anti-LC3B (NB100-2220) was from Novus Biological. Anti-p62 (GP62-C) was obtained from Progen Biotechnik. Anti-β-actin (A5441), vinculin (V9131) were from Sigma-Aldrich. Anti-phospho-ATG13 was a custom antibody obtained from Millennium Pharmaceuticals. For immunofluorescence microscopy, anti-LAMP1 (ab25630) was purchased from Abcam, anti-LC3B (PM036), anti-p62 (M162-3) and anti-ATG16L1 (PM040) were purchased from MBL. For immunohistochemistry, anti-p62 (ab207305) was purchased from Abcam, anti-LC3B (PM036) from MBL was used to stain LC3B.

Autophagy induction & inhibition

Cells were plated at the desired confluence the night before treatment. At 1 hour prior to starvation treatment, cells were replenished with fresh media. Starvation was performed using HBSS media (Multicell #311-513-CL), DMEM without amino acid, DMEM without

glucose, or DMEM without serum. Torin-1 (200nM, Tocris Bioscience) was added to cells for 2 hours to achieve mTORC inhibition. H_2O_2 (75μM, Fisher H325-500) was added to cells for 1 hour to induce ATG16L1 phosphorylation. Carbonyl cyanide m-chlorophenylhydrazone (CCCP. 100μM, Abcam ab141229) was added to cells for 5 hours to induce ATG16L1 phosphorylation. For samples treated with bafilomycin A1 (200nM, Cayman Chemicals), bafilomycin A1 was applied 15 minutes before treatment with stressors. VPS34 inhibitor (100nm, Calbiochem 5326280001) was added to cells for 2hours (IF) to 3 hours(WB) to achieve inhibition of autophagy.

Western blot

Cells were lysed directly with 1x Laemmil sample buffer. Samples were boiled at 95˚C for 10 minutes and then resolved by SDS-PAGE on 6%-18% gradient polyacrylamide gels. After transferring onto a PVDF membrane, the portions containing pATG16L1 were blocked with blocking solution (Ab126587) diluted in 1x PBS for 30 minutes. All other membranes were blocked with 5% skim milk dissolved in TBST for 30 minutes. Earlier pATG16L1 blots in this manuscript used 5% skim milk as the blocking agent, but had significantly higher background. Use of Ab126587 is strongly recommended. pATG16L1 was detected with overnight incubation in primary antibody diluted at 1:2000 with 2.5% BSA at 4°C, followed by 5x TBST washes and incubation in 1:15000 diluted anti-rabbit HRP conjugated secondary antibody at room temperature for 45 minutes.

Immunofluorescence (IF) microscopy

IF was performed on IBIDI-treated coverslips, cut to $1cm^2$ (ibidi, cat. 10814) which were deposited into 6 or 12 well plates. Cells were seeded onto coverslips 16 hours before

treatment. After treatment, cells were rinsed with PBS then fixed in 4% paraformaldehyde in PBS for 15 minutes. Cells were then permeabilized with 50 µg/mL of digitonin in PBS for 10 minutes. Blocking was performed in 1% BSA and 2% serum in PBS for 30 minutes. Cells were then incubated with primary antibodies in the blocking buffer for 1 hour at room temperature. Slides were then washed 3x with PBS, then incubated with secondary antibodies in blocking buffer for 30 minutes. Slides were then washed 3x with PBS and mounted onto glass microscope slides with ProLong gold anti-fade (Invitrogen). Epifluorescent images were captured with inverted Zeiss AxioObserver.Z1. High-resolution images were captured using Zeiss LSM 880 AxioObserverZ1 Confocal Microscope with AiryScan. Images were deconvoluted with AutoQuant x3.1 and 3D structures were constructed using Imaris.

Quantification of Immunofluorescence microscopy

Colocalization and average numbers of puncta per cell were determined by blinded manual counting of puncta from representative epifluorescent images. Quantification was performed on 3 independent experiments with at least 30 cells counted per treatment condition. Statistical analysis was performed with student's T-test.

Cyto-ID Autophagy Detection Kit assay

Cells were plated on ibidi 8 well µ-Slide (Ibidi, cat. 80826) overnight and subjected to the indicated treatments. Cells were then incubated in DMEM without phenol red containing Cyto-ID autophagy detection stain (Enzo, ENZ-KIT175-0050) for 30 minutes, then washed with PBS, re-incubated with either complete DMEM without phenol red or HBSS.

Images were acquired and deconvolved using an environmental chamber control microscope (DeltaVision Elite-Olympus IX-71 with FemtoJet Microinjector).

Immunohistochemistry (IHC)

Mice and tissue extraction

Muscle samples were harvested from CD1 wildtype mice that were either fed *ad libitum* or starved for 16 hours. Both groups of mice were provided with drinking water. Mice were sacrificed in the following morning after 16 hours; quadriceps muscle were harvested and immediately processed as described in the following sections.

Brain and liver samples were from mice fed ad libitum. These organs were harvested from mice perfused with PFA. Mice were anesthetized and transcardially perfused with cold phosphate buffered saline (PBS, pH7.4) followed by 4% paraformaldehyde in PBS. Brains were removed and post fixed for 1 hour in 4% paraformaldehyde and then transferred in cryoprotectant solution of 30% sucrose with 0.1% sodium azide in PBS. For brain section preparation brains were sectioned coronally into 30µm slices on a freezing microtome and stored in PBS with 0.1% sodium azide.

Tissue processing

Tissue samples were either: 1) Directly embedded in optimal cutting temperature compound (OCT) and snap frozen in liquid nitrogen-cooled isopentane bath. The frozen samples were sectioned into 10µm thick slices and mounted onto glass slides. Samples were then rinsed once with PBS and fixed in 4% PFA for 25 minutes. 2) Fixed in 10% formalin for 2 days. Then rinsed 3 times with 30% sucrose 3 times. The samples were

then dehydrated and paraffin embedded, sectioned into 4μm thick slices, and mounted onto glass microscope slides. Prior to staining, samples were rehydrated and deparffinized. Antigen-retrieval for both groups was performed in pH 9.0 EDTA solution, at 110°C for 12 minutes in a microwave processor (Histo5, Milestone).

Antibody staining

Samples were rinsed 3 times with PBS; treated with 3% H_2O_2 (in PBS) for 10 minutes; washed 3 times with TbT; blocked with 5% BSA for 2 hours; stained with primary antibody overnight at 4˚C (LC3 1:1000, p62 1:1000, pATG16L1 1:300); washed 3 times with TbT, incubated with secondary antibody (Alexa Fluor 555 anti-rabbit cat. A31572, 1:1000) for 1 hour; washed once with TbT; stained with DAPI (2mg/mL, Roche Diagnostics) for 10 minutes; washed 3 times with TbT; cover slip mounted with Fluoromount-G mounting solution (Invitrogen, 00-4958-02). All treatments were done at room temperature unless otherwise stated.

Image acquisition for IHC

IHC Images were acquired using Zeiss LSM 800 AxioObserverZ1 Confocal Microscope. Video was made by the 3D reconstruction function.

Quantification of Immunohistochemistry

Average numbers of puncta per cell were determined by blinded manual counting of puncta from representative images. Quantification was performed across at least 3 unique field of views and at least 15 cells counted per treatment condition.

Electron Microscopy

Q7 cells were treated with the indicated treatments then fixed with EM grade 4% paraformaldehyde and 3.5% glutaldehyde overnight. The cells were then washed with PBS 3 times and embedded in 4% agarose. The agarose embedded cells were sectioned into 50□m thick sections on a vibratome, then silver-enhanced for EM imaging. Quantifications of autophagosomes numbers were done by blinded manual counting from at least 14 unique field of views and at least 7 cells were counted per sample.

Discussion

Here, we describe methods for monitoring mammalian autophagy utilizing measurement of the direct signaling between two essential enzymes involved in autophagosome formation, the autophagy initiator kinase ULK, and the E3-like enzyme subunit ATG16L1. The selective presence of pATG16L1^{s278} on newly-forming autophagosomes indicates this signaling event is tightly tied to the biology of autophagosome formation, and therefore to the rate of autophagy induction. In a well-defined system, pATG16L1^{s278} levels largely follow the rate of LC3B lipidation, which is represented by the protein levels of LC3B-II. However, in the absence of lysosomal inhibitors, pATG16L1^{s278} consistently yielded a more reliable representation of the rate of ongoing autophagosome formation, likely due to the closer relationship between autophagy induction and pATG16L1^{s278} on the autophagy pathway than that of LC3B-II. The reliability of this assay will likely be of even greater benefit in more technically challenging experimental systems, where target cells may be rare, or drugs impractical. In fact, the ability of pATG16L1^{s278} to accurately measure autophagy rate without the need for an inhibitor chemical is one of the most significant strengths of assays utilizing this marker. Lysosomal inhibitors, while critical for the determination of autophagic flux in traditional LC3B-II based assays, inevitably introduce confounding factors to the experimental system, such as cytotoxicity or feedback inhibition, both of which would then affect the early regulation of the autophagy pathway. Another major advantage of pATG16L1^{s278} based assays over that of LC3B or autophagy adaptors such as p62 is that unlike the latter two proteins, pATG16L1^{s278} is not degraded by autophagy. This means that the cell would likely possess a near-constant pool of ATG16L1 that cycles between phosphorylated and dephosphorylated state based

on the cellular requirement to activate autophagy. Conversely, LC3B and p62 levels are affected not only by the rate of autophagosome turnover but also the transcriptional regulation. As we have already demonstrated in the case of p62, this can lead to situations where the change in protein level itself is no longer an accurate representation of autophagy rates.

The monoclonal pATG16L1^{s278} antibody characterized here is capable of endogenously detecting autophagy induction in multiple tissues and species across several common assays making it a robust method that can be easily adopted in most experimental situations. Based on these promising qualities, it could very well be applied in other established autophagy assays that were not explored in this study, such as flow cytometry or immunogold TEM, to be used in place of traditional autophagy markers such as LC3 or p62. Nevertheless, much more work is needed in this area of research, but the prospects are highly promising.

Additionally, the analysis of pATG16L1^{s278} may open new avenues for research into the mechanisms of autophagy induction and regulation. For example, the origin of membrane lipids used to form the autophagosome is still a much-contested topic in the field of autophagy research, pATG16L1^{s278} analysis may aid in demarcating the mechanisms and stages of autophagosomal membrane expansion, potentially paving the way to a more accurate model of autophagosome biogenesis, especially at the early stages.

Until recently, very little was known about the differences between the alpha and beta isoforms of ATG16L1 in terms of their physiological roles. In early 2019, a research group reported ATG16L1 isoforms differentially regulated LC3B lipidation mechanisms in canonical autophagy and VPS34-independent endosomal lipidation. They found that

ATG16L1 contained two distinct lipid-binding regions. An N-terminal region that was essential for LC3B lipidation under all scenarios *in vivo*, and an internal region unique to the beta isoform that was dispensable for canonical autophagy but required in VPS34-independent LC3B lipidation on endosomes. Since pATG16L1^{s278} is only present on the beta isoform, it might be possible that pATG16L1^{s278} is involved in beta ATG16L1-specific functions. A possible scenario is that pATG16L1^{s278} regulates the cellular localization of beta ATG16L1, such as facilitating membrane binding during the reported endosomal specific LC3B lipidation. Additionally, our lab has also recorded evidence suggesting that ATG16L1 tethering to cytoskeletal components seems to be regulated by phosphorylation events in a nutrient-sensitive manner. Despite whether this hypothesis turns out to be true or not, analysis of pATG16L1^{s278} will no doubt be beneficial in prospective research to further explore the different physiological functions of ATG16L1 isoforms and highlight additional ATG16L1 isoform-specific signaling pathways.

Previously, our lab has characterized the functions of pATG16L1^{s278} under both wildtype and Crohn's allele (caATG16L1) background of ATG16L1. We found that pATG16L1^{s278} enhanced intracellular bacteria capture and clearance by autophagy in wildtype cells but exacerbated the caspase-mediated cleavage of caATG16L1-containing cells, and as a result, lead to a decrease in clearance of intracellular bacteria. The caATG16L1 is one of several polymorphisms involving autophagy-related proteins that are associated with the onset of Crohn's disease. The pattern recognition receptor NOD2 is involved in xenophagic capture of bacteria, and also have mutations related to Crohn's. As pATG16L1^{s278} in wildtype cells was observed to preferentially localize to intracellular bacteria, this could imply a common defect on ATG16L1 function in these Crohn's

associated mutations. This hypothesis is further supported by the Crohn's associated SNP also being reported in ULK, albeit with less strength than caATG16L1, which could be explained by the functional redundancy of ULK1&2 isoforms. The exact mechanism of pATG16L1^{s278} promotion of caATG16L1 cleavage remains uncharacterized. However, further exploration of this topic and the role of ATG16L1 would surely improve our understandings of the impacts of autophagy defects in Crohn's disease development.

The 278th serine is one of many serine and threonine residues located in a conserved region on ATG16L1, which has not been well characterized. Based on high throughput mass spectrometry data that have been deposited, we have found that other sites in this region are also phosphorylated. It is highly unlikely that evolution would preserve a stretch of serine and threonine residues without any important function from the fruit fly to human. Therefore, it is quite possible that other regulatory events, either activating or inhibiting, are acting on this region of ATG16L1 and controlling the rate of autophagy initiation. The possibility of redundant activating pathways is highly likely, as we found the mutation of S278 was dispensable for activation. Taken together, pATG16L1^{s278} could very well only represent the tip of the iceberg when it comes to autophagy regulation via post-translational modifications on ATG16L1 and much work in this area remains to be done.

Lastly, we must reiterate that the use of pATG16L1^{s278} alone has the potential to be misleading in specific conditions that we have not yet determined, but likely exist. Therefore, the employment of multiple methods of autophagy analysis will remain the best approach to study the autophagy pathway. However, the use of pATG16L1^{s278} nonetheless represents an exciting new tool for autophagy researchers to utilize in the continued interrogation of the autophagy pathway.

References

1. Yang, Z. & Klionsky, D. J. Eaten alive: a history of macroautophagy. *Nat. Cell Biol.* **12**, 814–822 (2010).

2. Opperdoes, F. A Feeling for the Cell: Christian de Duve (1917–2013). *PLOS Biol.* **11**, e1001671 (2013).

3. Sabatini, D. D. & Adesnik, M. Christian de Duve: Explorer of the cell who discovered new organelles by using a centrifuge. *Proc. Natl. Acad. Sci. U. S. A.* **110**, 13234–13235 (2013).

4. Straus, W. Occurrence of phagosomes and phago-lysosomes in different segments of the nephron in relation to the reabsorption, transport, digestion, and extrusion of intravenously injected horseradish peroxidase. *J. Cell Biol.* **21**, 295–308 (1964).

5. Zanvil Alexander Cohn 1926-1993. *J. Exp. Med.* **179**, 1–30 (1994).

6. Klionsky, D. J. *et al.* Guidelines for the use and interpretation of assays for monitoring autophagy (3rd edition). *Autophagy* **12**, 1–222 (2016).

7. Matsuura, A., Tsukada, M., Wada, Y. & Ohsumi, Y. Apg1p, a novel protein kinase required for the autophagic process in Saccharomyces cerevisiae. *Gene* **192**, 245–250 (1997).

8. Mizushima, N., Sugita, H., Yoshimori, T. & Ohsumi, Y. A new protein conjugation system in human. The counterpart of the yeast Apg12p conjugation system essential for autophagy. *J. Biol. Chem.* **273**, 33889–33892 (1998).

9. Kabeya, Y. *et al.* LC3, a mammalian homologue of yeast Apg8p, is localized in autophagosome membranes after processing. *EMBO J.* **19**, 5720–5728 (2000).

10. Blommaart, E. F., Luiken, J. J., Blommaart, P. J., van Woerkom, G. M. & Meijer, A. J. Phosphorylation of ribosomal protein S6 is inhibitory for autophagy in isolated rat hepatocytes. *J. Biol. Chem.* **270**, 2320–2326 (1995).

11. Ganley, I. G. *et al.* ULK1.ATG13.FIP200 complex mediates mTOR signaling and is essential for autophagy. *J. Biol. Chem.* **284**, 12297–12305 (2009).

12. Mizushima, N. *et al.* Dissection of autophagosome formation using Apg5-deficient mouse embryonic stem cells. *J. Cell Biol.* **152**, 657–668 (2001).

13. Koyama-Honda, I., Itakura, E., Fujiwara, T. K. & Mizushima, N. Temporal analysis of recruitment of mammalian ATG proteins to the autophagosome formation site. *Autophagy* **9**, 1491–1499 (2013).

14. Ryter, S. W., Cloonan, S. M. & Choi, A. M. K. Autophagy: a critical regulator of cellular metabolism and homeostasis. *Mol. Cells* **36**, 7–16 (2013).

15. Kim, L. C., Cook, R. S. & Chen, J. mTORC1 and mTORC2 in cancer and the tumor microenvironment. *Oncogene* **36**, 2191–2201 (2017).

16. Saxton, R. A. & Sabatini, D. M. mTOR Signaling in Growth, Metabolism, and Disease. *Cell* **168**, 960–976 (2017).

17. Laplante, M. & Sabatini, D. M. mTOR signaling at a glance. *J. Cell Sci.* **122**, 3589–3594 (2009).

18. Foster, K. G. *et al.* Regulation of mTOR complex 1 (mTORC1) by raptor Ser863 and multisite phosphorylation. *J. Biol. Chem.* **285**, 80–94 (2010).

19. Kakumoto, K., Ikeda, J.-I., Okada, M., Morii, E. & Oneyama, C. mLST8 Promotes mTOR-Mediated Tumor Progression. *PloS One* **10**, e0119015 (2015).

20. Sohretoglu, D., Zhang, C., Luo, J. & Huang, S. ReishiMax inhibits mTORC1/2 by activating AMPK and inhibiting IGFR/PI3K/Rheb in tumor cells. *Signal Transduct. Target. Ther.* **4**, 21 (2019).

21. Tchevkina, E. & Komelkov, A. Protein Phosphorylation as a Key Mechanism of mTORC1/2 Signaling Pathways. *Protein Phosphorylation Hum. Health* (2012) doi:10.5772/48274.

22. Puertollano, R. mTOR and lysosome regulation. *F1000Prime Rep.* **6**, (2014).

23. Manifava, M. *et al.* Dynamics of mTORC1 activation in response to amino acids. *eLife* **5**, (2016).

24. Kirali, K., Goksedef, D. & Yakut, C. Reverse ‘U’ aortotomy for aortic valve replacement after previous coronary artery bypass grafting. *J. Card. Surg.* **20**, 269–270 (2005).

25. Manning, B. D. & Cantley, L. C. Rheb fills a GAP between TSC and TOR. *Trends Biochem. Sci.* **28**, 573–576 (2003).

26. Yu, J. S. L. & Cui, W. Proliferation, survival and metabolism: the role of PI3K/AKT/mTOR signalling in pluripotency and cell fate determination. *Dev. Camb. Engl.* **143**, 3050–3060 (2016).

27. Wong, P.-M., Puente, C., Ganley, I. G. & Jiang, X. The ULK1 complex: sensing nutrient signals for autophagy activation. *Autophagy* **9**, 124–137 (2013).

28. Lee, E.-J. & Tournier, C. The requirement of uncoordinated 51-like kinase 1 (ULK1) and ULK2 in the regulation of autophagy. *Autophagy* **7**, 689–695 (2011).

29. Mercer, C. A., Kaliappan, A. & Dennis, P. B. A novel, human Atg13 binding protein, Atg101, interacts with ULK1 and is essential for macroautophagy. *Autophagy* **5**, 649–662 (2009).

30. Suzuki, H., Kaizuka, T., Mizushima, N. & Noda, N. N. Structure of the Atg101-Atg13 complex reveals essential roles of Atg101 in autophagy initiation. *Nat. Struct. Mol. Biol.* **22**, 572–580 (2015).

31. Hara, T. *et al.* FIP200, a ULK-interacting protein, is required for autophagosome formation in mammalian cells. *J. Cell Biol.* **181**, 497–510 (2008).

32. Hosokawa, N. *et al.* Nutrient-dependent mTORC1 association with the ULK1-Atg13-FIP200 complex required for autophagy. *Mol. Biol. Cell* **20**, 1981–1991 (2009).

33. Alers, S., Löffler, A. S., Wesselborg, S. & Stork, B. Role of AMPK-mTOR-Ulk1/2 in the regulation of autophagy: cross talk, shortcuts, and feedbacks. *Mol. Cell. Biol.* **32**, 2–11 (2012).

34. Parzych, K. R. & Klionsky, D. J. An overview of autophagy: morphology, mechanism, and regulation. *Antioxid. Redox Signal.* **20**, 460–473 (2014).

35. Cicchini, M., Karantza, V. & Xia, B. Molecular pathways: autophagy in cancer--a matter of timing and context. *Clin. Cancer Res. Off. J. Am. Assoc. Cancer Res.* **21**, 498–504 (2015).

36. Raiborg, C., Schink, K. O. & Stenmark, H. Class III phosphatidylinositol 3-kinase and its catalytic product PtdIns3P in regulation of endocytic membrane traffic. *FEBS J.* **280**, 2730–2742 (2013).

37. Lőrincz, P. *et al.* Atg6/UVRAG/Vps34-Containing Lipid Kinase Complex Is Required for Receptor Downregulation through Endolysosomal Degradation and Epithelial Polarity during Drosophila Wing Development. *BioMed Research International* https://www.hindawi.com/journals/bmri/2014/851349/ (2014) doi:10.1155/2014/851349.

38. Funderburk, S. F., Wang, Q. J. & Yue, Z. The Beclin 1-VPS34 complex--at the crossroads of autophagy and beyond. *Trends Cell Biol.* **20**, 355–362 (2010).

39. Egan, D. F. *et al.* Small Molecule Inhibition of the Autophagy Kinase ULK1 and Identification of ULK1 Substrates. *Mol. Cell* **59**, 285–297 (2015).

40. Russell, R. C. *et al.* ULK1 induces autophagy by phosphorylating Beclin-1 and activating VPS34 lipid kinase. *Nat. Cell Biol.* **15**, 741–750 (2013).

41. Wold, M. S., Lim, J., Lachance, V., Deng, Z. & Yue, Z. ULK1-mediated phosphorylation of ATG14 promotes autophagy and is impaired in Huntington's disease models. *Mol. Neurodegener.* **11**, 76 (2016).

42. Di Bartolomeo, S. *et al.* The dynamic interaction of AMBRA1 with the dynein motor complex regulates mammalian autophagy. *J. Cell Biol.* **191**, 155–168 (2010).

43. Kim, J. *et al.* Differential regulation of distinct Vps34 complexes by AMPK in nutrient stress and autophagy. *Cell* **152**, 290–303 (2013).

44. Schu, P. V. *et al.* Phosphatidylinositol 3-kinase encoded by yeast VPS34 gene essential for protein sorting. *Science* **260**, 88–91 (1993).

45. Siddhanta, U., McIlroy, J., Shah, A., Zhang, Y. & Backer, J. M. Distinct roles for the p110alpha and hVPS34 phosphatidylinositol 3'-kinases in vesicular trafficking,

regulation of the actin cytoskeleton, and mitogenesis. *J. Cell Biol.* **143**, 1647–1659 (1998).

46. Obara, K. & Ohsumi, Y. PtdIns 3-Kinase Orchestrates Autophagosome Formation in Yeast. *J. Lipids* **2011**, 498768 (2011).

47. Jiang, P. *et al.* The HOPS complex mediates autophagosome-lysosome fusion through interaction with syntaxin 17. *Mol. Biol. Cell* **25**, 1327–1337 (2014).

48. Yuan, H.-X., Russell, R. C. & Guan, K.-L. Regulation of PIK3C3/VPS34 complexes by MTOR in nutrient stress-induced autophagy. *Autophagy* **9**, 1983–1995 (2013).

49. Munson, M. J. *et al.* mTOR activates the VPS34-UVRAG complex to regulate autolysosomal tubulation and cell survival. *EMBO J.* **34**, 2272–2290 (2015).

50. Kang, R., Zeh, H. J., Lotze, M. T. & Tang, D. The Beclin 1 network regulates autophagy and apoptosis. *Cell Death Differ.* **18**, 571–580 (2011).

51. Geng, J. & Klionsky, D. J. The Atg8 and Atg12 ubiquitin-like conjugation systems in macroautophagy. 'Protein Modifications: Beyond the Usual Suspects'' Review Series'. *EMBO Rep.* **9**, 859–864 (2008).

52. Qiu, Y., Zheng, Y., Taherbhoy, A. M., Kaiser, S. E. & Schulman, B. A. Crystallographic Characterization of ATG Proteins and Their Interacting Partners. *Methods Enzymol.* **587**, 227–246 (2017).

53. Tanida, I. *et al.* Apg7p/Cvt2p: A novel protein-activating enzyme essential for autophagy. *Mol. Biol. Cell* **10**, 1367–1379 (1999).

54. Shintani, T. *et al.* Apg10p, a novel protein-conjugating enzyme essential for autophagy in yeast. *EMBO J.* **18**, 5234–5241 (1999).

55. Mizushima, N., Noda, T. & Ohsumi, Y. Apg16p is required for the function of the Apg12p-Apg5p conjugate in the yeast autophagy pathway. *EMBO J.* **18**, 3888–3896 (1999).

56. Fujita, N. *et al.* The Atg16L complex specifies the site of LC3 lipidation for membrane biogenesis in autophagy. *Mol. Biol. Cell* **19**, 2092–2100 (2008).

57. Kirisako, T. *et al.* The reversible modification regulates the membrane-binding state of Apg8/Aut7 essential for autophagy and the cytoplasm to vacuole targeting pathway. *J. Cell Biol.* **151**, 263–276 (2000).

58. Fujita, N. *et al.* The Atg16L complex specifies the site of LC3 lipidation for membrane biogenesis in autophagy. *Mol. Biol. Cell* **19**, 2092–2100 (2008).

59. Mizushima, N. *et al.* A protein conjugation system essential for autophagy. *Nature* **395**, 395–398 (1998).

60. Birgisdottir, Å. B., Lamark, T. & Johansen, T. The LIR motif - crucial for selective autophagy. *J. Cell Sci.* **126**, 3237–3247 (2013).

61. Fujita, N. *et al.* An Atg4B mutant hampers the lipidation of LC3 paralogues and causes defects in autophagosome closure. *Mol. Biol. Cell* **19**, 4651–4659 (2008).

62. Proikas-Cezanne, T., Takacs, Z., Dönnes, P. & Kohlbacher, O. WIPI proteins: essential PtdIns3P effectors at the nascent autophagosome. *J. Cell Sci.* **128**, 207–217 (2015).

63. Dooley, H. C. *et al.* WIPI2 links LC3 conjugation with PI3P, autophagosome formation, and pathogen clearance by recruiting Atg12-5-16L1. *Mol. Cell* **55**, 238–252 (2014).

64. Yoshii, S. R. & Mizushima, N. Autophagy machinery in the context of mammalian mitophagy. *Biochim. Biophys. Acta* **1853**, 2797–2801 (2015).

65. Takahashi, Y. *et al.* Bif-1 regulates Atg9 trafficking by mediating the fission of Golgi membranes during autophagy. *Autophagy* **7**, 61–73 (2011).

66. Young, A. R. J. *et al.* Starvation and ULK1-dependent cycling of mammalian Atg9 between the TGN and endosomes. *J. Cell Sci.* **119**, 3888–3900 (2006).

67. Burman, C. & Ktistakis, N. T. Regulation of autophagy by phosphatidylinositol 3-phosphate. *FEBS Lett.* **584**, 1302–1312 (2010).

68. Zhuang, X. *et al.* ATG9 regulates autophagosome progression from the endoplasmic reticulum in Arabidopsis. *Proc. Natl. Acad. Sci. U. S. A.* **114**, E426–E435 (2017).

69. Ropolo, A. *et al.* The pancreatitis-induced vacuole membrane protein 1 triggers autophagy in mammalian cells. *J. Biol. Chem.* **282**, 37124–37133 (2007).

70. Vaccaro, M. I., Ropolo, A., Grasso, D. & Iovanna, J. L. A novel mammalian trans-membrane protein reveals an alternative initiation pathway for autophagy. *Autophagy* **4**, 388–390 (2008).

71. Grasso, D. *et al.* Zymophagy, a novel selective autophagy pathway mediated by VMP1-USP9x-p62, prevents pancreatic cell death. *J. Biol. Chem.* **286**, 8308–8324 (2011).

72. Carlsson, S. R. & Simonsen, A. Membrane dynamics in autophagosome biogenesis. *J. Cell Sci.* **128**, 193–205 (2015).

73. Molejon, M. I., Ropolo, A., Re, A. L., Boggio, V. & Vaccaro, M. I. The VMP1-Beclin 1 interaction regulates autophagy induction. *Sci. Rep.* **3**, 1055 (2013).

74. Nowak, J. *et al.* The TP53INP2 protein is required for autophagy in mammalian cells. *Mol. Biol. Cell* **20**, 870–881 (2009).

75. Levine, B. & Kroemer, G. Autophagy in the pathogenesis of disease. *Cell* **132**, 27–42 (2008).

76. Qu, X. *et al.* Promotion of tumorigenesis by heterozygous disruption of the beclin 1 autophagy gene. *J. Clin. Invest.* **112**, 1809–1820 (2003).

77. Mariño, G. *et al.* Tissue-specific autophagy alterations and increased tumorigenesis in mice deficient in Atg4C/autophagin-3. *J. Biol. Chem.* **282**, 18573–18583 (2007).

78. Rabinowitz, J. D. & White, E. Autophagy and metabolism. *Science* **330**, 1344–1348 (2010).

79. Degenhardt, K. *et al.* Autophagy promotes tumor cell survival and restricts necrosis, inflammation, and tumorigenesis. *Cancer Cell* **10**, 51–64 (2006).

80. Sweeney, P. *et al.* Protein misfolding in neurodegenerative diseases: implications and strategies. *Transl. Neurodegener.* **6**, 6 (2017).

81. Jaeger, P. A. & Wyss-Coray, T. All-you-can-eat: autophagy in neurodegeneration and neuroprotection. *Mol. Neurodegener.* **4**, 16 (2009).

82. Schulte, J. & Littleton, J. T. The biological function of the Huntingtin protein and its relevance to Huntington's Disease pathology. *Curr. Trends Neurol.* **5**, 65–78 (2011).

83. Ravikumar, B. *et al.* Inhibition of mTOR induces autophagy and reduces toxicity of polyglutamine expansions in fly and mouse models of Huntington disease. *Nat. Genet.* **36**, 585–595 (2004).

84. Abd-Elrahman, K. S. & Ferguson, S. S. G. Modulation of mTOR and CREB pathways following mGluR5 blockade contribute to improved Huntington's pathology in zQ175 mice. *Mol. Brain* **12**, 35 (2019).

85. Webb, J. L., Ravikumar, B., Atkins, J., Skepper, J. N. & Rubinsztein, D. C. Alpha-Synuclein is degraded by both autophagy and the proteasome. *J. Biol. Chem.* **278**, 25009–25013 (2003).

86. Yu, W. H. *et al.* Macroautophagy--a novel Beta-amyloid peptide-generating pathway activated in Alzheimer's disease. *J. Cell Biol.* **171**, 87–98 (2005).

87. Mei, Y., Thompson, M. D., Cohen, R. A. & Tong, X. Autophagy and oxidative stress in cardiovascular diseases. *Biochim. Biophys. Acta* **1852**, 243–251 (2015).

88. Nakai, A. *et al.* The role of autophagy in cardiomyocytes in the basal state and in response to hemodynamic stress. *Nat. Med.* **13**, 619–624 (2007).

89. Yano, T. *et al.* Autophagic control of listeria through intracellular innate immune recognition in drosophila. *Nat. Immunol.* **9**, 908–916 (2008).

90. Thurston, T. L. M., Ryzhakov, G., Bloor, S., von Muhlinen, N. & Randow, F. The TBK1 adaptor and autophagy receptor NDP52 restricts the proliferation of ubiquitin-coated bacteria. *Nat. Immunol.* **10**, 1215–1221 (2009).

91. Ogawa, M. *et al.* Escape of intracellular Shigella from autophagy. *Science* **307**, 727–731 (2005).

92. Andrade, R. M., Wessendarp, M., Gubbels, M.-J., Striepen, B. & Subauste, C. S. CD40 induces macrophage anti-Toxoplasma gondii activity by triggering autophagy-dependent fusion of pathogen-containing vacuoles and lysosomes. *J. Clin. Invest.* **116**, 2366–2377 (2006).

93. Nakagawa, I. *et al.* Autophagy defends cells against invading group A Streptococcus. *Science* **306**, 1037–1040 (2004).

94. Gutierrez, M. G. *et al.* Autophagy is a defense mechanism inhibiting BCG and Mycobacterium tuberculosis survival in infected macrophages. *Cell* **119**, 753–766 (2004).

95. Paludan, C. *et al.* Endogenous MHC class II processing of a viral nuclear antigen after autophagy. *Science* **307**, 593–596 (2005).

96. English, L. *et al.* Autophagy enhances the presentation of endogenous viral antigens on MHC class I molecules during HSV-1 infection. *Nat. Immunol.* **10**, 480–487 (2009).

97. Freeman, H. J. Natural history and long-term clinical course of Crohn's disease. *World J. Gastroenterol. WJG* **20**, 31–36 (2014).

98. Hendrickson, B. A., Gokhale, R. & Cho, J. H. Clinical aspects and pathophysiology of inflammatory bowel disease. *Clin. Microbiol. Rev.* **15**, 79–94 (2002).

99. Brest, P. *et al.* Autophagy and Crohn's disease: at the crossroads of infection, inflammation, immunity, and cancer. *Curr. Mol. Med.* **10**, 486–502 (2010).

100. Massey, D. C. O. & Parkes, M. Genome-wide association scanning highlights two autophagy genes, ATG16L1 and IRGM, as being significantly associated with Crohn's disease. *Autophagy* **3**, 649–651 (2007).

101. Sadaghian Sadabad, M. *et al.* The ATG16L1-T300A allele impairs clearance of pathosymbionts in the inflamed ileal mucosa of Crohn's disease patients. *Gut* **64**, 1546–1552 (2015).

102. Sorbara, M. T. *et al.* The protein ATG16L1 suppresses inflammatory cytokines induced by the intracellular sensors Nod1 and Nod2 in an autophagy-independent manner. *Immunity* **39**, 858–873 (2013).

103. Homer, C. R., Richmond, A. L., Rebert, N. A., Achkar, J.-P. & McDonald, C. ATG16L1 and NOD2 interact in an autophagy-dependent antibacterial pathway implicated in Crohn's disease pathogenesis. *Gastroenterology* **139**, 1630–1641, 1641.e1–2 (2010).

104. Diamanti, M. A. *et al.* IKKα controls ATG16L1 degradation to prevent ER stress during inflammation. *J. Exp. Med.* **214**, 423–437 (2017).

105. Gao, P. *et al.* The Inflammatory Bowel Disease-Associated Autophagy Gene Atg16L1T300A Acts as a Dominant Negative Variant in Mice. *J. Immunol. Baltim. Md 1950* **198**, 2457–2467 (2017).

106. Boada-Romero, E. *et al.* The T300A Crohn's disease risk polymorphism impairs function of the WD40 domain of ATG16L1. *Nat. Commun.* **7**, 11821 (2016).

107. Isidoro, C. *et al.* The role of autophagy on the survival of dopamine neurons. *Curr. Top. Med. Chem.* **9**, 869–879 (2009).

108. Wu, J. *et al.* Molecular cloning and characterization of rat LC3A and LC3B--two novel markers of autophagosome. *Biochem. Biophys. Res. Commun.* **339**, 437–442 (2006).

109. Kimura, S., Fujita, N., Noda, T. & Yoshimori, T. Monitoring autophagy in mammalian cultured cells through the dynamics of LC3. *Methods Enzymol.* **452**, 1–12 (2009).

110. Meléndez, A. *et al.* Autophagy genes are essential for dauer development and life-span extension in C. elegans. *Science* **301**, 1387–1391 (2003).

111. Rusten, T. E. *et al.* Programmed autophagy in the Drosophila fat body is induced by ecdysone through regulation of the PI3K pathway. *Dev. Cell* **7**, 179–192 (2004).

112. Bampton, E. T. W., Goemans, C. G., Niranjan, D., Mizushima, N. & Tolkovsky, A. M. The dynamics of autophagy visualized in live cells: from autophagosome formation to fusion with endo/lysosomes. *Autophagy* **1**, 23–36 (2005).

113. Amer, A. O. & Swanson, M. S. Autophagy is an immediate macrophage response to Legionella pneumophila. *Cell. Microbiol.* **7**, 765–778 (2005).

114. Ogawa, M. & Sasakawa, C. Intracellular survival of Shigella. *Cell. Microbiol.* **8**, 177–184 (2006).

115. Reyes, L. *et al.* Deletion of lipoprotein PG0717 in Porphyromonas gingivalis W83 reduces gingipain activity and alters trafficking in and response by host cells. *PloS One* **8**, e74230 (2013).

116. Kimura, S., Noda, T. & Yoshimori, T. Dissection of the autophagosome maturation process by a novel reporter protein, tandem fluorescent-tagged LC3. *Autophagy* **3**, 452–460 (2007).

117. Orvedahl, A. *et al.* Image-based genome-wide siRNA screen identifies selective autophagy factors. *Nature* **480**, 113–117 (2011).

118. Jain, A. *et al.* p62/SQSTM1 is a target gene for transcription factor NRF2 and creates a positive feedback loop by inducing antioxidant response element-driven gene transcription. *J. Biol. Chem.* **285**, 22576–22591 (2010).

119. Fujita, K.-I. & Srinivasula, S. M. TLR4-mediated autophagy in macrophages is a p62-dependent type of selective autophagy of aggresome-like induced structures (ALIS). *Autophagy* **7**, 552–554 (2011).

120. Salminen, A. *et al.* Emerging role of p62/sequestosome-1 in the pathogenesis of Alzheimer's disease. *Prog. Neurobiol.* **96**, 87–95 (2012).

121. Jiang, X. *et al.* VPS34 stimulation of p62 phosphorylation for cancer progression. *Oncogene* **36**, 6850–6862 (2017).

122. Clausen, T. H. *et al.* p62/SQSTM1 and ALFY interact to facilitate the formation of p62 bodies/ALIS and their degradation by autophagy. *Autophagy* **6**, 330–344 (2010).

123. Kirkin, V., Lamark, T., Johansen, T. & Dikic, I. NBR1 cooperates with p62 in selective autophagy of ubiquitinated targets. *Autophagy* **5**, 732–733 (2009).

124. Shi, J. *et al.* NBR1 is dispensable for PARK2-mediated mitophagy regardless of the presence or absence of SQSTM1. *Cell Death Dis.* **6**, e1943 (2015).

125. Gammoh, N., Florey, O., Overholtzer, M. & Jiang, X. Interaction Between FIP200 and ATG16L1 Distinguishes ULK1 Complex-Dependent and -Independent Autophagy. *Nat. Struct. Mol. Biol.* **20**, 144–149 (2013).

126. Nishimura, T. *et al.* FIP200 regulates targeting of Atg16L1 to the isolation membrane. *EMBO Rep.* **14**, 284–291 (2013).

127. Alsaadi, R. M. *et al.* ULK1-mediated phosphorylation of ATG16L1 promotes xenophagy, but destabilizes the ATG16L1 Crohn's mutant. *EMBO Rep.* **20**, e46885 (2019).

128. Nguyen, T. N. *et al.* Atg8 family LC3/GABARAP proteins are crucial for autophagosome-lysosome fusion but not autophagosome formation during PINK1/Parkin mitophagy and starvation. *J. Cell Biol.* **215**, 857–874 (2016).

129. Komatsu, M. *et al.* Homeostatic levels of p62 control cytoplasmic inclusion body formation in autophagy-deficient mice. *Cell* **131**, 1149–1163 (2007).

130. Pankiv, S. *et al.* p62/SQSTM1 binds directly to Atg8/LC3 to facilitate degradation of ubiquitinated protein aggregates by autophagy. *J. Biol. Chem.* **282**, 24131–24145 (2007).

131. Yuan, N. *et al.* Bafilomycin A1 targets both autophagy and apoptosis pathways in pediatric B-cell acute lymphoblastic leukemia. *Haematologica* **100**, 345–356 (2015).

132. Sahani, M. H., Itakura, E. & Mizushima, N. Expression of the autophagy substrate SQSTM1/p62 is restored during prolonged starvation depending on transcriptional upregulation and autophagy-derived amino acids. *Autophagy* **10**, 431–441 (2014).

133. Losier, T. T. *et al.* AMPK Promotes Xenophagy through Priming of Autophagic Kinases upon Detection of Bacterial Outer Membrane Vesicles. *Cell Rep.* **26**, 2150-2165.e5 (2019).

134. Mizushima, N., Yamamoto, A., Matsui, M., Yoshimori, T. & Ohsumi, Y. In vivo analysis of autophagy in response to nutrient starvation using transgenic mice expressing a fluorescent autophagosome marker. *Mol. Biol. Cell* **15**, 1101–1111 (2004).

135. Rosenfeldt, M. T., Nixon, C., Liu, E., Mah, L. Y. & Ryan, K. M. Analysis of macroautophagy by immunohistochemistry. *Autophagy* **8**, 963–969 (2012).

136. Xi, Y. *et al.* Knockout of Atg5 delays the maturation and reduces the survival of adult-generated neurons in the hippocampus. *Cell Death Dis.* **7**, e2127 (2016).

137. Hoffman, M. A. *et al.* von Hippel-Lindau protein mutants linked to type 2C VHL disease preserve the ability to downregulate HIF. *Hum. Mol. Genet.* **10**, 1019–1027 (2001).

138. Guo, H. *et al.* Atg5 Disassociates the V1V0-ATPase to Promote Exosome Production and Tumor Metastasis Independent of Canonical Macroautophagy. *Dev. Cell* **43**, 716-730.e7 (2017).

139. Mauthe, M. *et al.* Resveratrol-mediated autophagy requires WIPI-1-regulated LC3 lipidation in the absence of induced phagophore formation. *Autophagy* **7**, 1448–1461 (2011).

Permissions to reuse copyright contents

This thesis is based on the author's first author publication: Tian, W., Alsaadi, R., Guo, Z. *et al.* An antibody for analysis of autophagy induction. *Nat Methods* **17,** 232–239 (2020). https://doi.org/10.1038/s41592-019-0661-y. As per policy of the copyright holder Spring Nature, reuse of article by the original author does not need permission as long as the journal (Nature Methods) is credited with initial publication. For figures taken from published articles (Figs. 1-9, 11-14), written permission to reuse copyrighted material were obtained from the respective copyright holders and are listed below in order.

Figure 1

Figure 2

ASM authorizes an advanced degree candidate to republish the requested material in his/her doctoral thesis or dissertation. If your thesis, or dissertation, is to be published commercially, then you must reapply for permission.

Figure 3

AMERICAN ASSOCIATION FOR CANCER RESEARCH LICENSE
TERMS AND CONDITIONS
Jul 25, 2020

This Agreement between Mr. Wensheng Tian ("You") and American Association for Cancer Research ("American Association for Cancer Research") consists of your license details and the terms and conditions provided by American Association for Cancer Research and Copyright Clearance Center.

License Number	4876230069992
License date	Jul 25, 2020
Licensed Content Publisher	American Association for Cancer Research
Licensed Content Publication	Clinical Cancer Research
Licensed Content Title	Molecular Pathways: Autophagy in Cancer—A Matter of Timing and Context
Licensed Content Author	Michelle Cicchini,Vassiliki Karantza,Bing Xia
Licensed Content Date	Feb 1, 2015
Licensed Content Volume	21
Licensed Content Issue	3
Type of Use	Thesis/Dissertation
Requestor type	academic/educational
Format	electronic
Portion	figures/tables/illustrations
Number of figures/tables/illustrations	1
Will you be translating?	no
Circulation	999999
Territory of distribution	Worldwide
Title	Analysis of Autophagy Induction through ATG16L1 Phosphorylation
Institution name	University of Ottawa
Expected presentation date	Aug 2020
Portions	Figure 1
Requestor Location	University of Ottawa 451 Smyth Rd Apt 108 Ottawa, ON K1H 8L1 Canada Attn: University of Ottawa
Total	0.00 USD
Terms and Conditions	

American Association for Cancer Research (AACR) Terms and Conditions

INTRODUCTION
The Publisher for this copyright material is the American Association for Cancer Research (AACR). By clicking "accept" in connection with completing this licensing transaction, you agree to the following terms and conditions applying to this transaction. You also agree to the Billing and Payment terms and conditions established by Copyright Clearance Center (CCC) at the time you opened your Rightslink account.

LIMITED LICENSE
The AACR grants exclusively to you, the User, for onetime, non-exclusive use of this material for the purpose stated in your request and used only with a maximum distribution equal to the number you identified in the permission process. Any form of republication must be completed within one year although copies made before then may be distributed thereafter and any electronic posting is limited to a period of one year. Reproduction of this material is confined to the purpose and/or media for which permission is granted. Altering or modifying this material is not permitted. However, figures and illustrations may be minimally altered or modified to serve the new work.

GEOGRAPHIC SCOPE
Licenses may be exercised as noted in the permission process

RESERVATION OF RIGHTS
The AACR reserves all rights not specifically granted in the combination of 1) the license details provided by you and accepted in the course of this licensing transaction, 2) these terms and conditions , and 3) CCC's Billing and Payment terms and conditions.

DISCLAIMER
You may obtain permission via Rightslink to use material owned by AACR. When you are requesting permission to reuse a portion for an AACR publication, it is your responsibility to examine each portion of content as published to determine whether a credit to, or copyright notice of a third party owner is published next to the item. You must obtain permission from the third party to use any material which has been reprinted with permission from the said third party. If you have not obtained permission from the third party, AACR disclaims any responsibility for the use you make of items owned by them.

LICENSE CONTINGENT ON PAYMENT
While you may exercise the rights licensed immediately upon issuance of the license at the end of the licensing process for the transaction, provided that you have disclosed complete and accurate details of your proposed use, no license is finally effective unless and until full payment is received from you, either by the publisher or by the CCC, as provided in CCC's Billing and Payment terms and conditions. If full payment is not received on a timely basis, then any license preliminarily granted shall be deemed automatically revoked and shall be void as if never granted. Further, in the event that you breach any of these terms and conditions, or any of the CCC's Billing and Payment terms and conditions, the license is automatically revoked and shall be void as if never granted. Use of materials as described in a revoked license, as well as any use of the materials beyond the scope of an unrevoked license, may constitute copyright infringement and the publisher reserves the right to take any and all action to protect its copyright in the materials.

COPYRIGHT NOTICE
You must include the following credit line in connection with your reproduction of the licensed material: "Reprinted (or adapted) from Publication Title, Copyright Year, Volume/Issue, Page Range, Author, Title of Article, with permission from AACR".

TRANSLATION
This permission is granted for non-exclusive world English rights only.

WARRANTIES
Publisher makes no representations or warranties with respect to the licensed material.

INDEMNIFICATION
You hereby indemnify and agree to hold harmless the publisher and CCC, and their respective officers, directors, employees and agents, from and against any and all claims arising out of your use of the licensed material other than as specifically authorized pursuant to this license.

REVOCATION
The AACR reserves the right to revoke a license for any reason, including but not limited to advertising and promotional uses of AACR content, third party usage and incorrect figure source attribution.

NO TRANSFER OF LICENSE
This license is personal to you and may not be sublicensed, assigned, or transferred by you to any other person without publisher's written permission.

NO AMENDMENT EXCEPT IN WRITING
This license may not be amended except in a writing signed by both parties (or, in the case of publisher, by CCC on publisher's behalf).

OBJECTION TO CONTRARY TERMS
Publishers hereby objects to any terms contained in any purchase order, acknowledgement, check endorsement or other writing prepared by you, which terms are inconsistent with these terms and conditions or CCC's Billing and Payment terms and conditions. These terms and conditions together with CCC's Billing and Payment terms and conditions (which are incorporated herein) comprise the entire agreement between you and publisher (and CCC) concerning this licensing transaction. In the event of any conflict between your obligations established by these terms and conditions, and those established by CCC's Billing and Payment terms and conditions, these terms and conditions shall control.

THESIS/DISSERTATION TERMS
If your request is to reuse an article authored by you and published by the AACR in your dissertation/thesis, your thesis may be submitted to your institution in either in print or electronic form. Should your thesis be published commercially, please reapply.

ELECTRONIC RESERVE
If this license is made in connection with a course, and the Licensed Material or any portion thereof is to be posted to a website, the website is to be password protected and made available only to the students registered for the relevant course. The permission is granted

for the duration of the course. All content posted to the website must maintain the copyright information notice.

JURISDICTION
This license transaction shall be governed by and construed in accordance with the laws of Pennsylvania. You hereby agree to submit to the jurisdiction of the federal and state courts located in Pennsylvania for purposes of resolving any disputes that may arise in connection with this licensing transaction.

Other Terms and Conditions:
v1.0

Figure 4

ELSEVIER LICENSE
TERMS AND CONDITIONS
Jul 25, 2020

This Agreement between Mr. Wensheng Tian ("You") and Elsevier ("Elsevier") consists of your license details and the terms and conditions provided by Elsevier and Copyright Clearance Center.

License Number	4876230660175
License date	Jul 25, 2020
Licensed Content Publisher	Elsevier
Licensed Content Publication	Trends in Cell Biology
Licensed Content Title	The Beclin 1–VPS34 complex – at the crossroads of autophagy and beyond
Licensed Content Author	Sarah F. Funderburk,Qing Jun Wang,Zhenyu Yue
Licensed Content Date	Jun 1, 2010
Licensed Content Volume	20
Licensed Content Issue	6
Licensed Content Pages	8
Start Page	355
End Page	362
Type of Use	reuse in a thesis/dissertation
Portion	figures/tables/illustrations
Number of figures/tables/illustrations	1
Format	electronic
Are you the author of this Elsevier article?	No
Will you be translating?	No
Title	Analysis of Autophagy Induction through ATG16L1 Phosphorylation
Institution name	University of Ottawa
Expected presentation date	Aug 2020
Portions	Figure 1B
Requestor Location	University of Ottawa 451 Smyth Rd Apt 108 Ottawa, ON K1H 8L1 Canada Attn: University of Ottawa
Publisher Tax ID	GB 494 6272 12
Total	0.00 USD

Terms and Conditions

INTRODUCTION

1. The publisher for this copyrighted material is Elsevier. By clicking "accept" in connection with completing this licensing transaction, you agree that the following terms and conditions apply to this transaction (along with the Billing and Payment terms and conditions established by Copyright Clearance Center, Inc. ("CCC"), at the time that you opened your Rightslink account and that are available at any time at http://myaccount.copyright.com).

GENERAL TERMS

2. Elsevier hereby grants you permission to reproduce the aforementioned material subject to the terms and conditions indicated.

3. Acknowledgement: If any part of the material to be used (for example, figures) has appeared in our publication with credit or acknowledgement to another source, permission must also be sought from that source. If such permission is not obtained then that material may not be included in your publication/copies. Suitable acknowledgement to the source must be made, either as a footnote or in a reference list at the end of your publication, as follows:

"Reprinted from Publication title, Vol /edition number, Author(s), Title of article / title of chapter, Pages No., Copyright (Year), with permission from Elsevier [OR APPLICABLE SOCIETY COPYRIGHT OWNER]." Also Lancet special credit - "Reprinted from The Lancet, Vol. number, Author(s), Title of article, Pages No., Copyright (Year), with permission from Elsevier."

4. Reproduction of this material is confined to the purpose and/or media for which permission is hereby given.

5. Altering/Modifying Material: Not Permitted. However figures and illustrations may be altered/adapted minimally to serve your work. Any other abbreviations, additions, deletions and/or any other alterations shall be made only with prior written authorization of Elsevier Ltd. (Please contact Elsevier at permissions@elsevier.com). No modifications can be made to any Lancet figures/tables and they must be reproduced in full.

6. If the permission fee for the requested use of our material is waived in this instance, please be advised that your future requests for Elsevier materials may attract a fee.

7. Reservation of Rights: Publisher reserves all rights not specifically granted in the combination of (i) the license details provided by you and accepted in the course of this licensing transaction, (ii) these terms and conditions and (iii) CCC's Billing and Payment terms and conditions.

8. License Contingent Upon Payment: While you may exercise the rights licensed immediately upon issuance of the license at the end of the licensing process for the transaction, provided that you have disclosed complete and accurate details of your proposed use, no license is finally effective unless and until full payment is received from

you (either by publisher or by CCC) as provided in CCC's Billing and Payment terms and conditions. If full payment is not received on a timely basis, then any license preliminarily granted shall be deemed automatically revoked and shall be void as if never granted. Further, in the event that you breach any of these terms and conditions or any of CCC's Billing and Payment terms and conditions, the license is automatically revoked and shall be void as if never granted. Use of materials as described in a revoked license, as well as any use of the materials beyond the scope of an unrevoked license, may constitute copyright infringement and publisher reserves the right to take any and all action to protect its copyright in the materials.

9. Warranties: Publisher makes no representations or warranties with respect to the licensed material.

10. Indemnity: You hereby indemnify and agree to hold harmless publisher and CCC, and their respective officers, directors, employees and agents, from and against any and all claims arising out of your use of the licensed material other than as specifically authorized pursuant to this license.

11. No Transfer of License: This license is personal to you and may not be sublicensed, assigned, or transferred by you to any other person without publisher's written permission.

12. No Amendment Except in Writing: This license may not be amended except in a writing signed by both parties (or, in the case of publisher, by CCC on publisher's behalf).

13. Objection to Contrary Terms: Publisher hereby objects to any terms contained in any purchase order, acknowledgment, check endorsement or other writing prepared by you, which terms are inconsistent with these terms and conditions or CCC's Billing and Payment terms and conditions. These terms and conditions, together with CCC's Billing and Payment terms and conditions (which are incorporated herein), comprise the entire agreement between you and publisher (and CCC) concerning this licensing transaction. In the event of any conflict between your obligations established by these terms and conditions and those established by CCC's Billing and Payment terms and conditions, these terms and conditions shall control.

14. Revocation: Elsevier or Copyright Clearance Center may deny the permissions described in this License at their sole discretion, for any reason or no reason, with a full refund payable to you. Notice of such denial will be made using the contact information provided by you. Failure to receive such notice will not alter or invalidate the denial. In no event will Elsevier or Copyright Clearance Center be responsible or liable for any costs, expenses or damage incurred by you as a result of a denial of your permission request, other than a refund of the amount(s) paid by you to Elsevier and/or Copyright Clearance Center for denied permissions.

LIMITED LICENSE

The following terms and conditions apply only to specific license types:

15. **Translation**: This permission is granted for non-exclusive world **English** rights only unless your license was granted for translation rights. If you licensed translation rights you may only translate this content into the languages you requested. A professional translator

must perform all translations and reproduce the content word for word preserving the integrity of the article.

16. **Posting licensed content on any Website**: The following terms and conditions apply as follows: Licensing material from an Elsevier journal: All content posted to the web site must maintain the copyright information line on the bottom of each image; A hyper-text must be included to the Homepage of the journal from which you are licensing at http://www.sciencedirect.com/science/journal/xxxxx or the Elsevier homepage for books at http://www.elsevier.com; Central Storage: This license does not include permission for a scanned version of the material to be stored in a central repository such as that provided by Heron/XanEdu.

Licensing material from an Elsevier book: A hyper-text link must be included to the Elsevier homepage at http://www.elsevier.com . All content posted to the web site must maintain the copyright information line on the bottom of each image.

Posting licensed content on Electronic reserve: In addition to the above the following clauses are applicable: The web site must be password-protected and made available only to bona fide students registered on a relevant course. This permission is granted for 1 year only. You may obtain a new license for future website posting.

17. **For journal authors:** the following clauses are applicable in addition to the above:

Preprints:

A preprint is an author's own write-up of research results and analysis, it has not been peer-reviewed, nor has it had any other value added to it by a publisher (such as formatting, copyright, technical enhancement etc.).

Authors can share their preprints anywhere at any time. Preprints should not be added to or enhanced in any way in order to appear more like, or to substitute for, the final versions of articles however authors can update their preprints on arXiv or RePEc with their Accepted Author Manuscript (see below).

If accepted for publication, we encourage authors to link from the preprint to their formal publication via its DOI. Millions of researchers have access to the formal publications on ScienceDirect, and so links will help users to find, access, cite and use the best available version. Please note that Cell Press, The Lancet and some society-owned have different preprint policies. Information on these policies is available on the journal homepage.

Accepted Author Manuscripts: An accepted author manuscript is the manuscript of an article that has been accepted for publication and which typically includes author-incorporated changes suggested during submission, peer review and editor-author communications.

Authors can share their accepted author manuscript:

- immediately

    - via their non-commercial person homepage or blog
    - by updating a preprint in arXiv or RePEc with the accepted manuscript
    - via their research institute or institutional repository for internal institutional uses or as part of an invitation-only research collaboration work-group
    - directly by providing copies to their students or to research collaborators for their personal use
    - for private scholarly sharing as part of an invitation-only work group on commercial sites with which Elsevier has an agreement
- After the embargo period
    - via non-commercial hosting platforms such as their institutional repository
    - via commercial sites with which Elsevier has an agreement

In all cases accepted manuscripts should:

- link to the formal publication via its DOI
- bear a CC-BY-NC-ND license - this is easy to do
- if aggregated with other manuscripts, for example in a repository or other site, be shared in alignment with our hosting policy not be added to or enhanced in any way to appear more like, or to substitute for, the published journal article.

Published journal article (JPA): A published journal article (PJA) is the definitive final record of published research that appears or will appear in the journal and embodies all value-adding publishing activities including peer review co-ordination, copy-editing, formatting, (if relevant) pagination and online enrichment.

Policies for sharing publishing journal articles differ for subscription and gold open access articles:

Subscription Articles: If you are an author, please share a link to your article rather than the full-text. Millions of researchers have access to the formal publications on ScienceDirect, and so links will help your users to find, access, cite, and use the best available version.

Theses and dissertations which contain embedded PJAs as part of the formal submission can be posted publicly by the awarding institution with DOI links back to the formal publications on ScienceDirect.

If you are affiliated with a library that subscribes to ScienceDirect you have additional private sharing rights for others' research accessed under that agreement. This includes use for classroom teaching and internal training at the institution (including use in course packs and courseware programs), and inclusion of the article for grant funding purposes.

Gold Open Access Articles: May be shared according to the author-selected end-user license and should contain a CrossMark logo, the end user license, and a DOI link to the formal publication on ScienceDirect.

Please refer to Elsevier's posting policy for further information.

18. **For book authors** the following clauses are applicable in addition to the above: Authors are permitted to place a brief summary of their work online only. You are not allowed to download and post the published electronic version of your chapter, nor may you scan the printed edition to create an electronic version. **Posting to a repository:** Authors are permitted to post a summary of their chapter only in their institution's repository.

19. **Thesis/Dissertation**: If your license is for use in a thesis/dissertation your thesis may be submitted to your institution in either print or electronic form. Should your thesis be published commercially, please reapply for permission. These requirements include permission for the Library and Archives of Canada to supply single copies, on demand, of the complete thesis and include permission for Proquest/UMI to supply single copies, on demand, of the complete thesis. Should your thesis be published commercially, please reapply for permission. Theses and dissertations which contain embedded PJAs as part of the formal submission can be posted publicly by the awarding institution with DOI links back to the formal publications on ScienceDirect.

Elsevier Open Access Terms and Conditions

You can publish open access with Elsevier in hundreds of open access journals or in nearly 2000 established subscription journals that support open access publishing. Permitted third party re-use of these open access articles is defined by the author's choice of Creative Commons user license. See our open access license policy for more information.

Terms & Conditions applicable to all Open Access articles published with Elsevier:

Any reuse of the article must not represent the author as endorsing the adaptation of the article nor should the article be modified in such a way as to damage the author's honour or reputation. If any changes have been made, such changes must be clearly indicated.

The author(s) must be appropriately credited and we ask that you include the end user license and a DOI link to the formal publication on ScienceDirect.

If any part of the material to be used (for example, figures) has appeared in our publication with credit or acknowledgement to another source it is the responsibility of the user to ensure their reuse complies with the terms and conditions determined by the rights holder.

Additional Terms & Conditions applicable to each Creative Commons user license:

CC BY: The CC-BY license allows users to copy, to create extracts, abstracts and new works from the Article, to alter and revise the Article and to make commercial use of the Article (including reuse and/or resale of the Article by commercial entities), provided the user gives appropriate credit (with a link to the formal publication through the relevant DOI), provides a link to the license, indicates if changes were made and the licensor is not

represented as endorsing the use made of the work. The full details of the license are available at http://creativecommons.org/licenses/by/4.0.

CC BY NC SA: The CC BY-NC-SA license allows users to copy, to create extracts, abstracts and new works from the Article, to alter and revise the Article, provided this is not done for commercial purposes, and that the user gives appropriate credit (with a link to the formal publication through the relevant DOI), provides a link to the license, indicates if changes were made and the licensor is not represented as endorsing the use made of the work. Further, any new works must be made available on the same conditions. The full details of the license are available at http://creativecommons.org/licenses/by-nc-sa/4.0.

CC BY NC ND: The CC BY-NC-ND license allows users to copy and distribute the Article, provided this is not done for commercial purposes and further does not permit distribution of the Article if it is changed or edited in any way, and provided the user gives appropriate credit (with a link to the formal publication through the relevant DOI), provides a link to the license, and that the licensor is not represented as endorsing the use made of the work. The full details of the license are available at http://creativecommons.org/licenses/by-nc-nd/4.0. Any commercial reuse of Open Access articles published with a CC BY NC SA or CC BY NC ND license requires permission from Elsevier and will be subject to a fee.

Commercial reuse includes:

- Associating advertising with the full text of the Article
- Charging fees for document delivery or access
- Article aggregation
- Systematic distribution via e-mail lists or share buttons

Posting or linking by commercial companies for use by customers of those companies.

20. **Other Conditions**:

v1.9

Figure 5

JOHN WILEY AND SONS LICENSE
TERMS AND CONDITIONS
Jul 25, 2020

This Agreement between Mr. Wensheng Tian ("You") and John Wiley and Sons ("John Wiley and Sons") consists of your license details and the terms and conditions provided by John Wiley and Sons and Copyright Clearance Center.

License Number	4876261372135
License date	Jul 25, 2020
Licensed Content Publisher	John Wiley and Sons
Licensed Content Publication	EMBO Reports
Licensed Content Title	The Atg8 and Atg12 ubiquitin-like conjugation systems in macroautophagy
Licensed Content Author	Jiefei Geng, Daniel J. Klionsky
Licensed Content Date	Aug 15, 2008
Licensed Content Volume	9
Licensed Content Issue	9
Licensed Content Pages	6
Type of use	Dissertation/Thesis
Requestor type	University/Academic
Format	Electronic
Portion	Figure/table
Number of figures/tables	1
Will you be translating?	No
Title	Analysis of Autophagy Induction through ATG16L1 Phosphorylation
Institution name	University of Ottawa
Expected presentation date	Aug 2020
Portions	Figure 2b, 2c
Requestor Location	University of Ottawa 451 Ottawa, ON K1H 8L1 Canada Attn: University of Ottawa
Publisher Tax ID	EU826007151
Total	0.00 USD

Terms and Conditions

TERMS AND CONDITIONS

- The Wiley Materials and all of the intellectual property rights therein shall at all times remain the exclusive property of John Wiley & Sons Inc, the Wiley Companies, or their respective licensors, and your interest therein is only that of having possession of and the right to reproduce the Wiley Materials pursuant to Section 2 herein during the continuance of this Agreement. You agree that you own no right, title or interest in or to the Wiley Materials or any of the intellectual property rights therein. You shall have no rights hereunder other than the license as provided for above in Section 2. No right, license or interest to any trademark, trade name, service mark or other branding ("Marks") of WILEY or its licensors is granted hereunder, and you agree that you shall not assert any such right, license or interest with respect thereto

- NEITHER WILEY NOR ITS LICENSORS MAKES ANY WARRANTY OR REPRESENTATION OF ANY KIND TO YOU OR ANY THIRD PARTY, EXPRESS, IMPLIED OR STATUTORY, WITH RESPECT TO THE MATERIALS OR THE ACCURACY OF ANY INFORMATION CONTAINED IN THE MATERIALS, INCLUDING, WITHOUT LIMITATION, ANY IMPLIED WARRANTY OF MERCHANTABILITY, ACCURACY, SATISFACTORY QUALITY, FITNESS FOR A PARTICULAR PURPOSE, USABILITY, INTEGRATION OR NON-INFRINGEMENT AND ALL SUCH WARRANTIES ARE HEREBY EXCLUDED BY WILEY AND ITS LICENSORS AND WAIVED BY YOU.

- WILEY shall have the right to terminate this Agreement immediately upon breach of this Agreement by you.

- You shall indemnify, defend and hold harmless WILEY, its Licensors and their respective directors, officers, agents and employees, from and against any actual or threatened claims, demands, causes of action or proceedings arising from any breach of this Agreement by you.

- IN NO EVENT SHALL WILEY OR ITS LICENSORS BE LIABLE TO YOU OR ANY OTHER PARTY OR ANY OTHER PERSON OR ENTITY FOR ANY SPECIAL, CONSEQUENTIAL, INCIDENTAL, INDIRECT, EXEMPLARY OR PUNITIVE DAMAGES, HOWEVER CAUSED, ARISING OUT OF OR IN CONNECTION WITH THE DOWNLOADING, PROVISIONING, VIEWING OR USE OF THE MATERIALS REGARDLESS OF THE FORM OF ACTION, WHETHER FOR BREACH OF CONTRACT, BREACH OF WARRANTY, TORT, NEGLIGENCE, INFRINGEMENT OR OTHERWISE (INCLUDING, WITHOUT LIMITATION, DAMAGES BASED ON LOSS OF PROFITS, DATA, FILES, USE, BUSINESS OPPORTUNITY OR CLAIMS OF THIRD PARTIES), AND WHETHER OR NOT THE PARTY HAS BEEN ADVISED OF THE POSSIBILITY OF SUCH DAMAGES. THIS LIMITATION SHALL APPLY NOTWITHSTANDING ANY FAILURE OF ESSENTIAL PURPOSE OF ANY LIMITED REMEDY PROVIDED HEREIN.

- Should any provision of this Agreement be held by a court of competent jurisdiction to be illegal, invalid, or unenforceable, that provision shall be deemed amended to achieve as nearly as possible the same economic effect as the original provision, and the legality, validity and enforceability of the remaining provisions of this Agreement shall not be affected or impaired thereby.

- The failure of either party to enforce any term or condition of this Agreement shall not constitute a waiver of either party's right to enforce each and every term and condition of this Agreement. No breach under this agreement shall be deemed waived or excused by either party unless such waiver or consent is in writing signed by the party granting such waiver or consent. The waiver by or consent of a party to a breach of any provision of this Agreement shall not operate or be construed as a waiver of or consent to any other or subsequent breach by such other party.

- This Agreement may not be assigned (including by operation of law or otherwise) by you without WILEY's prior written consent.

- Any fee required for this permission shall be non-refundable after thirty (30) days from receipt by the CCC.

- These terms and conditions together with CCC's Billing and Payment terms and conditions (which are incorporated herein) form the entire agreement between you and WILEY concerning this licensing transaction and (in the absence of fraud) supersedes all prior agreements and representations of the parties, oral or written. This Agreement may not be amended except in writing signed by both parties. This Agreement shall be binding upon and inure to the benefit of the parties' successors, legal representatives, and authorized assigns.

- In the event of any conflict between your obligations established by these terms and conditions and those established by CCC's Billing and Payment terms and conditions, these terms and conditions shall prevail.

- WILEY expressly reserves all rights not specifically granted in the combination of (i) the license details provided by you and accepted in the course of this licensing transaction, (ii) these terms and conditions and (iii) CCC's Billing and Payment terms and conditions.

- This Agreement will be void if the Type of Use, Format, Circulation, or Requestor Type was misrepresented during the licensing process.

- This Agreement shall be governed by and construed in accordance with the laws of the State of New York, USA, without regards to such state's conflict of law rules. Any legal action, suit or proceeding arising out of or relating to these Terms and Conditions or the breach thereof shall be instituted in a court of competent jurisdiction in New York County in the State of New York in the United States of America and each party hereby consents and submits to the personal jurisdiction of such court, waives any objection to venue in such court and consents to service of process by registered or certified mail, return receipt requested, at the last known address of such party.

WILEY OPEN ACCESS TERMS AND CONDITIONS

Wiley Publishes Open Access Articles in fully Open Access Journals and in Subscription journals offering Online Open. Although most of the fully Open Access journals publish open access articles under the terms of the Creative Commons Attribution (CC BY)

License only, the subscription journals and a few of the Open Access Journals offer a choice of Creative Commons Licenses. The license type is clearly identified on the article.

The Creative Commons Attribution License

The Creative Commons Attribution License (CC-BY) allows users to copy, distribute and transmit an article, adapt the article and make commercial use of the article. The CC-BY license permits commercial and non-

Creative Commons Attribution Non-Commercial License

The Creative Commons Attribution Non-Commercial (CC-BY-NC)License permits use, distribution and reproduction in any medium, provided the original work is properly cited and is not used for commercial purposes.(see below)

Creative Commons Attribution-Non-Commercial-NoDerivs License

The Creative Commons Attribution Non-Commercial-NoDerivs License (CC-BY-NC-ND) permits use, distribution and reproduction in any medium, provided the original work is properly cited, is not used for commercial purposes and no modifications or adaptations are made. (see below)

Use by commercial "for-profit" organizations

Use of Wiley Open Access articles for commercial, promotional, or marketing purposes requires further explicit permission from Wiley and will be subject to a fee.

Further details can be found on Wiley Online Library http://olabout.wiley.com/WileyCDA/Section/id-410895.html

Other Terms and Conditions:

v1.10 Last updated September 2015

Figure 6

Figure 7

Figure 8

This is a License Agreement between University of Ottawa -- Wensheng Tian ("You") and The Company of Biologists Ltd. ("Publisher") provided by Copyright Clearance Center ("CCC"). The license consists of your order details, the terms and conditions provided by The Company of Biologists Ltd., and the CCC terms and conditions.

All payments must be made in full to CCC.

Order Date
25-Jul-2020
Order license ID
1050889-1
ISSN
1477-9137
Type of Use
Republish in a thesis/dissertation
Publisher
COMPANY OF BIOLOGISTS LTD.
Portion
Chart/graph/table/figure

LICENSED CONTENT

Publication Title
Journal of cell science
Author/Editor
Company of Biologists.
Date
01/01/1966
Language
English
Country
United Kingdom of Great Britain and Northern Ireland
Rightsholder
The Company of Biologists Ltd.
Publication Type
e-Journal
URL
http://jcs.biologists.org/

REQUEST DETAILS

Portion Type
Chart/graph/table/figure
Number of charts / graphs / tables / figures requested
1
Format (select all that apply)
Electronic
Who will republish the content?
Academic institution

Duration of Use
Life of current edition
Lifetime Unit Quantity
Up to 999
Rights Requested
Main product
Distribution
Worldwide
Translation
Original language of publication
Copies for the disabled?
No
Minor editing privileges?
No
Incidental promotional use?
No
Currency
USD

NEW WORK DETAILS

Title
Analysis of Autophagy Induction through ATG16L1 Phosphorylation
Instructor name
Wensheng Tian
Institution name
University of Ottawa
Expected presentation date
2020-08-05

ADDITIONAL DETAILS

Order reference number
N/A
The requesting person / organization to appear on the license
University of Ottawa -- Wensheng Tian

REUSE CONTENT DETAILS

Title, description or numeric reference of the portion(s)
Figure 8
Editor of portion(s)
N/A
Volume of serial or monograph
N/A
Page or page range of portion
17
Title of the article/chapter the portion is from
Analysis of Autophagy Induction through ATG16L1 Phosphorylation
Author of portion(s)

Wensheng Tian
Issue, if republishing an article from a serial
N/A
Publication date of portion
2020-08-05

PUBLISHER TERMS AND CONDITIONS

The acknowledgement should state "Reproduced / adapted with permission" and give the source journal name. The acknowledgement should either provide full citation details or refer to the relevant citation in the article reference list. The full citation details should include authors, journal, year, volume, issue and page citation. Where appearing online or in other electronic media, a link should be provided to the original article (e.g. via DOI): Development: dev.biologists.org Disease Models & Mechanisms: dmm.biologists.org Journal of Cell Science: jcs.biologists.org The Journal of Experimental Biology: jeb.biologists.org
CCC Republication Terms and Conditions

1. Description of Service; Defined Terms. This Republication License enables the User to obtain licenses for republication of one or more copyrighted works as described in detail on the relevant Order Confirmation (the "Work(s)"). Copyright Clearance Center, Inc. ("CCC") grants licenses through the Service on behalf of the rightsholder identified on the Order Confirmation (the "Rightsholder"). "Republication", as used herein, generally means the inclusion of a Work, in whole or in part, in a new work or works, also as described on the Order Confirmation. "User", as used herein, means the person or entity making such republication.
2. The terms set forth in the relevant Order Confirmation, and any terms set by the Rightsholder with respect to a particular Work, govern the terms of use of Works in connection with the Service. By using the Service, the person transacting for a republication license on behalf of the User represents and warrants that he/she/it (a) has been duly authorized by the User to accept, and hereby does accept, all such terms and conditions on behalf of User, and (b) shall inform User of all such terms and conditions. In the event such person is a "freelancer" or other third party independent of User and CCC, such party shall be deemed jointly a "User" for purposes of these terms and conditions. In any event, User shall be deemed to have accepted and agreed to all such terms and conditions if User republishes the Work in any fashion.
3. Scope of License; Limitations and Obligations.
    1. All Works and all rights therein, including copyright rights, remain the sole and exclusive property of the Rightsholder. The license created by the exchange of an Order Confirmation (and/or any invoice) and payment by User of the full amount set forth on that document includes only those rights expressly set forth in the Order Confirmation and in these terms and conditions, and conveys no other rights in the Work(s) to User. All rights not expressly granted are hereby reserved.
    2. General Payment Terms: You may pay by credit card or through an account with us payable at the end of the month. If you and we agree that you may establish a standing account with CCC, then the following terms apply: Remit Payment to: Copyright Clearance Center, 29118 Network Place, Chicago, IL 60673-1291. Payments Due: Invoices are payable upon their delivery to you (or upon our notice to you that they are available to you for downloading). After 30 days, outstanding amounts will be subject to a service charge of 1-1/2% per month or, if less, the maximum rate allowed by applicable law. Unless otherwise specifically set forth in the Order Confirmation or in a separate written agreement signed by CCC, invoices are due and payable on "net 30" terms. While

User may exercise the rights licensed immediately upon issuance of the Order Confirmation, the license is automatically revoked and is null and void, as if it had never been issued, if complete payment for the license is not received on a timely basis either from User directly or through a payment agent, such as a credit card company.

3. Unless otherwise provided in the Order Confirmation, any grant of rights to User (i) is "one-time" (including the editions and product family specified in the license), (ii) is non-exclusive and non-transferable and (iii) is subject to any and all limitations and restrictions (such as, but not limited to, limitations on duration of use or circulation) included in the Order Confirmation or invoice and/or in these terms and conditions. Upon completion of the licensed use, User shall either secure a new permission for further use of the Work(s) or immediately cease any new use of the Work(s) and shall render inaccessible (such as by deleting or by removing or severing links or other locators) any further copies of the Work (except for copies printed on paper in accordance with this license and still in User's stock at the end of such period).
4. In the event that the material for which a republication license is sought includes third party materials (such as photographs, illustrations, graphs, inserts and similar materials) which are identified in such material as having been used by permission, User is responsible for identifying, and seeking separate licenses (under this Service or otherwise) for, any of such third party materials; without a separate license, such third party materials may not be used.
5. Use of proper copyright notice for a Work is required as a condition of any license granted under the Service. Unless otherwise provided in the Order Confirmation, a proper copyright notice will read substantially as follows: "Republished with permission of [Rightsholder's name], from [Work's title, author, volume, edition number and year of copyright]; permission conveyed through Copyright Clearance Center, Inc. " Such notice must be provided in a reasonably legible font size and must be placed either immediately adjacent to the Work as used (for example, as part of a by-line or footnote but not as a separate electronic link) or in the place where substantially all other credits or notices for the new work containing the republished Work are located. Failure to include the required notice results in loss to the Rightsholder and CCC, and the User shall be liable to pay liquidated damages for each such failure equal to twice the use fee specified in the Order Confirmation, in addition to the use fee itself and any other fees and charges specified.
6. User may only make alterations to the Work if and as expressly set forth in the Order Confirmation. No Work may be used in any way that is defamatory, violates the rights of third parties (including such third parties' rights of copyright, privacy, publicity, or other tangible or intangible property), or is otherwise illegal, sexually explicit or obscene. In addition, User may not conjoin a Work with any other material that may result in damage to the reputation of the Rightsholder. User agrees to inform CCC if it becomes aware of any infringement of any rights in a Work and to cooperate with any reasonable request of CCC or the Rightsholder in connection therewith.

4. Indemnity. User hereby indemnifies and agrees to defend the Rightsholder and CCC, and their respective employees and directors, against all claims, liability, damages, costs and expenses, including legal fees and expenses, arising out of any use of a Work beyond the scope of the rights granted herein, or any use of a Work which has been altered in any unauthorized way by User, including claims of defamation or infringement of rights of copyright, publicity, privacy or other tangible or intangible property.
5. Limitation of Liability. UNDER NO CIRCUMSTANCES WILL CCC OR THE RIGHTSHOLDER BE LIABLE FOR ANY DIRECT, INDIRECT, CONSEQUENTIAL OR INCIDENTAL DAMAGES (INCLUDING WITHOUT LIMITATION DAMAGES FOR LOSS OF BUSINESS PROFITS OR INFORMATION, OR FOR BUSINESS INTERRUPTION) ARISING OUT OF THE USE OR INABILITY TO USE A WORK, EVEN IF ONE OF THEM HAS BEEN

ADVISED OF THE POSSIBILITY OF SUCH DAMAGES. In any event, the total liability of the Rightsholder and CCC (including their respective employees and directors) shall not exceed the total amount actually paid by User for this license. User assumes full liability for the actions and omissions of its principals, employees, agents, affiliates, successors and assigns.

6. Limited Warranties. THE WORK(S) AND RIGHT(S) ARE PROVIDED "AS IS". CCC HAS THE RIGHT TO GRANT TO USER THE RIGHTS GRANTED IN THE ORDER CONFIRMATION DOCUMENT. CCC AND THE RIGHTSHOLDER DISCLAIM ALL OTHER WARRANTIES RELATING TO THE WORK(S) AND RIGHT(S), EITHER EXPRESS OR IMPLIED, INCLUDING WITHOUT LIMITATION IMPLIED WARRANTIES OF MERCHANTABILITY OR FITNESS FOR A PARTICULAR PURPOSE. ADDITIONAL RIGHTS MAY BE REQUIRED TO USE ILLUSTRATIONS, GRAPHS, PHOTOGRAPHS, ABSTRACTS, INSERTS OR OTHER PORTIONS OF THE WORK (AS OPPOSED TO THE ENTIRE WORK) IN A MANNER CONTEMPLATED BY USER; USER UNDERSTANDS AND AGREES THAT NEITHER CCC NOR THE RIGHTSHOLDER MAY HAVE SUCH ADDITIONAL RIGHTS TO GRANT.
7. Effect of Breach. Any failure by User to pay any amount when due, or any use by User of a Work beyond the scope of the license set forth in the Order Confirmation and/or these terms and conditions, shall be a material breach of the license created by the Order Confirmation and these terms and conditions. Any breach not cured within 30 days of written notice thereof shall result in immediate termination of such license without further notice. Any unauthorized (but licensable) use of a Work that is terminated immediately upon notice thereof may be liquidated by payment of the Rightsholder's ordinary license price therefor; any unauthorized (and unlicensable) use that is not terminated immediately for any reason (including, for example, because materials containing the Work cannot reasonably be recalled) will be subject to all remedies available at law or in equity, but in no event to a payment of less than three times the Rightsholder's ordinary license price for the most closely analogous licensable use plus Rightsholder's and/or CCC's costs and expenses incurred in collecting such payment.
8. Miscellaneous.
    1. User acknowledges that CCC may, from time to time, make changes or additions to the Service or to these terms and conditions, and CCC reserves the right to send notice to the User by electronic mail or otherwise for the purposes of notifying User of such changes or additions; provided that any such changes or additions shall not apply to permissions already secured and paid for.
    2. Use of User-related information collected through the Service is governed by CCC's privacy policy, available online here:https://marketplace.copyright.com/rs-ui-web/mp/privacy-policy
    3. The licensing transaction described in the Order Confirmation is personal to User. Therefore, User may not assign or transfer to any other person (whether a natural person or an organization of any kind) the license created by the Order Confirmation and these terms and conditions or any rights granted hereunder; provided, however, that User may assign such license in its entirety on written notice to CCC in the event of a transfer of all or substantially all of User's rights in the new material which includes the Work(s) licensed under this Service.
    4. No amendment or waiver of any terms is binding unless set forth in writing and signed by the parties. The Rightsholder and CCC hereby object to any terms contained in any writing prepared by the User or its principals, employees, agents or affiliates and purporting to govern or otherwise relate to the licensing transaction described in the Order Confirmation, which terms are in any way inconsistent with any terms set forth in the Order Confirmation and/or in these terms and conditions or CCC's standard operating

procedures, whether such writing is prepared prior to, simultaneously with or subsequent to the Order Confirmation, and whether such writing appears on a copy of the Order Confirmation or in a separate instrument.

5. The licensing transaction described in the Order Confirmation document shall be governed by and construed under the law of the State of New York, USA, without regard to the principles thereof of conflicts of law. Any case, controversy, suit, action, or proceeding arising out of, in connection with, or related to such licensing transaction shall be brought, at CCC's sole discretion, in any federal or state court located in the County of New York, State of New York, USA, or in any federal or state court whose geographical jurisdiction covers the location of the Rightsholder set forth in the Order Confirmation. The parties expressly submit to the personal jurisdiction and venue of each such federal or state court.If you have any comments or questions about the Service or Copyright Clearance Center, please contact us at 978-750-8400 or send an e-mail to support@copyright.com.

v 1.1

Figures 9, 11 and 12

Thesis/Dissertation Reuse Request

Taylor & Francis is pleased to offer reuses of its content for a thesis or dissertation free of charge contingent on resubmission of permission request if work is published.

Figures 13 and 14

JOHN WILEY AND SONS LICENSE
TERMS AND CONDITIONS
Jul 25, 2020

This Agreement between Mr. Wensheng Tian ("You") and John Wiley and Sons ("John Wiley and Sons") consists of your license details and the terms and conditions provided by John Wiley and Sons and Copyright Clearance Center.

License Number	4876280464611
License date	Jul 25, 2020
Licensed Content Publisher	John Wiley and Sons
Licensed Content Publication	EMBO Reports
Licensed Content Title	ULK1-mediated phosphorylation of ATG16L1 promotes xenophagy, but destabilizes the ATG16L1 Crohn's mutant
Licensed Content Author	Ryan C Russell, David C Rubinsztein, Zhihao Guo, et al
Licensed Content Date	May 24, 2019
Licensed Content Volume	20
Licensed Content Issue	7
Licensed Content Pages	12
Type of use	Dissertation/Thesis
Requestor type	University/Academic
Format	Electronic
Portion	Figure/table
Number of figures/tables	2
Will you be translating?	No
Title	Analysis of Autophagy Induction through ATG16L1 Phosphorylation
Institution name	University of Ottawa
Expected presentation date	Aug 2020
Portions	Figure 1E, Figure 2A
Requestor Location	University of Ottawa 451 Smyth Rd Ottawa, ON K1H 8L1 Canada Attn: University of Ottawa
Publisher Tax ID	EU826007151
Total	0.00 USD
Terms and Conditions	

TERMS AND CONDITIONS

This copyrighted material is owned by or exclusively licensed to John Wiley & Sons, Inc. or one of its group companies (each a"Wiley Company") or handled on behalf of a society with which a Wiley Company has exclusive publishing rights in relation to a particular work (collectively "WILEY"). By clicking "accept" in connection with completing this licensing transaction, you agree that the following terms and conditions apply to this transaction (along with the billing and payment terms and conditions established by the Copyright Clearance Center Inc., ("CCC's Billing and Payment terms and conditions"), at the time that you opened your RightsLink account (these are available at any time at http://myaccount.copyright.com).

Terms and Conditions

- The materials you have requested permission to reproduce or reuse (the "Wiley Materials") are protected by copyright.

- You are hereby granted a personal, non-exclusive, non-sub licensable (on a stand-alone basis), non-transferable, worldwide, limited license to reproduce the Wiley Materials for the purpose specified in the licensing process. This license, **and any CONTENT (PDF or image file) purchased as part of your order,** is for a one-time use only and limited to any maximum distribution number specified in the license. The first instance of republication or reuse granted by this license must be completed within two years of the date of the grant of this license (although copies prepared before the end date may be distributed thereafter). The Wiley Materials shall not be used in any other manner or for any other purpose, beyond what is granted in the license. Permission is granted subject to an appropriate acknowledgement given to the author, title of the material/book/journal and the publisher. You shall also duplicate the copyright notice that appears in the Wiley publication in your use of the Wiley Material. Permission is also granted on the understanding that nowhere in the text is a previously published source acknowledged for all or part of this Wiley Material. Any third party content is expressly excluded from this permission.

- With respect to the Wiley Materials, all rights are reserved. Except as expressly granted by the terms of the license, no part of the Wiley Materials may be copied, modified, adapted (except for minor reformatting required by the new Publication), translated, reproduced, transferred or distributed, in any form or by any means, and no derivative works may be made based on the Wiley Materials without the prior permission of the respective copyright owner.**For STM Signatory Publishers clearing permission under the terms of the STM Permissions Guidelines only, the terms of the license are extended to include subsequent editions and for editions in other languages, provided such editions are for the work as a whole in situ and does not involve the separate exploitation of the permitted figures or extracts,** You may not alter, remove or suppress in any manner any copyright, trademark or other notices displayed by the Wiley Materials. You may not license, rent, sell, loan, lease, pledge, offer as security, transfer or assign the

Wiley Materials on a stand-alone basis, or any of the rights granted to you hereunder to any other person.

- The Wiley Materials and all of the intellectual property rights therein shall at all times remain the exclusive property of John Wiley & Sons Inc, the Wiley Companies, or their respective licensors, and your interest therein is only that of having possession of and the right to reproduce the Wiley Materials pursuant to Section 2 herein during the continuance of this Agreement. You agree that you own no right, title or interest in or to the Wiley Materials or any of the intellectual property rights therein. You shall have no rights hereunder other than the license as provided for above in Section 2. No right, license or interest to any trademark, trade name, service mark or other branding ("Marks") of WILEY or its licensors is granted hereunder, and you agree that you shall not assert any such right, license or interest with respect thereto

- NEITHER WILEY NOR ITS LICENSORS MAKES ANY WARRANTY OR REPRESENTATION OF ANY KIND TO YOU OR ANY THIRD PARTY, EXPRESS, IMPLIED OR STATUTORY, WITH RESPECT TO THE MATERIALS OR THE ACCURACY OF ANY INFORMATION CONTAINED IN THE MATERIALS, INCLUDING, WITHOUT LIMITATION, ANY IMPLIED WARRANTY OF MERCHANTABILITY, ACCURACY, SATISFACTORY QUALITY, FITNESS FOR A PARTICULAR PURPOSE, USABILITY, INTEGRATION OR NON-INFRINGEMENT AND ALL SUCH WARRANTIES ARE HEREBY EXCLUDED BY WILEY AND ITS LICENSORS AND WAIVED BY YOU.

- WILEY shall have the right to terminate this Agreement immediately upon breach of this Agreement by you.

- You shall indemnify, defend and hold harmless WILEY, its Licensors and their respective directors, officers, agents and employees, from and against any actual or threatened claims, demands, causes of action or proceedings arising from any breach of this Agreement by you.

- IN NO EVENT SHALL WILEY OR ITS LICENSORS BE LIABLE TO YOU OR ANY OTHER PARTY OR ANY OTHER PERSON OR ENTITY FOR ANY SPECIAL, CONSEQUENTIAL, INCIDENTAL, INDIRECT, EXEMPLARY OR PUNITIVE DAMAGES, HOWEVER CAUSED, ARISING OUT OF OR IN CONNECTION WITH THE DOWNLOADING, PROVISIONING, VIEWING OR USE OF THE MATERIALS REGARDLESS OF THE FORM OF ACTION, WHETHER FOR BREACH OF CONTRACT, BREACH OF WARRANTY, TORT, NEGLIGENCE, INFRINGEMENT OR OTHERWISE (INCLUDING, WITHOUT LIMITATION, DAMAGES BASED ON LOSS OF PROFITS, DATA, FILES, USE, BUSINESS OPPORTUNITY OR CLAIMS OF THIRD PARTIES), AND WHETHER OR NOT THE PARTY HAS BEEN ADVISED OF THE POSSIBILITY OF SUCH DAMAGES. THIS LIMITATION SHALL APPLY NOTWITHSTANDING ANY FAILURE OF ESSENTIAL PURPOSE OF ANY LIMITED REMEDY PROVIDED HEREIN.

- Should any provision of this Agreement be held by a court of competent jurisdiction to be illegal, invalid, or unenforceable, that provision shall be deemed amended to achieve as nearly as possible the same economic effect as the original provision,

and the legality, validity and enforceability of the remaining provisions of this Agreement shall not be affected or impaired thereby.

- The failure of either party to enforce any term or condition of this Agreement shall not constitute a waiver of either party's right to enforce each and every term and condition of this Agreement. No breach under this agreement shall be deemed waived or excused by either party unless such waiver or consent is in writing signed by the party granting such waiver or consent. The waiver by or consent of a party to a breach of any provision of this Agreement shall not operate or be construed as a waiver of or consent to any other or subsequent breach by such other party.

- This Agreement may not be assigned (including by operation of law or otherwise) by you without WILEY's prior written consent.

- Any fee required for this permission shall be non-refundable after thirty (30) days from receipt by the CCC.

- These terms and conditions together with CCC's Billing and Payment terms and conditions (which are incorporated herein) form the entire agreement between you and WILEY concerning this licensing transaction and (in the absence of fraud) supersedes all prior agreements and representations of the parties, oral or written. This Agreement may not be amended except in writing signed by both parties. This Agreement shall be binding upon and inure to the benefit of the parties' successors, legal representatives, and authorized assigns.

- In the event of any conflict between your obligations established by these terms and conditions and those established by CCC's Billing and Payment terms and conditions, these terms and conditions shall prevail.

- WILEY expressly reserves all rights not specifically granted in the combination of (i) the license details provided by you and accepted in the course of this licensing transaction, (ii) these terms and conditions and (iii) CCC's Billing and Payment terms and conditions.

- This Agreement will be void if the Type of Use, Format, Circulation, or Requestor Type was misrepresented during the licensing process.

- This Agreement shall be governed by and construed in accordance with the laws of the State of New York, USA, without regards to such state's conflict of law rules. Any legal action, suit or proceeding arising out of or relating to these Terms and Conditions or the breach thereof shall be instituted in a court of competent jurisdiction in New York County in the State of New York in the United States of America and each party hereby consents and submits to the personal jurisdiction of such court, waives any objection to venue in such court and consents to service of process by registered or certified mail, return receipt requested, at the last known address of such party.

WILEY OPEN ACCESS TERMS AND CONDITIONS

Wiley Publishes Open Access Articles in fully Open Access Journals and in Subscription journals offering Online Open. Although most of the fully Open Access journals publish open access articles under the terms of the Creative Commons Attribution (CC BY) License only, the subscription journals and a few of the Open Access Journals offer a choice of Creative Commons Licenses. The license type is clearly identified on the article.

The Creative Commons Attribution License

The Creative Commons Attribution License (CC-BY) allows users to copy, distribute and transmit an article, adapt the article and make commercial use of the article. The CC-BY license permits commercial and non-

Creative Commons Attribution Non-Commercial License

The Creative Commons Attribution Non-Commercial (CC-BY-NC)License permits use, distribution and reproduction in any medium, provided the original work is properly cited and is not used for commercial purposes.(see below)

Creative Commons Attribution-Non-Commercial-NoDerivs License

The Creative Commons Attribution Non-Commercial-NoDerivs License (CC-BY-NC-ND) permits use, distribution and reproduction in any medium, provided the original work is properly cited, is not used for commercial purposes and no modifications or adaptations are made. (see below)

Use by commercial "for-profit" organizations

Use of Wiley Open Access articles for commercial, promotional, or marketing purposes requires further explicit permission from Wiley and will be subject to a fee.

Further details can be found on Wiley Online Library http://olabout.wiley.com/WileyCDA/Section/id-410895.html

Other Terms and Conditions:

v1.10 Last updated September 2015